

Felipe Silveira de Souza Schneider

Quantitative computational contributions to the elucidation of chemical reaction mechanisms

Florianópolis, Santa Catarina, Brazil

November 22, 2022

Felipe Silveira de Souza Schneider

Quantitative computational contributions to the elucidation of chemical reaction mechanisms

Tese de Doutorado submetida ao Programa de Pós-graduação em Química da Universidade Federal de Santa Catarina como pré-requisito parcial para obtenção do Grau de Doutor em Química, na área de concentração em Físico-Química.

Universidade Federal de Santa Catarina — UFSC

Centro de Ciências Físicas e Matemáticas

Departamento de Química

Programa de Pós-Graduação em Química

Supervisor: Prof. Dr. Giovanni F. Caramori

Co-supervisor: Prof. Dr. Faruk Nome (*in memoriam*)

Florianópolis, Santa Catarina, Brazil

November 22, 2022

Felipe Silveira de Souza Schneider

Quantitative computational contributions to the
elucidation of chemical reaction mechanisms / Felipe Silveira de Souza Schneider. —
Florianópolis, Santa Catarina, Brazil, November 22, 2022—
105 p.: il. (algumas color.); 30 cm.

Supervisor: Prof. Dr. Giovanni F. Caramori

Co-supervisor: Prof. Dr. Faruk Nome (*in memoriam*)

Tese (Doutorado) – Universidade Federal de Santa Catarina — UFSC
Centro de Ciências Físicas e Matemáticas

Departamento de Química

Programa de Pós-Graduação em Química, November 22, 2022.

1. Química computacional. 2. Elucidação de mecanismos de reação. 3. Desenvolvimento de software. I. Prof. Dr. Giovanni F. Caramori. II. Prof. Dr. Faruk Nome (*in memoriam*). III. Universidade Federal de Santa Catarina. IV. Programa de Pós-Graduação em Química. V. Quantitative computational contributions to the elucidation of chemical reaction mechanisms.

Felipe Silveira de Souza Schneider

Quantitative computational contributions to the elucidation of chemical reaction mechanisms

Tese de Doutorado submetida ao Programa de Pós-graduação em Química da Universidade Federal de Santa Catarina como pré-requisito parcial para obtenção do Grau de Doutor em Química, na área de concentração em Físico-Química.

Tese de Doutorado submetida à banca examinadora e aprovada pelo colegiado do Programa de Pós-graduação em Química, sendo julgada adequada para a obtenção do grau de Doutor em Química.

Florianópolis, Santa Catarina, Brazil, November 22, 2022:

Prof. Dr. Giovanni F. Caramori
Orientador

Professor
Convidado 1

Professor
Convidado 2

Professor
Convidado 3

Professor
Convidado 4

Florianópolis, Santa Catarina, Brazil
November 22, 2022

*Este trabalho é dedicado ao Prof. Dr. Faruk Nome (in memoriam),
motivador original destas ideias.*

Acknowledgements

I would like to acknowledge the following people for their support in the development of this thesis.

Prof. Dr. Giovanni F. Caramori by his confidence and trust in myself and in this work, and by the opportunity he gave me to pursue these ideas. Prof. Dr. Faruk Nome (*in memoriam*) for his kind support at a time where this work was in its infancy. I thank both for their support, kindness, advice and mentoring.

The thesis committee for taking the time and effort to read, evaluate and discuss the present thesis.

To all professors in the Chemistry Department and in the Graduate Programme, and to the Federal University of Santa Catarina as a whole for the high-quality education and excellent work. A special thanks goes to Prof. Dr. Josiel D. Barbosa and Dr. Bernardo de Souza for their enthusiasm and outstanding collaboration, advice and support.

To all the members of our research group, colleagues and friends at GEEM for their support. I would like to thank particularly the following people: Alechania Miszturini, Alexandre Osmar Ortolan, Denner Ferreira, Letícia Maria Pequeno, Marina Briese, Matheus Colaço, Rômulo Peixoto, Vinícius Glitz, and, Vinícius Port. Without you I could not have made until here.

To Scheila and Manssur for helping me when I most needed it.

To my parents (Edson Schneider and Laureci Silveira de Souza Schneider) for their love and support in all these years.

To Deise Munaro for being so kind and special, and for standing on my side for so long and in such difficult times.

I am also grateful for the funding and resources provided by the following institutions: CNPq, for a PhD scholarship (grant number 140485/2017–1); and FAPESC, FAPESP, and CESUP/UFRGS, whose valuable resources make, directly or indirectly, our computing facilities viable.

To the developers of software I have used throughout these years, in special for the developers of the following projects: Julia, NumPy/SciPy, Vim/Neovim, L^AT_EX and abnT_EX, and, cclib.

“We’re in the position of a visitor from another dimension who comes to earth and sees a chess match. Assuming he knows it’s a game, he’s got two problems: first, figure out the rules, and second, figure out how to win. Ninety percent of science (including virtually all of chemistry) is in that second category. They’re trying to apply the laws that are already known.”

(Sheldon Lee Glashow, 1979)

Abstract

CHECK THE QUALIFICATION.

The key question is whether we can calculate reaction mechanisms quantitatively using solely computational methods.

We have developed a framework for the calculation of reaction mechanisms and contributed to the elucidation of some key mechanisms with and without the use of the framework.

Especial contributions were given in detail for some of the mechanisms. In particular, we pinpointed the most important sources of error in the calculations.

In conclusion, further work is needed to include the role of solvents and conformations in a quantitative way.

REMEMBER: ABSTRACT IS A STANDALONE DOCUMENT.

Keywords: catalysis. computational chemistry. chemical reaction mechanisms.



Resumo

A ser escrito.

Palavras-chave: catálise. química computational. mecanismos de reações químicas.



List of Figures

Figure 1 – Typical scheme of an intramolecular reactions	37
Figure 2 – Beesley-Thorpe-Ingold effect, also known as geminal dimethyl effect. . .	103
Figure 3 – Kinetic effects of geminal and vicinal disubstitutions.	104
Figure 4 – Intramolecular hydrolysis of the amidic bond in maleamic acids and their N-methyl substitutional kinetic effect.	105



List of Schemes

List of Tables

List of Abbreviations

ABNT Associação Brasileira de Normas Técnicas

abnTeX ABsurdas Normas para TeX

List of Symbols

Γ Letra grega Gama

Λ Lambda

ζ Letra grega minúscula zeta

\in Pertence

Contents

1	PRESENTATION AND STRUCTURE	27
I	STATE OF THE ART AND THEORY	29
2	INTRODUCTION	31
3	METHODS AND TECHNIQUES	33
3.1	Theoretical Background	33
3.1.1	Density functional theory (DFT)	33
3.1.2	Single-molecule property predictions	34
3.1.2.1	Transition state optimizations	34
3.1.3	Prediction of kinetics and thermodynamics for chemical reactions	35
3.1.3.1	Transition state theory	35
3.1.4	When things go wrong: bulk effects	35
3.1.4.1	Determining <i>pK</i> as	35
3.2	Chemical reaction mechanisms	36
3.2.1	Bell-Evans-Polanyi principle	36
3.2.2	Hammond's postulate	36
3.3	Intramolecular and substitutional effects: a key step to understand enzyme-like catalysis	37
3.4	Automatic determination of kinetics using overreact	38
3.5	Thermochemical partition functions	38
3.6	Why predicting chemical reactions is hard	38
3.7	"First-principle" calculations	39
3.7.1	Quantum tunneling effects	39
3.8	Microkinetic modelling	40
3.8.1	Design	40
3.8.2	Automatic differentiation	40
II	PUBLICATIONS	43
3.9	Contributions to the computational elucidation of reaction mechanisms	45
3.9.1	Minor contributions	45
3.9.2	Major contributions	45

4	PAPER I: MECHANISM OF PD(II)-MEDIATED UNCAGING REACTIONS OF PROPARGYLIC SUBSTRATES	47
4.1	Paper	48
5	PAPER II: PT-TRIGGERED BOND-CLEAVAGE OF PENTYNOYL AMIDE AND N-PROPARGYL HANDLES FOR DRUG-ACTIVATION .	57
5.1	Paper	58
6	PAPER III: OVERREACT, AN IN SILICO LAB: AUTOMATIVE QUANTUM CHEMICAL MICROKINETIC SIMU- LATIONS FOR COMPLEX CHEMICAL REACTIONS	71
6.1	Paper	71
7	CONCLUDING REMARKS AND CLOSING	81
	BIBLIOGRAPHY	83
	APPENDICES	93
	Appendix A – LIST OF WORKS	95
	Appendix B – PRACTICAL COMPUTATIONAL CHEMISTRY FOR THE INVESTIGATION OF REACTION MECHA- NISMS AND TRANSITION STATE SEARCHES	99
B.1	General remarks about transition state structures	99
B.1.1	Using Hammond's postulate for estimating transition state structures	99
B.2	Some methods for obtaining transition states	100
B.2.1	What if this don't work?	101
B.3	What to do once you found a transition state candidate	101
B.3.1	If you are finding a set of homologous transition states	102
	Appendix C – GEM- AND VIC DISUBSTITUTIONS	103

1 Presentation and structure

The present thesis is organized in two parts. Part I encompasses a brief overview of the current state of the art in the area of computational elucidation of reaction mechanisms. Part II is divided into three chapters, each of which presents an application or development to certain problems in the field.

The chapters in Part I provide a detailed account of the field. Chapter 2 summarizes the broad theme of reaction mechanism elucidation by computational means and its promising applications. Chapter 3 describes the methods available to computationally investigate reaction mechanisms and, in particular, the methods used in the present thesis. In Section 3.4, attention is paid to the design of `overreact` [1, 2], a software package developed by the author for the purpose of automating the investigation of reaction mechanisms in general.

MAKE THE FOLLOWING TEXT MORE ORGANIC, SUGGEST THAT THE APPLICATIONS ARE INTERTWINED. The chapters in Part II revolve around papers that have been published in the field and co-authored by the author. Chapter 4 deals with computational-experimental collaboration on the elucidation of the Palladium(II)-mediated uncaging reaction of propargylic substrates, with applications to the activation of prodrug molecules. It was published in COELHO, S. E. et al. Mechanism of palladium(ii)-mediated uncaging reactions of propargylic substrates. *ACS Catalysis*, American Chemical Society (ACS), v. 9, n. 5, p. 3792–3799, Mar 2019. ISSN 2155-5435. Disponível em: <<http://dx.doi.org/10.1021/acscatal.9b00210>>.. Chapter 5 provides an account of another computational-experimental collaboration on prodrug activation, this time on the Platinum(II)-triggered bond-cleavage of pentynoyl amide and N-propargyl handles. The relevant publication is OLIVEIRA, B. L. et al. Platinum-triggered bond-cleavage of pentynoyl amide and n-propargyl handles for drug-activation. *Journal of the American Chemical Society*, American Chemical Society (ACS), v. 142, n. 24, p. 10869–10880, May 2020. ISSN 1520-5126. Disponível em: <<http://dx.doi.org/10.1021/jacs.0c01622>>.. Finally, Chapter 6 introduces the `overreact` package, a software that performs microkinetic simulations from first principles in an automated way. It was published under SCHNEIDER, F. S. S.; CARAMORI, G. F. Overreact, an *in silico* lab: Automative quantum chemical microkinetic simulations for complex chemical reactions. *Journal of Computational Chemistry*, Wiley, Apr 2022. ISSN 1096-987x. Disponível em: <<http://dx.doi.org/10.1002/jcc.26861>>..

In all three chapters, the papers are presented in full text. These encompass what the author believes to be his most relevant contributions to the field, as detailed in Sec-

tion 3.9.2. Other minor contributions that tangentially relate to the field are commented on in the text (see Section 3.9.1). Furthermore, works not directly related to the field but were nevertheless published during the course of the thesis are presented in Appendix A.

A brief, closing perspective is given in Chapter 7, where the author concludes the thesis with an eye on what he believes to be the future of the field.

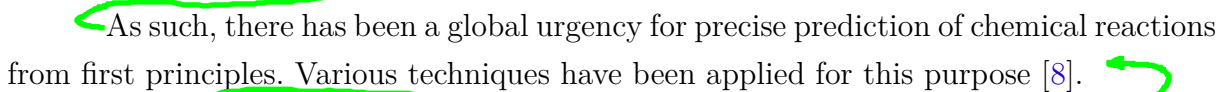
The present thesis contains two appendices. Together with the already mentioned Appendix A, which lists all the contributions co-authored, Appendix B provides a practical but short walkthrough over technical issues and methodologies developed during the thesis in the context of the main field, but that are rarely mentioned in the literature. Since most of the computational work in obtaining transition state geometries is still performed by trial and error, the author believes that Appendix B is an important contribution to the field as well.

Part I

State of the art and theory

2 Introduction

 Given the advent of environmental and energetic challenges [5], chemical reaction rational design is more important than ever. And today's economy demands fast chemical reactions: catalysts are employed in the production of over 80% of all chemical goods of industrial importance [6, 7]. In fact, the 2014 global market share of catalysts was evaluated in US\$ 33.5 billion, with an annual share in the global economy estimated to be worth US\$ 10 trillion [7].

 As such, there has been a global urgency for precise prediction of chemical reactions from first principles. Various techniques have been applied for this purpose [8].

 But there is natural room for improvement: currently industrially-employed catalysts do not reach near the throughput, atomic economy, selectivity and efficiency that are so frequently attained by natural enzymes [9]. If we are to rationally design chemical reactions on par with natural enzymes' billion years worth of evolution, we need to be able to predict chemical reactions from first principles with a high degree of accuracy. Such predictions must go beyond simple Gibbs' free energy diagrams and consider important aspects of complex chemical reaction networks such as concentrations, quantum tunneling, diffusion effects and others.



The present part presents an overview of methods for predicting chemical kinetics and thermodynamics from first principles. It starts with a brief introduction to the general state of the art in quantum chemistry and its applications to the study of chemical reactions. It then goes on to describe the methods employed in `overreact` [1], a software package for predicting chemical kinetics and simulating microkinetics automatically from first principles.

3 Methods and techniques

Since the works described in Chapters 4 to 6 consist of contributions related to the computational elucidation of reaction mechanisms, this chapter presents an account of the relevant computational methods and techniques used in the investigations, with background and context given for the various topics where appropriate. A basic background on computational chemistry applied to mechanistic elucidation is given in Section 3.1. Details about the methods used in the development of the `overreact` software package are given in Section 3.4.

3.1 Theoretical Background



Each of the steps in a proposed reaction mechanism is computational modelled by optimizing reactant, product and transition states. While the first two are minima on the potential energy surface, transition states represent a local maximum on the potential energy surface connecting reactants and products. This characterizes transition states as saddle points and, therefore, requires a different method of optimization than the other structures. In any case, optimization methods require an estimate of energies and gradients of the potential energy surface and the works presented in this thesis made use of the density functional theory (DFT) method [10, 11, 12, 13, 14] for that. A brief discussion of the theory can be found in Section 3.1.1.



3.1.1 Density functional theory (DFT)

This work has made extensive use of the density functional theory (DFT). As such, a very brief introduction to the theory is provided here. The interested reader is invited to read the cited references for more details [10, 11].

The main equation used in the DFT is the following (Equation (3.1)):

$$\left(-\frac{1}{2} \nabla^2 + v_{\text{ext}} + v_{\text{eff}} \right) \psi_i = \epsilon_i \psi_i \quad (3.1)$$

where ψ_i is i th molecular orbital, v_{ext} is the external potential due to the atomic nuclei, ϵ_i is the electronic energy of the i th orbital and v_{eff} is the effective potential for a given density functional (an approximation of the actual electron-electron interaction). This equation is analogous to the Hartree-Fock one [15] and is solved self-consistently as well. v_{eff} consists of classical Coulomb interactions, as well as exchange and correlation approximation potentials [12, 13, 14]. Other additive terms can appear in the potential as well, such as solvation approximations when employed [16, 17]. The various ways of

approximating the exchange and correlation potentials give rise to a number of different density functionals developed in the literature [18, 19, 20, 21, 22, 23, 24, 25].



In the present work, all problems were treated by expanding the molecular orbitals as a linear combination of basis functions centered at the atomic nuclei [15, 26, 27, 28]. The literature on basis set functions is extensive [29, 30, 31, 32, 33, 34, 35, 36, 37, 38, 39, 40]. We invite the interested reader to the references on each work for more about the levels of theory used in each case.

3.1.2 Single-molecule property predictions

Equation (3.1) allows us to obtain energy and gradient estimates (required for the prediction of geometrical, thermochemical and kinetic properties) with a reasonably good cost-effectiveness.



The most basic property required for any computational study is the molecular geometry. It is obtained by minimizing the energy with respect to the atomic positions. Commonly used and powerful family of optimization methods employed in the literature is the quasi-Newton method, where energies and gradients are computed, while an approximation to the second-derivative matrix (also known as a Hessian matrix) is updated at each step [41, 42].



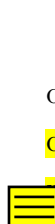
An approximation to the second-derivative matrix is employed in the algorithm for efficiency, but the actual matrix can be computed after the minimization is complete. This matrix provides important information about the region in the potential energy surface where the energy is minimum as we will see in the following.



3.1.2.1 Transition state optimizations



A structure to be a minimum on the potential energy surface means that any displacement of the structure will result in an increase in the potential energy. As a consequence, its second-derivative matrix is positive semi-definite (all eigenvalues are non-negative). On the other hand, first-order saddle points are characterized by behaving as a minimum with respect to all displacements of the structure except in a single direction. Displacement in this particular direction leads to a decrease in the potential energy and is associated with a single negative eigenvalue of the second-derivative matrix. By calculating the second-derivative matrix, we can determine whether a structure is a minimum, saddle point or otherwise.



Obtaining transition states can be done by a number of methods. For instance, eigenvector following (*EF*) method [41, 42, 43] attempts to maximize the energy along a given promising direction, while minimizing the energy along all other directions. Another very much used is the *STQN* method, developed by Peng and Schlegel [44, 45], It consists

in obtaining an estimate of the transition state from the known structures of reactants and products (QST2). An associated method allows the use of a custom guess for the transition state (QST3). The method is useful since i. knowledge of the transition state is optional, ii. it avoids calculating the second-derivative matrix for each step. The nudge-elastic band method is in the same vein as the *STQN* method, but attempts to minimize a discretized trajectory connecting reactants and products along the transition state, and can thus make use of information about this curve.

3.1.3 Prediction of kinetics and thermodynamics for chemical reactions

3.1.3.1 Transition state theory

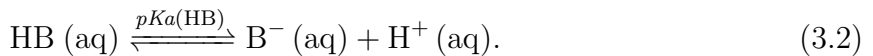
Transition state theory is based on the idea that the reactant ground state complex is in equilibrium with the transition state structure [46]. It is summarized by the Eyring equation.

3.1.4 When things go wrong: bulk effects

Here are some situations where predictions become poor due to the fact that our calculations are too small.

3.1.4.1 Determining pK_a s

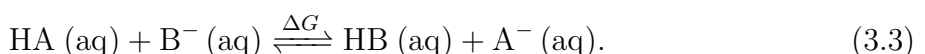
In the computational prediction of pK_a values, the direct dissociation approach (Equation (3.2)) leads to problems in the evaluation of the solvated proton, first because it is impossible to do electronic calculations for a zero-electron system [47, 48].



Second, due to the covalent nature of the interaction between the H^+ ion and the surrounding environment, which leads to the formation of clusters such as H_3O^+ , H_5O_2^+ , etc. [48].

One can employ the experimental proton solvation free energy ($-1104,5 \pm 0,3 \text{ kJ/mol}$ [49, 16]) in a semi-empirical fashion, but the trustworthiness of the results is still highly debated in the literature [50]. In fact, this often produces pK_a values that are far from the expected for simple carboxylic acids, for instance. Errors in the order of 7 pK_a units can be expected with this approach, as can be found in the literature [51, 47]. The major source of error can be attributed to the lack of explicit solute-solvent interactions [51].

A better approach is to use a relative determination method [47]. This avoids the problems associated with the direct dissociation approach by calculating the associated problem of proton exchange with a known reference acid, such as acetic acid [52]:



Since both sides of the Equation (3.3) have the same net charge and, hopefully both acid and conjugated base are, in general, of similar structure and size, favorable error cancelation is expected in the Gibbs free energy (ΔG). The $pK_a(\text{HA})$ can thus be written as a function of $pK_a(\text{HB, exp.})$:

$$pK_a(\text{HA}) = pK_a(\text{HB, exp.}) + \frac{\Delta G}{\ln(10)RT}. \quad (3.4)$$

It is customary that the error obtained by this method to be less than 1 pK_a unit for many solutes and solvents [47].

3.2 Chemical reaction mechanisms

Hypothetical reaction mechanisms consist of the interpretation of the available data for a chemical reaction in terms of a model that is self-consistent. Proposals for reaction mechanisms must be compared with each other and with the available experimental data. Many different hypotheses for the same reaction can exist, and, after pruning the ones in disagreement with the available data, it is still possible to have several different plausible models at hand. Computational modelling of chemical reactions provides one with a way of formulating, analyzing and comparing hypotheses to each other, to the literature and to the available experimental data. This way, one is able to come up with a “most probable” one.

3.2.1 Bell-Evans-Polanyi principle

The Bell-Evans-Polanyi (BEP) principle is a fundamental principle in the study of chemical reactions. It states that the more exothermic reactions usually have to overcome lower reaction barriers and are therefore faster.



It is customary to successfully extend this concept to exergonic reactions. But since the largest contribution is the electronic energy, it is reasonably safe to apply the BEP principle (and Hammer’s postulate, as we will see later) using electronic energies in the context of quantum chemistry calculations.

IN THE NOTES. CITATION.

3.2.2 Hammond’s postulate

IN THE NOTES. CITATION.

3.3 Intramolecular and substitutional effects: a key step to understand enzyme-like catalysis

Despite the great advancements in the developments of artificial enzymes [53], the synthetic reproduction of the reaction rate accelerations attained by natural enzymes is far from being reached. To get there, we will need a more detailed comprehension of the ways enzymes work at the molecular level [9]. Much effort has been put in this direction, with at least six Nobel Prizes awarded to this and related areas [54, 55, 56, 57, 58, 59]. These and other progresses show that the main source of acceleration in enzymatic reactions is to be found in the events that accompany the enzyme-substrate complex formation that leads to bond breaking and formation [9]. These events induce conformational changes in both substrate and enzyme, which enhances the interactions in the active site [60, 61, 62, 63, 64]. As a result, substrate active centers adequately orient themselves towards their counterparts in the active site, which leads to i. a decrease in stability of the ground state (if compared with the free substrate state), ii. a lowering of the transition state energy (if compared with the non-catalyzed reaction), iii. energy relaxation through the formation of intermediates and products.

These driving forces are also found in intramolecular reactions (Figure 1). In fact,

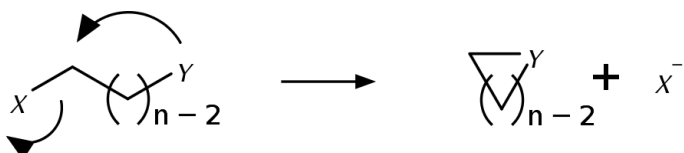


Figure 1 – Reaction scheme of a typical intramolecular reaction, whose products or intermediates are often cycles. Smaller rings ($n \leq 4$) tend to be disfavored by enthalpy, while larger rings ($n \geq 7$) have less probable formation due to entropy.

the similarities between monomolecular enzymatic processes and intramolecular reactions have been already recognized [65, 66, 67]. Despite the limitations of using intramolecular reactions as a model for enzymatic reactions, it is natural to suppose that the detailed understanding of enzyme catalysis has, as a prerequisite, the ability to understand the related processes in simpler systems. [68].

We have studied some of these effects.

Particular details concerning the intramolecular effects of geminal and vicinal disubstitutions can be found in Appendix C.

3.4 Automatic determination of kinetics using `overreact`

`overreact` is an open-source library, software package and command-line application for building and analyzing homogeneous microkinetic models from first-principles calculations [1, 2]. It propagates chemical reactions over time using only data available from computational chemistry calculations.

All differential equations are and their parameters are inferred from a reaction model and calculations provided by the user. Simultaneous reactions are easily solved, including parallel and concurrent reactions, pre-equilibration and even constant concentration reactants.

Furthermore, `overreact` is able to take most of the relevant physics of the problem into account in a semi-automated fashion. This includes concentration effects, symmetries, quantum tunneling, standard state corrections, implicit and explicit solvation, proper treatment of energy contributions and dispersion corrections. In most cases, in particular where solvation effects are weak, results matching experimental data are obtained.

It is open source¹, free of charge, available through the Python Package Index (PyPI) and is distributed under the MIT license. An online user manual is also available².

3.5 Thermochemical partition functions

It is possible to make use of computational calculations to obtain thermochemical data and, in particular, the thermochemical partition functions. This is routinely achieved by standard computational chemistry packages. This data can be used to estimate the thermodynamic properties of molecules and whole systems.

Não apenas seus autovalores nos permitem checar se uma otimização alcançou de fato um mínimo local, mas importantes funções de estado termodinâmicas são acessíveis através da matriz hessiana, valendo-se da aproximação QRRHO para gases ideais.

teoria do estado de transição [46].

3.6 Why predicting chemical reactions is hard

Perfect prediction of chemical reactions is an unforgiving problem. Since reaction rate constants depend exponentially on the activation Gibbs' free energy, small deviations on the latter exponentially increase errors on the latter. As such, given an activation energy

¹ Code is available at <<https://github.com/geem-lab/overreact-guide>>.

² The user guide can be found at <<https://geem-lab.github.io/overreact-guide/>>.

estimate ΔG^\ddagger on the true value $\widehat{\Delta G}^\ddagger$ with error ϵ ,

$$k = \kappa \frac{k_B T}{h} e^{\frac{-\Delta G^\ddagger}{RT}} = \kappa \frac{k_B T}{h} e^{\frac{-(\Delta \widehat{G}^\ddagger + \epsilon)}{RT}} = \widehat{k} e^{\frac{-\epsilon}{RT}} \quad (3.5)$$

where k and \widehat{k} are the predicted and true chemical reaction constants, respectively. Thus, at room temperature, an error of 1.36–2.73 kcal·mol⁻¹ gives rise to 10–100× error in the reaction rate constant, with larger errors found in lower temperatures. This is particularly important, as popular DFT methods commonly achieve accuracies of 2–3 kcal·mol⁻¹ for many molecules [69, 70]. Moreover, an error of 0.41 kcal·mol⁻¹ produces a twofold error in the constant. This goes to show that the so called “quantum chemical accuracy” of <1 kcal·mol⁻¹ [70] is not enough for the prediction of chemical reactions on par with experimental results. It goes without saying that this gives rise not only to a demand for more precise quantum chemical methods, but also for methods aiming at mitigating the effect of such errors in computational predictions of chemical reactions.

One might go one step further and investigate how this error in the reaction rate constant is related to individual errors in activation enthalpy and entropy errors.

$$k = \kappa \frac{k_B T}{h} e^{\frac{-\Delta H^\ddagger}{RT}} e^{\frac{\Delta S^\ddagger}{R}} = \kappa \frac{k_B T}{h} e^{\frac{-(\Delta \widehat{H}^\ddagger + \chi)}{RT}} e^{\frac{(\Delta \widehat{S}^\ddagger + \sigma)}{R}} = \widehat{k} e^{\frac{-\chi}{RT}} e^{\frac{\sigma}{R}} \quad (3.6)$$

The above suggests that, all things equal, errors in the predicted activation entropy dominate at high temperatures, while being less significant than activation enthalpy errors at low temperatures. The balance between the two will on the other hand depend on the actual reaction at hand.

3.7 “First-principle” calculations

Strictly speaking, computational first-principle calculations encompass methodologies that do not use experimental data either in their development or application. Broadly speaking, the first-principle calculations can be referred to wavefunction or density-functional theory (DFT) calculations.

Os perfis reacionais resultantes são suficientes para a predição de parâmetros cinéticos e termodinâmicos das reações, que foram comparados aos resultados disponíveis na literatura.

3.7.1 Quantum tunneling effects

Hydrogen abstraction reactions (HAA) comprise a class of reactions where quantum tunneling is often very important [71]. A particular group therein is the homolysis of C–H bonds by strong oxidants, which oftentimes the rate-limiting step in many transformations, and a particularly key step in the substrate activation by numerous metalloenzymes [71].

3.8 Microkinetic modelling

Microkinetic modelling is a technique used to predict the outcome of complex chemical reactions. It can be used to investigate the catalytic transformations of molecules by propagating a system of ordinary differential equations modelling the chemical reactions.

The technique can be made first-principle by making use of pure computational chemistry predictions. It is able to take into account effects that sole use of Gibbs' free energies are not able to, such as concentrations of species and complex time dynamics.

3.8.1 Design

`overreact` is a second iteration on an earlier attempt to build a homogeneous microkinetic analyzer from first-principles calculations [72]. Some things were learned from that first attempt: i. data is relatively easy to obtain from computational chemistry calculations, but it is not always in its optimal form; ii. solving differential equations is relatively easy in general, but hard to make it work for a wide range of problems mostly due to stiffness of the equations; iii. transforming knowledge about chemical structures into knowledge about the chemical reactions is hard to be done in an automated fashion; iv. having a good pipeline for data processing makes it easy to add new features to the system.

3.8.2 Automatic differentiation

Instead of employing numerical differentiation, whose precision depends on the particular step size, automatic differentiation can be used to produce analytical derivatives in a precise, efficient and automated way.

One conceptually simple way of doing this is by *forward differentiation* through dual numbers, where the real values are extended by an infinitesimal part in a trick that is not far from the concept of imaginary numbers. The pair of numbers can be added component-wise, and form a commutative algebra by making use of a simple multiplication rule that follows from the property $\epsilon^2 = 0$:

$$(a, b) * (c, d) \equiv (a + b\epsilon)(c + d\epsilon) = ac + (ad + bc)\epsilon \equiv (ac, ad + bc) \quad (3.7)$$

It is not hard to show that, by extending the domain of any real polynomial to dual numbers, one obtains

$$P((a, b)) \equiv P(a + b\epsilon) = P(a) + bP'(a)\epsilon \quad (3.8)$$

where $P'(a)$ is the *analytic* derivative of $P(a)$.

`overreact` employs a slightly more complex scheme called *backward differentiation*, available through Google's JAX library, that is more efficient for functions of many variables.

The main problem with this section of computational methodologies and models is the la

Part II

Publications

The present part presents contributed works, co-authored by me during the course of my PhD at the Federal University of Santa Catarina, to the field of computational elucidation of reaction mechanisms.

Other papers (and open-source software) not relevant or only tangentially related to the field can be found in the Appendix A.

3.9 Contributions to the computational elucidation of reaction mechanisms

3.9.1 Minor contributions

The following papers were co-authored by me and were published during my time as a PhD student, but in my view constitute only minor contributions and will thus only be mentioned in the present thesis.

- GROSS, I. P. et al. Polylactic acid, maleic anhydride and dicumyl peroxide: Nmr study of the free-radical melt reaction product. *Polymer Degradation and Stability*, Elsevier BV, v. 155, p. 1–8, Sep 2018. ISSN 0141-3910. Disponível em: <<http://dx.doi.org/10.1016/j.polymdegradstab.2018.06.016>>.
- SCHNEIDER, F. S. et al. A theoretical investigation on the aminolysis of pyromellitic and 1,4,5,8-naphthalenetetracarboxylic dianhydrides. *Computational and Theoretical Chemistry*, Elsevier BV, v. 1147, p. 13–19, Jan 2019. ISSN 2210-271x. Disponível em: <<http://dx.doi.org/10.1016/j.comptc.2018.11.008>>.
- ALMERINDO, G. I. et al. Kinetics and adsorption calculations: insights into the mgo-catalyzed detoxification of simulants of organophosphorus biocides. *Journal of Materials Chemistry A*, Royal Society of Chemistry (RSC), v. 8, n. 36, p. 19011–19021, 2020. ISSN 2050-7496. Disponível em: <<http://dx.doi.org/10.1039/C9TA14028J>>.

3.9.2 Major contributions

The rest of this part presents papers that I co-authored, were published as part of my PhD (after March 2017) and, in my view, constitute major contributions to the field.

4 Paper I: Mechanism of Pd(II)-mediated uncaging reactions of propargylic substrates

COELHO, S. E. et al. Mechanism of palladium(ii)-mediated uncaging reactions of propargylic substrates. *ACS Catalysis*, American Chemical Society (ACS), v. 9, n. 5, p. 3792–3799, Mar 2019. ISSN 2155-5435. Disponível em: <<http://dx.doi.org/10.1021/acscatal.9b00210>>.



In order to develop better C–O bond cleavage promoters, recently, bioorthogonal approaches have been devised to promote C–O bond cleavage by transition metals for uncaging protected molecules, normally with hydroxyl and amino functional groups. Palladium (II) has been extensively used for such biocompatible processes. Uncaging of propargyl groups has remained challenging. This reaction has been added to the bioorthogonal arsenal of chemical biology and medicinal chemistry for activating bio and prodrug molecules recently.

It is normally assumed that the process goes through *in situ* formation of catalytic Pd(0), promoted by a base through intramolecular ligand exchange reduction or nucleophilic attack by the solvent and then suffering reductive elimination. This Pd(0) could then undergo oxidative addition with the propargyl group, producing an allenylpalladium intermediate, which is then hydrolyzed, regenerating the Pd(0) and producing acetol as the side product. A less common hypothetical alternative is the Pd(II)-mediated hydration mechanism to form an intermediate that then decomposes by hydrolisys (Wacker-like oxidation WHAT IS THIS).

In this work, we attempted to unveil through which mechanism does the Palladium(II)-mediated chemical uncaging reaction of propargyl-protected hydroxyl groups takes place. The reactions were monitored in the lab by UV-vis spectroscopy and a deviation from first-order kinetics was observed. A distinct biexponential shape was found, consistent with biphasic kinetics, which produce the same product (DNP) at different reaction rates. The fastest reaction has a half-life of 1 hour, and was found to be around 15 times faster than the other, and 650 times faster than the uncatalyzed one.

It was observed that the fast phase was responsible for only two turnovers, which indicates that, although faster, it shuts down after two turnovers. Further experiments evidenced that the catalyst may not be stable and is changing through the course of the reaction, changing its activity. Furthermore, neither DNP or acetol seem to inhibit the

reaction.

With the XAS results, we proceeded to perform computational studies. We employed the $[\text{PdCl}_4]_2^-$ complex as the catalyst species, and chose a model substrate methyl-propargyl ether to simplify calculations. We employed an implicit solvation model in water, and used two explicit extra water molecules to consider the effect of hydrogen bonding, one interacting with the enol part and the other with the leaving group. We used PBE0 to obtain geometries and frequencies, and adjusted the electronic energy with DLPNO-CCSD(T) and HF-gCP to correct for basis set artifacts.

We found out that both Markovnikov and anti-Markovnikov regiochemical hydrations of the Pd-propargyl complex to form enols are competitive and within the method's error ($< 1 \text{ kcal}\cdot\text{mol}^{-1}$).

Our evidence suggested that the reaction proceeds through biphasic kinetics with different rates, where the most favorable path involves a Pd(II) anti-Markovnikov hydration of the propargyl group, followed by C-O bond breaking by β -O elimination. The process lasts two turnovers as the product inhibits further reactivity.

An application to metallocatalysis [3]. A computational-experimental collaboration.

4.1 Paper

The publication can be read in full next.

Mechanism of Palladium(II)-Mediated Uncaging Reactions of Propargylic Substrates

Sara E. Coelho,^{†,‡} Felipe S. S. Schneider,^{†,‡} Daniela C. de Oliveira,[‡] Guilherme L. Tripodi,[§] Marcos N. Eberlin,[§] Giovanni F. Caramori,^{†,‡} Bernardo de Souza,[†] and Josiel B. Domingos^{*,†,‡}

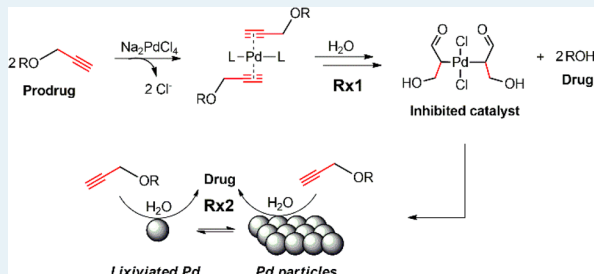
[†]Department of Chemistry, Federal University of Santa Catarina - UFSC, Campus Trindade, C.P. 476, Florianópolis, Santa Catarina 88040-900, Brazil

[‡]Brazilian Synchrotron Light Laboratory, LNLS, C.P. 6192, Campinas, São Paulo 13083-970, Brazil

[§]Thomson Mass Spectrometry Laboratory, University of Campinas-UNICAMP, Campinas, São Paulo 13083-872, Brazil

Supporting Information

ABSTRACT: The palladium(II)-mediated chemical uncaging reaction of propargylic substrates is a recent addition to the field of chemical biology and medicinal chemistry in the activation of bio and prodrug molecules. Most of the strategies used involve C–O bond breaking in molecules bearing protected amino and hydroxyl groups. Although this reaction has been known for many decades, its catalytic cycle in aqueous milieu remains unclear. Our mechanistic investigation results unveil that full propargylic substrate conversion occurs through biphasic kinetics of different rates, where the fastest reaction phase involves a Pd(II) anti-Markovnikov hydration of the propargyl moiety, followed by the C–O bond breaking through a β -O elimination and lasts only for two turnovers due to product inhibition. The second slower reaction phase involves the hydrolysis of the substrate promoted by Pd(0) species formed during the first phase of the reaction. These findings are crucial for the potential development of bioorthogonal Pd catalysts for the uncaging of propargylic protected bioactive and drugs molecules.



KEYWORDS: depropargylation reaction, palladium, mechanism, catalysis, hydrolysis

1. INTRODUCTION

The promotion of C–O bond cleavage by transition metals is one of the key strategies recently described for uncaging protected molecules possessing hydroxyl and amino functional groups under biocompatible conditions, extra- or intracellularly.^{1,2} In particular, palladium-mediated bond-cleavage reactions have gained great interest owing to their unique catalytic properties.^{3–8} Cell-surface engineering⁹ and protein^{10,11} and prodrug^{5,12–15} activation outside or inside living cells, through the C–O bond cleavage of propargylic ethers, carbamates, and carbonates (Figure 1a), are examples of the recent applications of palladium-mediated uncaging reactions, taking advantage of a bioorthogonal approach.^{16,17} Although it has been argued that carbamate groups are not truly bioorthogonal because they can be deprotected in vivo through the reaction with various nucleophiles and digestive enzymes, propargylic amines and ethers, while less reactive, are more suitable for in vivo applications.¹⁸ Deallylation reactions are also a common strategy, although they are less efficient with simple palladium catalysts than depropargylation.¹⁰ Whereas the mediation of dealylation by Pd(0) through a π -allylpalladium mechanism is well established,¹⁹ the Pd-mediated depropargylation reaction mechanism remains challenging in the current stage, and no systematic mechanistic

studies have been performed.¹⁶ However, it has been most frequently postulated that even when the initial forms of the catalyst are simple Pd(II) salts, the depropargylation reaction mechanism involves the in situ formation of the catalytic species Pd(0). This process is normally assumed to be promoted by a base through an intramolecular ligand exchange reduction or by an attack of a nucleophilic solvent, followed by a reductive elimination pathway.^{10–13,16,20–23} The Pd(0) is then assumed to undergo an oxidative addition with the propargyl group to form an allenylpalladium intermediate, which can be hydrolyzed to produce acetol as a side product and to regenerate the Pd(0) (pathway (i), Figure 1b). The less common hypothesis is a Pd(II)-mediated hydration mechanism (pathway (ii)) to form an intermediate that can decompose to form Pd(II) by hydrolysis (iii) in a Wacker-like oxidation.^{10,16,24}

However, these uncaging reactions are reported to be relatively slow and present low product yields, requiring high doses of catalyst. The catalyst solubility and toxicity therefore need to be considered when designing a bioorthogonal

Received: January 16, 2019

Revised: February 28, 2019

Published: March 21, 2019

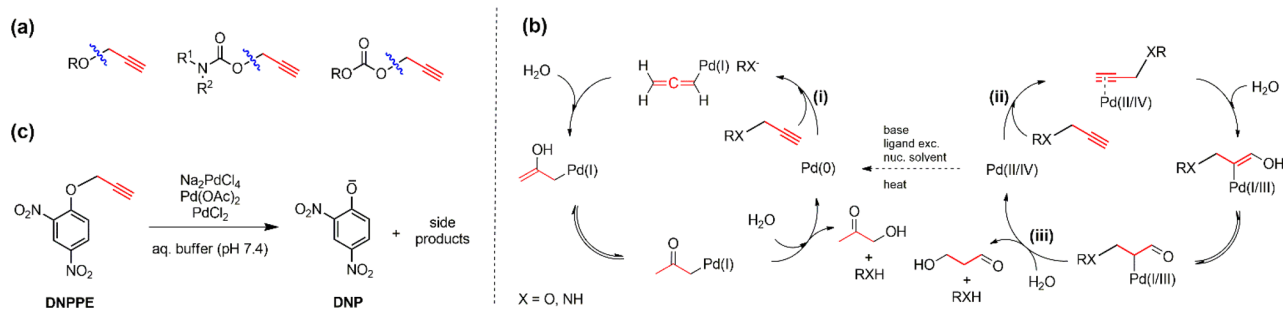


Figure 1. (a) Representative examples of C–O bond cleavage of propargyl protected hydroxyl and amino groups. (b) As suggested in the literature, the mechanism for the depropargylation reaction is mediated by Pd(0)[†] (pathway i) and Pd(II/IV) (pathway ii). (c) Proposed model reaction for the mechanistic studies in this work: prodrug DNPPE uncaging reaction in a phosphate-buffered aqueous medium (pH 7.4) mediated by simple Pd(II) salts.

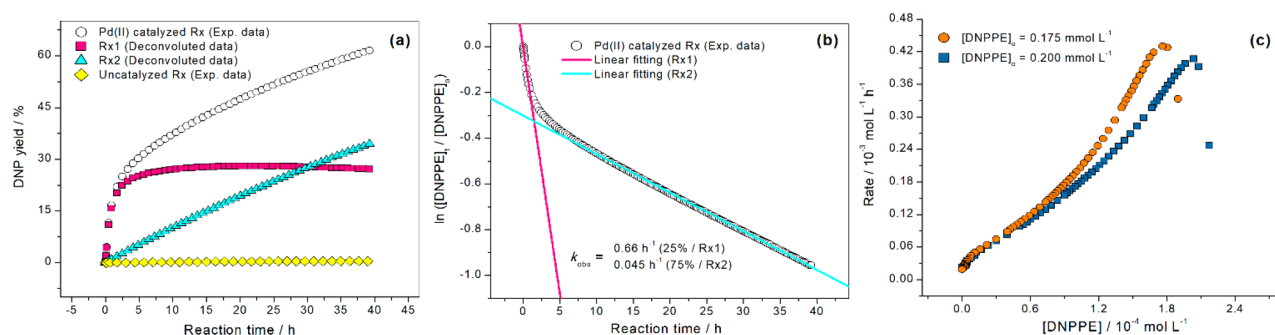


Figure 2. (a) Kinetics profiles of product conversion. (b) Natural log of the normalized experimental kinetic data for the DNPPE depropargylation reaction. (c) RPKA of on-cycle catalyst stability during the conversion of DNPPE (experiment 1: $[DNPPE]_0 = 0.2 \text{ mmol L}^{-1}$, $[Pd]_0 = 0.05 \text{ mmol L}^{-1}$ and experiment 2: $[DNPPE]_0 = 0.175 \text{ mmol L}^{-1}$, $[Pd]_0 = 0.05 \text{ mmol L}^{-1}$).

protocol.²⁵ Thus rational designs of highly elaborate transition-metal catalysts for uncaging reactions will rely on the understanding of fundamental organometallic mechanistic pathways, which can be achieved via both experiments and theoretical calculations to determine the coordination and reaction behavior of reactive intermediates.²⁶

In this article, we investigated the mechanism of the C–O bond-cleavage reaction of propargyl protected hydroxyl groups, triggered by the addition of simple Pd(II) salts (Na_2PdCl_4 , $\text{Pd}(\text{OAc})_2$, and PdCl_2), without the addition of base or ligands, in phosphate-buffered aqueous medium (pH 7.4). The prodrug compound 2,4-dinitrophenyl propargyl ether (DNPPE) was chosen as a model substrate for these studies (Figure 1c). DNPPE is a caged protonophore that becomes an active mitochondrial uncoupler (DNP)²⁷ after the removal of the propargyl protecting group. DNP is a widely studied pharmacological uncoupling agent used in experimental models of neurodegenerative conditions.^{28–30} Moreover, DNP is a tyrosine analogue, a catalytic residue present in many enzymes, and consequently a model compound for the bioconjugation of proteins.^{11,31} Also, the deprotection yield of DNPPE can be linked directly to UV–vis spectroscopy readouts, which offers a simple approach for an assessment of the reaction progress.

2. RESULTS AND DISCUSSION

In phosphate-buffered aqueous medium (pH 7.4), the reactions mediated by the Pd(II) salts were monitored by UV–vis spectroscopy through the appearance of the product DNP at a wavelength of 400 nm (Figure S1). For all Pd(II)

salts, a deviation from the first-order kinetics was observed (open circles, Figure 2a, for the reaction mediated by Na_2PdCl_4 and Figure S2 for the other salts). The distinct biexponential shape of the curve is not consistent with a simple reaction mechanism. Indeed, these profiles were typical of biphasic kinetics, producing the same product (DNP) at different rates (eq 1).^{32,33} The linear fit of eq 1 enabled the determination of two observed macroscopic rate constants (k_1 and k_2 , Figure 2b).

$$\frac{[\text{DNPPE}]_t}{[\text{DNPPE}]_0} = F^0 e^{-k_1 t} + S^0 e^{-k_2 t} \quad (1)$$

The yield magnitudes of the fast (k_1) and slow (k_2) phases are denoted by F^0 (25%) and S^0 (75%), respectively. On the basis of these macroscopic rate constants, the evolution of the DNP product was deconvoluted into two reaction kinetics profiles (Figure 2a, red squares and blue triangles for the fast and slow phases, respectively), namely, Rx1 and Rx2, respectively. It can be observed that Rx1 was ~15 times faster than Rx2 ($k = 0.66$ and 0.045 h^{-1} , respectively) and ~650 times faster than the uncatalyzed reaction ($k_{\text{unc}} = 1.02 \times 10^{-3} \text{ h}^{-1}$) under the same conditions. The half life for Rx1 is ~1 h, which makes this reaction feasible for bioorthogonal applications.³⁴

It is important to note that the fast phase (Rx1) is responsible for the conversion of ~20 mol % into the product DNP, that is, only two turnovers (Figure S3). Mechanistically, this information shows that although Rx1 is faster than Rx2, it shuts down after two turnovers. In fact, sequential addition of the catalyst after different reaction times leads to a sharp increase in the DNP production, which also lasts for around

two turnovers (Figure S4). We found this to be very important because for many of the Pd catalysts reported herein, the reaction was monitored during a short period, and the turnover, especially intracellularly, was not properly established.¹⁷

For a single-substrate catalytic cleavage reaction, a biphasic time course is consistent with a change in mechanism owed to a change in the activity of the catalyst. Thus an experiment by reaction progress kinetic analysis (RPKA) was performed to establish catalyst stability over the entire reaction course. RPKA can suggest a few initial sets of experiments to find any evidence of catalyst deactivation or product inhibition.³⁵ Therefore, two reactions initiated with different initial concentrations of DNPPE and the same catalyst concentration should display identical rate versus substrate concentration profiles in the absence of catalyst deactivation or product inhibition processes. Consequently, two reactions were performed: experiment 1 with $[DNPPE]_0 = 0.2 \text{ mmol L}^{-1}$ and experiment 2 with $[DNPPE]_0 = 0.175 \text{ mmol L}^{-1}$ (Figure 2c). Figure 2c shows an unmatched rate behavior through the graphical overlay, suggesting that $[Pd]$ is unequal for both experiments. These results indicate that the catalyst is not stable, which is further supported by later experiments revealing that the catalyst is changing to accommodate a switch in the mechanism. Moreover, further kinetic experiments adding DNP or acetol (the most frequently reported byproduct for this reaction) to the reaction medium show that neither affects the reaction profile (Figure S5). Thus a possible inhibition due the presence of DNP or possibly acetol products is ruled out.

Other parameters can also influence the reaction rate; for instance, increasing the Pd concentration from 2 to 12 mol % of Pd(II) resulted in an increase in the reaction rate by factors of 10 for Rx1 and 45 for Rx2 (Figure S6). The nonlinear response of Rx1/Rx2 reaction rates with changes in Pd concentration suggests a different nuclearity in the catalyst for these two processes. The phosphate buffer concentration also altered the reaction rate for Rx1, with a decrease observed from 0.01 to 0.15 mol L⁻¹, but it had no effect in the case of Rx2 (Figure S7). The amount of cosolvent DMSO affected the reaction rate as well; an increase from 10 to 50% of DMSO almost completely inhibited both reactions (Figure S8). This is important because DMSO is by far the most common cosolvent used in these reactions for substrate solubilization in aqueous solution *in vitro* or *in vivo* experiments. Because of the known coordination capabilities of phosphate and DMSO toward transition metals, the concentrated buffer and cosolvent are probably inhibiting the reaction through complexation with the catalytic species. The stronger inhibition effect of the buffer in the case of Rx1 shows that the Pd species involved in this reaction is a more labile one.

As discussed before, the most general assumption in the literature is that this reaction mechanism occurs via oxidative addition of the propargyl C–O bond to Pd(0) (Figure 1b, pathway i). Thus to investigate the true nature of the catalytic species, we tested the hypothesis that the involvement of Pd(0) formed spontaneously from the reduction of Pd(II) in the reaction medium. First, we performed X-ray absorption spectroscopy (XAS) analysis of the reaction medium after 3 h under the same conditions used during the standard reaction (buffered aqueous medium, pH 7.4, at 48 °C) but without the addition of substrate. The Na₂PdCl₄ salt was chosen due to its higher solubility in water, and the XAS data were collected on a

synchrotron-based setup in transmission mode at the Pd–K edge (24.35 keV). (See the Supporting Information for details of the XAS setup.) As shown in Figure S9, the extended X-ray absorption fine structure (EXAFS) fitting results show an intense Pd(II)–Cl bond signal and the absence of the Pd(0)–Pd(0) or Pd(II)–O bond signals, which would be observed if Pd(0) species or Pd(II) hydrolysis products had been formed in the reaction medium during the 3 h of the experiment.^{36,37} It is clear from these results that under these reaction conditions, no Pd(0) is spontaneously formed, but we do not rule out the possible formation of Pd(0) in the presence of the substrate, for example, due to a Wacker-type reaction. The nature of the catalysts in the presence of substrate was not investigated by XAS due to the low solubility of DNPPE.

Thus two mechanistic scenarios could possibly act in the faster kinetic phase. If Pd(0) was somehow formed in the presence of substrate, then the reaction would occur via an oxidative addition at the propargyl group, or the other scenario would be a hydration of the propargyl group coordinated to a Pd(II) (Figure 1b, pathways i and ii, respectively). To distinguish between these possible pathways, we have performed a kinetic experiment adding CS₂ at 0 h and after 2 h of reaction time. CS₂ acts as a catalyst poison for homogeneous and heterogeneous Pd(0) catalysts at temperatures below 50 °C, whereas Pd(II) species are unaffected.³⁸ As shown in Figure S10, the initial reaction rate for the faster phase in all cases is similar. This result indicates that there is no participation of Pd(0) species in the faster phase (Rx1). On the contrary, the slower phase (Rx2) rate has been intensely affected by the addition of CS₂, most probably due the participation of Pd(0) in this reaction phase.

Continuing with the aim to unveil the nature of the catalytic species, high-resolution electrospray ionization mass spectrometry (ESI–HRMS) was used to monitor the reaction and possible detection of key reaction intermediates.^{39–42} ESI is a soft ionization technique that can be used to analyze both cations and anions, displays high sensitivity, and allows the immediate transfer to the gas phase of most ionic species present in the reaction solution. Working in negative ion mode, the *in situ* ESI(–)–HRMS monitoring of the reaction, with 20 mol % of Na₂PdCl₄ in phosphate-buffered aqueous solution pH 7.4 (5% DMSO) provided 10 min after the start of the reaction, identified the following proposed species: the product DNP (*m/z* = 183) as the major species (Figure 3a) and three other Pd species interacting with the substrate at *m/z* 434.8, 416.9, and 638.9 (Figure 3b–d). The species at *m/z* 434.8 (1, Figure 3b) is a π complex of PdCl₃ with DNPPE, and the Pd signal at *m/z* 416.9 may be one of the several possible carbopalladate isomers formed from the hydration (Markovnikov or anti-Markovnikov) of the π complex [DNPPE–PdCl₃] (2, Figure 3c). We shall see later that computational calculations revealed that the ketone isomer is more stable (~16 kcal mol⁻¹).

The third species identified is a hydrolyzed (Markovnikov or anti-Markovnikov) carbopalladate intermediate complexed with another DNPPE molecule through a π interaction (3, Figure 3d). The agreement between the experimental and calculated (Figure S11) isotopologue patterns and exact masses corroborates the proposed structures and elemental compositions. Moreover, the ESI–HRMS analysis after 35 min of reaction shows that species 1 and 2 are still present, but after 120 min, only the DNP product can be observed. In addition, the analysis of a precipitate formed after 35 min of reaction

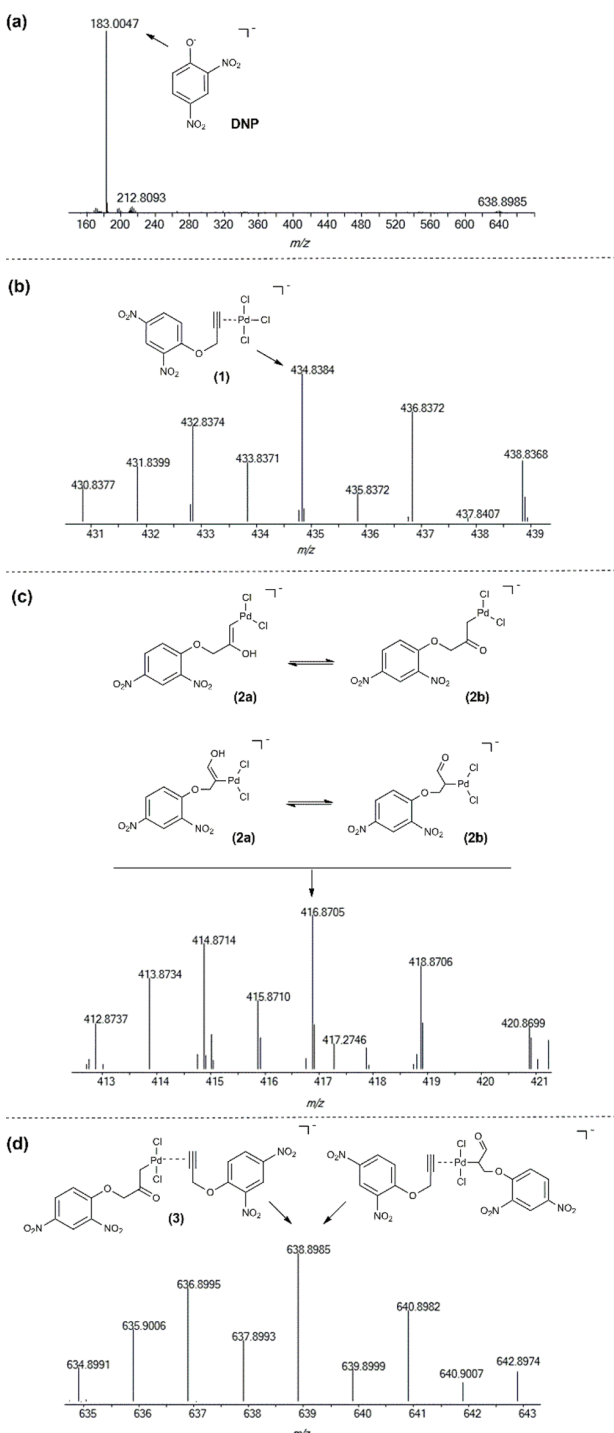


Figure 3. ESI($-$)-HRMS of the reaction medium 10 min after the start of the DNPPE depropargylation reaction. The ions at m/z 434.8 (b), m/z 416.9 (c), and m/z 638.9 (d) were detected in lower abundance compared with the product ion DNP (a), so the spectral regions of interest were amplified ($[DNPPE] = 2.12 \text{ mmol L}^{-1}$, $[\text{Na}_2\text{PdCl}_4] = 20 \text{ mol \%}$, in H_2O (5% DMSO), pH 7.4 at 48 °C).

also identified an ion at m/z 473 (Figure S12), corresponding to another hydrolyzed carbopalladate intermediate. Ion 3 was then further characterized by ESI collision-induced dissociation tandem mass spectrometry (ESI-CID-MS/MS). The

observed fragmentation pathways of these reaction intermediates reflect their intrinsic reactivity and support the proposed structures of 3. (See Figure S13 for further discussion.)

These species identified by ESI-HRMS, together with the results from the kinetic studies, align more with an alkyne hydration pathway than with an oxidative addition pathway, at least for the initial part of the reaction, that is, for the faster reaction phase. To explore the details of the fast Rx1 and possibly exploit it in the future, we also performed computational studies. On the basis of the XAS results, the complex $[\text{PdCl}_4]^{2-}$ was used as the catalyst species, and we chose the model substrate methyl-propargyl ether to simplify the calculations. All simulations were performed with an implicit solvent model, and we added two extra water molecules to consider the effect of explicit solvation, one interacting with the enol part and the other interacting with the leaving group. Geometries and frequencies were calculated with the functional PBE0,⁴³ and, to obtain very accurate energetics, DLPNO-CCSD(T)⁴⁴ was used to compute the energies, and the HF-gCP⁴⁵ correction was added to minimize basis set artifacts.

Surprisingly, the energy difference between the Markovnikov and anti-Markovnikov regiochemical hydrations of the Pd-propargyl complex to form enols is low (<1 kcal mol⁻¹), falling within the error of the method (Figure S14). Thus both pathways to product formation were explored. After the formation of the enol, a tautomerization can occur (also suggested by ESI-HRMS, Figure 3c), and we found that keto tautomers are the most stable. Next, we searched for the C–O bond break step for both regiochemical keto tautomer intermediates. For the anti-Markovnikov keto intermediate (\mathbf{C}_2 , Figure S14), the first-expected S_N^2 -like hydrolysis is not much faster than the uncatalyzed reaction, with the transition state being stabilized by only ca. 8 kcal mol⁻¹. We then searched for other mechanistic pathways, such as an intramolecular attack of the oxygen ($\Delta G^\ddagger = 58.7 \text{ kcal mol}^{-1}$), β -H elimination of Pd, followed by hydrolysis (this pathway was discarded due to the high acidity of methylene H) and concluded that a β -O elimination mechanism was most likely, with the C–O bond breaking prior to a subsequent attack of water ($\Delta G^\ddagger = 38 \text{ kcal mol}^{-1}$). For the Markovnikov keto intermediate (\mathbf{C}_2' , Figure S14), the S_N^2 -like hydrolysis presented much higher activation energy ($\Delta G^\ddagger = 54.02 \text{ kcal mol}^{-1}$) than the β -O elimination of the anti-Markovnikov keto intermediate. The complete calculation for the first reaction turnover of the main mechanism is depicted in Figure 4.

Thus we propose that the most probable operating reaction pathway for Rx1 involves the coordination of DNPPE molecules to Pd(II), followed by an anti-Markovnikov attack of water molecules at the propargyl moiety, prior to the C–O bond breaking by β -O elimination and hydration (Figure 5). The proposed pathways for Rx1 shown in Figure 5 involve the stepwise C–O bond cleavages ($2 \rightarrow 4 \rightarrow 5 \rightarrow 6 \rightarrow 7 \rightarrow 8$). In this scenario, the final products are two equivalents of DNP and the bis(1-hydroxy-3-oxopropyl)palladium(II) chloride, the carbopalladate complex 8. Although the formation of 8 could not be confirmed by analytical tools such as ESI-HRMS or even by H^1 NMR (Figure S15), its existence is supported by the detection of only two turnovers during Rx1 because the binding of a third DNPPE molecule is less likely due to steric hindrance.

The K_{eq} values calculated for two insertions of the propargyl ether substrate are 4.9×10^{-4} for the first and 6.3×10^{-4} for

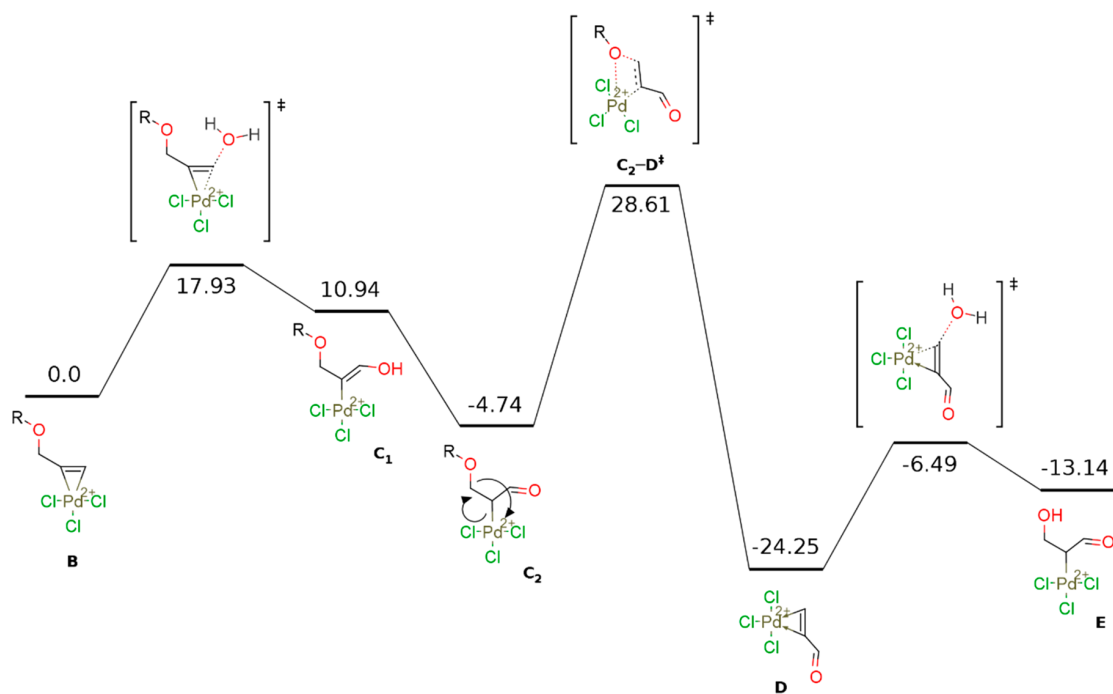


Figure 4. Energy profile (kcal mol^{-1}) calculated for the first turnover of the depropargylation reaction catalyzed by $[\text{PdCl}_4]^{2-}$ in water.

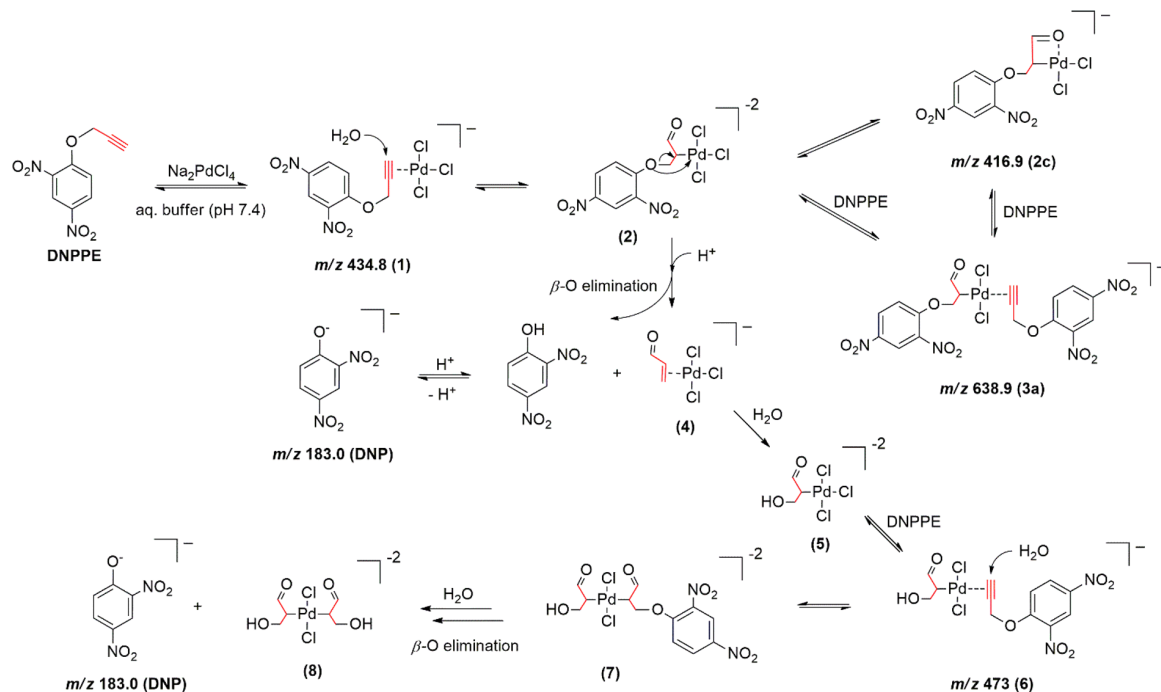


Figure 5. Proposed pathways for Rx1 in the depropargylation reaction of DNPPE mediated by Pd(II) salts.

the second insertion, but the binding of a third molecule, displacing a chloride, has a constant of 7.6×10^{-8} (Figure S14) and probably does not happen at all; in this case, complex 8 can be considered a product-inhibited Pd catalyst. Indeed, when 50 mol % of Pd is used, the quantitative formation of DNP is reached in <2 h in a monophasic first-order kinetic profile (Figure S16) for all three Pd(II) salts used in this study. As can be seen, the role of the metal in this first step is two-

fold: It facilitates the hydration of the triplet bond and stabilizes the keto tautomer intermediate during the C–O bond breaking. We assume that when a second substrate is coordinated, the same hydrolytic mechanism is followed.

To test the hypothesis of complex 8 formation, we added propargyl alcohol in the reaction medium and waited for 2 h before the addition of the substrate. The idea is that under this time, the propargyl alcohol, complexed with Pd(II), would be

hydrolyzed and inhibit further complexation of DNPPE molecules. In fact, as shown in Figure S17, Rx1 was much slower with the addition of propargyl alcohol. This result corroborates the proposed mechanism for Rx1.

On the basis of the kinetic evidence and poisoning studies (see below), it is more likely that after these first two turnovers, Rx2 is undergoing a different mechanism. When the reaction was performed with a higher substrate concentration, a dark precipitate was observed after the reaction completion. This precipitate was analyzed by transmission electron microscopy (Figure S18) and synchrotron-based X-ray absorption spectroscopy (XANES/EXAFS) (Figure S19). These experiments revealed the presence of 5 nm Pd nanoparticles (Pd NPs) and palladium with a mixed oxidation state. (See the Supporting Information for further details and discussion.) The reaction was then monitored by dynamic light scattering (DLS, Figure S20), and the presence of nanoparticles (hydrodynamic ratio between 8 and 15 nm) was observed beginning at 5 min of reaction, although in very low concentration.

These observations motivated us to perform further poisoning experiments to determine the catalytically active species for Rx2. Figure S21 shows the reaction kinetic profiles with CS_2 and $\text{Hg}(0)$ added after 120 min of reaction compared with the reactions without the additives. As discussed before, CS_2 acts as a catalyst poison for homogeneous and heterogeneous catalysts,³⁸ whereas $\text{Hg}(0)$ poisons metal-particle heterogeneous catalysts by amalgamating the metal or adsorbing onto the metal surface, especially palladium, with homogeneous complexes remaining unaffected.⁴⁶ The addition of CS_2 completely inhibits the catalytic activity of Rx2, but the presence of mercury inhibits the DNP formation by ~60%. These results indicate that the catalytic activity of the slower phase of the reaction (Rx2) is mainly a result of Pd(0) NPs formed during the reaction or lixiviated Pd(0) atoms from the NPs (Figure 6); the formation of these Pd(0) species from the Pd(II) complex 8 may explain why this product has not been detect by any analytical tools employed. In fact, when the reaction was performed in the presence of as-synthesized Pd(0) NPs, the reaction was extremely slow (Figure S22), supporting the nature of the Rx2 phase of the reaction.

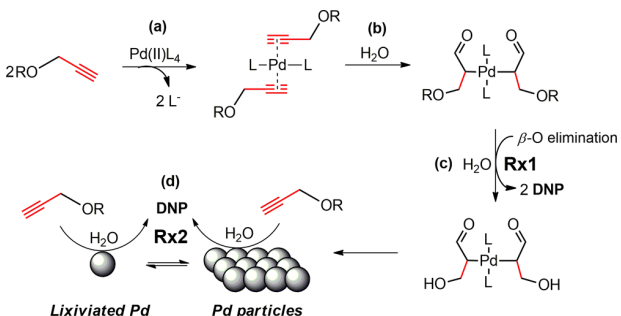


Figure 6. Pd(II) catalytic fate in the DNPPE O-depropargylation reaction. The full substrate conversion is a consequence of two different catalytic cycles: (i) Two equivalents of substrate are converted in a fast reaction, where the initial step is a ligand exchange (a), followed by hydration of the triple bond (b) and C–O bond cleavage by β -O elimination, followed by hydration (c). (ii) The second and less effective cycle might be the result of a Pd(0) nanoparticles/lixiviated catalytic species formed after the first cycle (d). L = ligand (e.g., Cl^- and AcO^-). R = 2,4-dinitrophenyl group.

3. CONCLUSIONS

We have shown that simple Pd(II) salts can effectively act as catalysts for the O-depropargylation reaction under biocompatible conditions, but the reaction is biphasic, presenting a fast and a slow phase, revealing that the catalyst is changing to accommodate a switch in the mechanism. The faster phase ends after two turnovers due to product inhibition. This explains the frequently reported need for high doses of these catalysts for a fast full conversion of the substrate. The mechanism for the faster phase involves key intermediates where the Pd(II) is inserted with anti-Markovnikov orientation at the propargyl moiety prior to the C–O bond cleavage by a β -O elimination, as suggested by theoretical modeling, whereas the slow phase involves the hydrolysis of the substrate promoted by Pd(0) species formed during the first phase of the reaction. These findings will help to design and control the selective reactivity of new palladium catalysts for uncaging reactions of O-propargyl substrates, especially discrete Pd complexes.⁴⁷ For example, we envision that Pd complexes with bulky ligands may be a better choice for this reaction because the expulsion of the reaction product can be tuned by the steric bulkiness of the ligands, avoiding the inhibition of the catalyst by the reaction product derived from the propargyl moiety. These studies are currently underway in our laboratory.

■ ASSOCIATED CONTENT

Supporting Information

The Supporting Information is available free of charge on the ACS Publications website at DOI: [10.1021/acscatal.9b00210](https://doi.org/10.1021/acscatal.9b00210).

Detailed experimental procedures, reaction kinetics profiles, and spectroscopic analysis ([PDF](#))

■ AUTHOR INFORMATION

Corresponding Author

*E-mail: josiel.domingos@ufsc.br.

ORCID

Sara E. Coelho: [0000-0001-9145-5657](https://orcid.org/0000-0001-9145-5657)

Felipe S. S. Schneider: [0000-0001-8090-2976](https://orcid.org/0000-0001-8090-2976)

Giovanni F. Caramori: [0000-0002-6455-7831](https://orcid.org/0000-0002-6455-7831)

Josiel B. Domingos: [0000-0002-6001-4522](https://orcid.org/0000-0002-6001-4522)

Notes

The authors declare no competing financial interest.

■ ACKNOWLEDGMENTS

We are grateful to CNPq and CAPES for the financial support received for this study. We also thank the Brazilian Synchrotron Light Laboratory (LNLS) team for XAS experiments carried out under proposals 20160243/20170351 on the XDS beamline, using the experimental station developed for the EMA beamline at SIRIUS source, the Central Laboratory of Electron Microscopy (LCME) at UFSC (for the TEM analysis), and the Brazilian National Center for Supercomputing (CESUP/UFRGS). This paper is dedicated in memory of Professor Faruk José Nome Aguilera (1947–2018).

■ REFERENCES

- (1) Li, J.; Chen, P. R. Development and Application of Bond Cleavage Reactions in Bioorthogonal Chemistry. *Nat. Chem. Biol.* **2016**, *12*, 129–137.
- (2) Pérez-López, A. M.; Rubio-Ruiz, B.; Sebastián, V.; Hamilton, L.; Adam, C.; Bray, T. L.; Irusta, S.; Brennan, P. M.; Lloyd-Jones, G. C.;

- Sieger, D.; Santamaría, J.; Unciti-Broceta, A. Gold-Triggered Uncaging Chemistry in Living Systems. *Angew. Chem., Int. Ed.* **2017**, *56*, 12548–12552.
- (3) Yusop, R. M.; Unciti-Broceta, A.; Johansson, E. M. V.; Sánchez-Martín, R. M.; Bradley, M. Palladium-Mediated Intracellular Chemistry. *Nat. Chem.* **2011**, *3*, 239–243.
- (4) Yang, M. Y.; Li, J.; Chen, P. R. Transition Metal-Mediated Bioorthogonal Protein Chemistry in Living Cells. *Chem. Soc. Rev.* **2014**, *43*, 6511–6526.
- (5) Völker, T.; Meggers, E. Transition-Metal-Mediated Uncaging in Living Human Cells — an Emerging Alternative to Photolabile Protecting Groups. *Curr. Opin. Chem. Biol.* **2015**, *25*, 48–54.
- (6) Dumas, A.; Couvreur, P. Palladium: A Future Key Player in the Nanomedical Field? *Chemical Science* **2015**, *6*, 2153–2157.
- (7) Chankeshwara, S. V.; Indrigo, E.; Bradley, M. Palladium-Mediated Chemistry in Living Cells. *Curr. Opin. Chem. Biol.* **2014**, *21*, 128–135.
- (8) Jbara, M.; Maity, S. K.; Brik, A. Palladium in the Chemical Synthesis and Modification of Proteins. *Angew. Chem., Int. Ed.* **2017**, *56*, 10644–10655.
- (9) Wang, J.; Cheng, B.; Li, J.; Zhang, Z.; Hong, W.; Chen, X.; Chen, P. R. Chemical Remodeling of Cell-Surface Sialic Acids through a Palladium-Triggered Bioorthogonal Elimination Reaction. *Angew. Chem., Int. Ed.* **2015**, *54*, 5364–5368.
- (10) Li, J.; Yu, J.; Zhao, J.; Wang, J.; Zheng, S.; Lin, S.; Chen, L.; Yang, M.; Jia, S.; Zhang, X.; Chen, P. R. Palladium-Triggered Deprotection Chemistry for Protein Activation in Living Cells. *Nat. Chem.* **2014**, *6*, 352–361.
- (11) Wang, J.; Zheng, S.; Liu, Y.; Zhang, Z.; Lin, Z.; Li, J.; Zhang, G.; Wang, X.; Li, J.; Chen, P. R. Palladium-Triggered Chemical Rescue of Intracellular Proteins Via Genetically Encoded Allene-Caged Tyrosine. *J. Am. Chem. Soc.* **2016**, *138*, 15118–15121.
- (12) Weiss, J. T.; Dawson, J. C.; Macleod, K. G.; Rybski, W.; Fraser, C.; Torres-Sánchez, C.; Patton, E. E.; Bradley, M.; Carragher, N. O.; Unciti-Broceta, A. Extracellular Palladium-Catalysed Dealkylation of 5-Fluoro-1-Propargyl-Uracil as a Bioorthogonally Activated Prodrug Approach. *Nat. Commun.* **2014**, *5*, 3277.
- (13) Weiss, J. T.; Dawson, J. C.; Fraser, C.; Rybski, W.; Torres-Sánchez, C.; Bradley, M.; Patton, E. E.; Carragher, N. O.; Unciti-Broceta, A. Development and Bioorthogonal Activation of Palladium-Labile Prodrugs of Gemcitabine. *J. Med. Chem.* **2014**, *57*, 5395–5404.
- (14) Tonga, G. Y.; Jeong, Y.; Duncan, B.; Mizuhara, T.; Mout, R.; Das, R.; Kim, S. T.; Yeh, Y.-C.; Yan, B.; Hou, S.; Rotello, V. M. Supramolecular Regulation of Bioorthogonal Catalysis in Cells Using Nanoparticle-Embedded Transition Metal Catalysts. *Nat. Chem.* **2015**, *7*, 597–603.
- (15) Stenton, B. J.; Oliveira, B. L.; Matos, M. J.; Sinatra, L.; Bernardes, G. J. L. A Thioether-Directed Palladium-Cleavable Linker for Targeted Bioorthogonal Drug Decaging. *Chemical Science* **2018**, *9*, 4185–4189.
- (16) Martínez-Calvo, M.; Mascareñas, J. L. Organometallic Catalysis in Biological Media and Living Settings. *Coord. Chem. Rev.* **2018**, *359*, 57–79.
- (17) Bai, Y.; Chen, J.; Zimmerman, S. C. Designed Transition Metal Catalysts for Intracellular Organic Synthesis. *Chem. Soc. Rev.* **2018**, *47*, 1811–1821.
- (18) Vinogradova, E. V. Organometallic Chemical Biology: An Organometallic Approach to Bioconjugation. *Pure Appl. Chem.* **2017**, *89*, 1619–1640.
- (19) Garner, A. L.; Song, F.; Koide, K. Enhancement of a Catalysis-Based Fluorometric Detection Method for Palladium through Rational Fine-Tuning of the Palladium Species. *J. Am. Chem. Soc.* **2009**, *131*, 5163–5171.
- (20) Amatore, C.; Jutand, A.; Thuilliez, A. Formation of Palladium(0) Complexes from Pd(OAc)₂ and a Bidentate Phosphine Ligand (Dppp) and Their Reactivity in Oxidative Addition. *Organometallics* **2001**, *20*, 3241–3249.
- (21) Pal, M.; Parasuraman, K.; Yeleswarapu, K. R. Palladium-Catalyzed Cleavage of O/N-Propargyl Protecting Groups in Aqueous Media under a Copper-Free Condition. *Org. Lett.* **2003**, *5*, 349–352.
- (22) Rambabu, D.; Bhavani, S.; Swamy, N. K.; Basaveswara Rao, M. V.; Pal, M. Pd/C-Mediated Depropargylation of Propargyl Ethers/Amines in Water. *Tetrahedron Lett.* **2013**, *54*, 1169–1173.
- (23) Wei, C. S.; Davies, G. H. M.; Soltani, O.; Albrecht, J.; Gao, Q.; Pathirana, C.; Hsiao, Y.; Tummala, S.; Eastgate, M. D. The Impact of Palladium(II) Reduction Pathways on the Structure and Activity of Palladium(0) Catalysts. *Angew. Chem., Int. Ed.* **2013**, *52*, 5822–5826.
- (24) Liu, B.; Wang, H.; Wang, T.; Bao, Y.; Du, F.; Tian, J.; Li, Q.; Bai, R. A New Ratiometric Esipr Sensor for Detection of Palladium Species in Aqueous Solution. *Chem. Commun. (Cambridge, U. K.)* **2012**, *48*, 2867–2869.
- (25) Sletten, E. M.; Bertozzi, C. R. Bioorthogonal Chemistry: Fishing for Selectivity in a Sea of Functionality. *Angew. Chem., Int. Ed.* **2009**, *48*, 6974–6998.
- (26) Murahashi, T.; Ogoshi, S.; Kurosawa, H. New Direction in Organopalladium Chemistry: Structure and Reactivity of Unsaturated Hydrocarbon Ligands Bound to Multipalladium Units. *Chem. Rec.* **2003**, *3*, 101–111.
- (27) Chalmers, S.; Caldwell, S. T.; Quin, C.; Prime, T. A.; James, A. M.; Cairns, A. G.; Murphy, M. P.; McCarron, J. G.; Hartley, R. C. Selective Uncoupling of Individual Mitochondria within a Cell Using a Mitochondria-Targeted Photoactivated Protonophore. *J. Am. Chem. Soc.* **2012**, *134*, 758–761.
- (28) Wu, B.; Jiang, M.; Peng, Q.; Li, G.; Hou, Z.; Milne, G. L.; Mori, S.; Alonso, R.; Geisler, J. G.; Duan, W. 2,4 Dnp Improves Motor Function, Preserves Medium Spiny Neuronal Identity, and Reduces Oxidative Stress in a Mouse Model of Huntington's Disease. *Exp. Neurol.* **2017**, *293*, 83–90.
- (29) Khan, R. S.; Dine, K.; Geisler, J. G.; Shindler, K. S. Mitochondrial Uncoupler Prodrug of 2,4-Dinitrophenol, Mp201, Prevents Neuronal Damage and Preserves Vision in Experimental Optic Neuritis. *Oxid. Med. Cell. Longevity* **2017**, *2017*, 1–10.
- (30) Geisler, J. G.; Marosi, K.; Halpern, J.; Mattson, M. P. Dnp, Mitochondrial Uncoupling, and Neuroprotection: A Little Dab'll Do Ya. *Alzheimer's Dementia* **2017**, *13*, 582–591.
- (31) Trader, D. J.; Carlson, E. E. Chemoselective Hydroxyl Group Transformation: An Elusive Target. *Mol. BioSyst.* **2012**, *8*, 2484–2493.
- (32) Kayastha, A. M.; Gupta, A. K. An Easy Method to Determine the Kinetic-Parameters of Biphasic Reactions. *Biochem. Educ.* **1987**, *15*, 135–135.
- (33) Anderson, T. G.; McConnell, H. M. Interpretation of Biphasic Dissociation Kinetics for Isomeric Class II Major Histocompatibility Complex-Peptide Complexes. *Biophys. J.* **1999**, *77*, 2451–2461.
- (34) Devaraj, N. K. The Future of Bioorthogonal Chemistry. *ACS Cent. Sci.* **2018**, *4*, 952–959.
- (35) Blackmond, D. G. Reaction Progress Kinetic Analysis: A Powerful Methodology for Mechanistic Studies of Complex Catalytic Reactions. *Angew. Chem., Int. Ed.* **2005**, *44*, 4302–4320.
- (36) Yao, Y.; Patzig, C.; Hu, Y.; Scott, R. W. J. In Situ X-Ray Absorption Spectroscopic Study of Fe@Fexoy/Pd and Fe@Fexoy/Cu Nanoparticle Catalysts Prepared by Galvanic Exchange Reactions. *J. Phys. Chem. C* **2015**, *119*, 21209–21218.
- (37) Chang, S. Y.; Grunder, Y.; Booth, S. G.; Molleta, L. B.; Uehara, A.; Mosselmans, J. F. W.; Cibin, G.; Pham, V. T.; Nataf, L.; Dryfe, R. A. W.; Schroeder, S. L. M. Detection and Characterisation of Sub-Critical Nuclei During Reactive Pd Metal Nucleation by X-Ray Absorption Spectroscopy. *CrystEngComm* **2016**, *18*, 674–682.
- (38) Charbonneau, M.; Addoumeh, G.; Ogundinma, P.; Schmitzer, A. R. Support-Free Palladium-Nhc Catalyst for Highly Recyclable Heterogeneous Suzuki–Miyaura Coupling in Neat Water. *Organometallics* **2014**, *33*, 6544–6549.
- (39) Santos, L. S. In *Reactive Intermediates*; Wiley-VCH Verlag GmbH & Co. KGaA: 2010; pp 133–198.
- (40) Roglans, A.; Pla-Quintana, A. In *Reactive Intermediates*; Wiley-VCH Verlag GmbH & Co. KGaA: 2010; pp 229–275.

- (41) Qian, R.; Zhou, J.; Yao, S.; Wang, H.; Guo, Y. In *Reactive Intermediates*; Wiley-VCH Verlag GmbH & Co. KGaA: 2010; pp 113–131.
- (42) Nachtigall, F. M.; Eberlin, M. N. In *Reactive Intermediates*; Wiley-VCH Verlag GmbH & Co. KGaA: 2010; pp 63–111.
- (43) Adamo, C.; Barone, V. Toward Reliable Density Functional Methods without Adjustable Parameters: The Pbe0Model. *J. Chem. Phys.* **1999**, *110*, 6158–6170.
- (44) Ripplinger, C.; Sandhoefer, B.; Hansen, A.; Neese, F. Natural Triple Excitations in Local Coupled Cluster Calculations with Pair Natural Orbitals. *J. Chem. Phys.* **2013**, *139*, 134101–134113.
- (45) Kruse, H.; Grimme, S. A Geometrical Correction for the Inter- and Intra-Molecular Basis Set Superposition Error in Hartree-Fock and Density Functional Theory Calculations for Large Systems. *J. Chem. Phys.* **2012**, *136*, 154101–154116.
- (46) Widegren, J. A.; Finke, R. G. A Review of the Problem of Distinguishing True Homogeneous Catalysis from Soluble or Other Metal-Particle Heterogeneous Catalysis under Reducing Conditions. *J. Mol. Catal. A: Chem.* **2003**, *198*, 317–341.
- (47) Martínez-Calvo, M.; Couceiro, J. R.; Destito, P.; Rodríguez, J.; Mosquera, J.; Mascareñas, J. L. Intracellular Deprotection Reactions Mediated by Palladium Complexes Equipped with Designed Phosphine Ligands. *ACS Catal.* **2018**, *8*, 6055–6061.

5 Paper II: Pt-triggered bond-cleavage of pentynoyl amide and n-propargyl handles for drug-activation

OLIVEIRA, B. L. et al. Platinum-triggered bond-cleavage of pentynoyl amide and n-propargyl handles for drug-activation. *Journal of the American Chemical Society*, American Chemical Society (ACS), v. 142, n. 24, p. 10869–10880, May 2020. ISSN 1520-5126. Disponível em: <<http://dx.doi.org/10.1021/jacs.0c01622>>.

Here we present a new Pt-based smart drug was developed for cancer therapy [4]. We studied a biorthogonal Pt-complex for prodrug applications whose controlled activation consists of a water-directed bond-cleavage reaction, releasing a therapeutical protecting group. This application to metallocatalysis was done in a joint computational-experimental collaboration.

In order for such prodrugs to work, they must be selective to the type of tumor being treated, as well as having low toxicity. Metal-mediated decaging prodrugs offer the possibility of being catalytic, allowing them to be used in substoichiometric amounts, which thus reduces the required dosage.

Other metals were already studied in the literature, including Pd [3], Ru and Au. Pt was chosen since other complexes such as Cisplatin are widely used in the clinic, having short half-life in humans, not being present in human biology, and having the ability to concentrate in the tumor site.

We introduce a new biorthogonal cleavage reaction catalyzed by platinum for prodrug activation. We demonstrate that pentynoyl tertiary amide and N-propargyl amide handles in small-molecule drugs decage successfully in both aqueous and cell media under nontoxic quantities of Pt salts. Studies in zebrafish models for the treatment of colorectal cancer showed promising results.

As a highlight, it was experimentally found that water was required to generate the active catalyst, which means activation of metal-chloride bonds by water, which is rare [76].

Calculations indicate that the reaction takes place through a stepwise process starting with coordination of the substrate molecule to Pt(II), followed by an intramolecular attack of the carbonyl oxygen to the pentynoyl moiety, producing a five-membered ring intermediate. From this intermediate, different decomposition pathways were explored. The one with lowest energy encompasses a hydration of the intermediate, which then fur-

ther decomposes to liberate the free amine. A subsequent hydrolysis recovers the metal complex.

The intermediate CS_0 identified by LC-MS was determined by the computational methodology. The difference in activation free energy between both substrates was found to be around $2.8 \text{ kcal}\cdot\text{mol}^{-1}$.

A new decaging reaction of alkynes with platinum complexes were developed, aiming at the release secondary amines from stable tertiary amides. The reaction happens successfully both in cell cultures and living organisms. We showed that the reaction takes place by a platinum-mediated intramolecular cyclization mechanism and that water works as the metal-activating agent. Our computational model matches well the thorough LC-MS characterization of the reaction intermediates. The reaction was further extended to work with N-propargyl groups with comparable efficacies to palladium-mediated depropargylation [3].

In the group of Prof. Bernardes, it was adapted for the synthesis of a noninternalizing ADC (WHAT IS THIS?), resulting in drug release upon administration of platinum complexes in cancer cells. It was also demonstrated to work effectively in colorectal cancer zebrafish xenograft model employing nontoxic amounts of CisPt in order to activate a prodrug of the anticancer agent 5-FU (WHAT IS THIS AGAIN?), which effectively led to significant tumor reduction *in vivo*.

This adds a significant decaging strategy for the toolbox of chemical biology applications. It reaction is effective in aqueous systems encompassing high concentrations of salts with high yields and reaction rates, similar to the standard palladium decaging metal (WHAT?). A downside is the suetibility of the reaction towards the presence of nucleophiles, which leads to one order of magnitude slower rates. It is also compatible with cellular environments, although the presence of biomolecules/nucleophiles reduces overall yields considerably. These results pave the way for future developments of platinum-mediated decaging reactions.

5.1 Paper

The publication can be read in full next.

Platinum-Triggered Bond-Cleavage of Pentynoyl Amide and N-Propargyl Handles for Drug-Activation

Bruno L. Oliveira,*[▼] Benjamin J. Stenton,[▼] V. B. Unnikrishnan, Cátila Rebelo de Almeida, João Conde, Magda Negrão, Felipe S. S. Schneider, Carlos Cordeiro, Miguel Godinho Ferreira, Giovanni F. Caramori, Josiel B. Domingos, Rita Fior,* and Gonçalo J. L. Bernardes*



Cite This: *J. Am. Chem. Soc.* 2020, 142, 10869–10880



Read Online

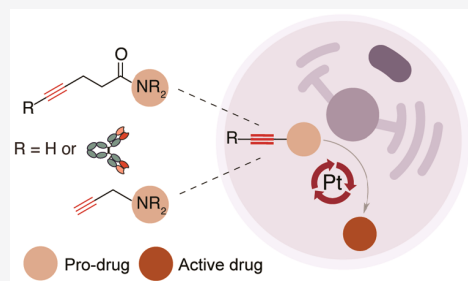
ACCESS

Metrics & More

Article Recommendations

Supporting Information

ABSTRACT: The ability to create ways to control drug activation at specific tissues while sparing healthy tissues remains a major challenge. The administration of exogenous target-specific triggers offers the potential for traceless release of active drugs on tumor sites from antibody-drug conjugates (ADCs) and caged prodrugs. We have developed a metal-mediated bond-cleavage reaction that uses platinum complexes [K_2PtCl_4 or Cisplatin (CisPt)] for drug activation. Key to the success of the reaction is a water-promoted activation process that triggers the reactivity of the platinum complexes. Under these conditions, the decaging of pentynoyl tertiary amides and N-propargyls occurs rapidly in aqueous systems. In cells, the protected analogues of cytotoxic drugs 5-fluorouracil (5-FU) and monomethyl auristatin E (MMAE) are partially activated by nontoxic amounts of platinum salts. Additionally, a noninternalizing ADC built with a pentynoyl traceless linker that features a tertiary amide protected MMAE was also decaged in the presence of platinum salts for extracellular drug release in cancer cells. Finally, CisPt-mediated prodrug activation of a propargyl derivative of 5-FU was shown in a colorectal zebrafish xenograft model that led to significant reductions in tumor size. Overall, our results reveal a new metal-based cleavable reaction that expands the application of platinum complexes beyond those in catalysis and cancer therapy.



INTRODUCTION

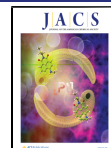
The targeting of potent drugs with tumor-specific ligands is an essential feature of drug delivery and cancer therapy.¹ Notable in this field are antibody-drug conjugates (ADCs) that use an antibody to transport a drug to cancerous cells and endogenously release it by hydrolysis (low pH, reduction of disulfide bonds) or by proteolysis (e.g., cathepsin B protease).^{2,3} Although the cleavage of ADC linkers with endogenous triggers is the simplest method for drug release, external small-molecule triggers for extracellular drug release may be more advantageous because they avoid any disparity in cleavage rates caused by variable biology across subjects, and drug release is not dependent on the concentrations of cellular triggers.^{4–7} In fact, ADCs built with protease cleavable linkers for drug release have been shown recently to not depend on the cathepsin B protease function for efficient and targeted cancer-cell killing.⁴ The promise of controlled prodrug activation has fueled research into new triggers that enable bond-cleavage reactions to unleash bioorthogonal protecting groups, which deactivate otherwise potent drugs.⁸ Robillard and co-workers pioneered the development of tetrazine-triggered drug delivery from ADCs.⁹ By using a noninternalizing ADC consisting of a diabody conjugated to *trans*-cyclooctene-linked drug monomethyl auristatin E (MMAE),¹⁰ the allylic carbamate-containing linker can rapidly

react with a tetrazine through an inverse-electron-demand Diels–Alder reaction.^{10,11} The drug is released within the extracellular tumor environment and showed efficacy in delaying tumor growth in xenograft mice models.¹⁰ Other chemical- or light-mediated decaging reactions have also been developed with an array of applications that range from *in situ* activation of prodrugs to the gain-of-function study on proteins.^{12–15}

Although the recent results with noninternalizing ADCs for click-triggered drug release show promise, there are several issues that remain to be improved, such as the lack of tumor-selectivity of the chemical triggers or their short *in vivo* retention times that may result in reduced release of the cytotoxic payloads and thus lower efficacy. Additionally, in such applications the tumor payload concentration is determined by the cell-surface antigen expression, which in some cases may be too low to achieve a useful therapeutic

Received: February 10, 2020

Published: May 26, 2020



response.^{7,16} This contrasts with the use of internalizing ADCs that have an accumulative effect inside the tumor cells.^{7,16,17}

Metal-mediated decaging of prodrugs has been more extensively reported than small-molecule-mediated decaging.¹⁸ Unlike chemical triggers, transition metals can be catalytic, which allows their use in substoichiometric amounts. In these cases, only very small amounts of catalytic metal are required to achieve the desired pharmacologic effect, thereby reducing toxicity and side reactions.^{19,20} This feature was recently demonstrated by Weissleder and co-workers using palladium nanoparticles that accumulate in tumor cells and serve as cellular catalysts for the activation of different model prodrugs and resulted in tumor growth inhibition.²¹

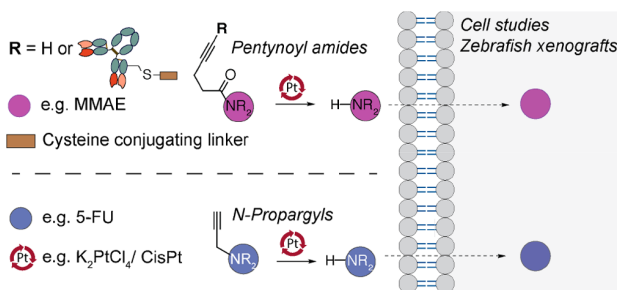
Palladium-mediated decaging is indeed the most studied method for prodrug activation, which relies on the cleavage of terminal propargylic and allylic carbamates moieties introduced into small molecule drugs.^{21–26} Recently, our group developed an internal bifunctional thioether propargyl carbamate linker with a conjugating unit for protein modification and MMAE for palladium-mediated drug release from a nanobody-drug conjugate in cellular systems.²⁷ Other metals, such as ruthenium^{28–30} and gold,^{31,32} have been also explored for cleavage and drug release. One of the latest additions to this field was the recent report by Peng Chen and co-workers³³ on a copper-releasable reaction for protein gain-of-function and drug activation. Together, these examples highlight the potential of metal-mediated cleavage as a means to achieve controlled and chemically defined drug release.

Whereas the utility of the above-mentioned metals for decaging applications has been extensively demonstrated, other metals have not yet been sufficiently explored. For instance, platinum is widely used in catalysis,³⁴ but has found few applications in chemical biology, possibly as a result of its intrinsic cytotoxicity. However, in the context of cancer therapy, we hypothesized that the use of platinum complexes [e.g., Cisplatin (CisPt) used in the clinic]^{35,36} as catalysts for cleavage reactions could be propitious for bioorthogonal activation of prodrugs in tumor cells.

“Bioorthogonal” is perhaps unfitting terminology for a compound known to react with water, nucleic acids, amino acids, and proteins.^{37,38} However, CisPt is one of the most commonly used chemotherapy drugs, being used to treat up to 20% of cancer patients.^{39,40} CisPt was deemed a suitable reagent for the development of a drug decaging reaction because it is highly reactive (half-life in humans of ~30 min),^{41,42} accumulates in the tumor, and most importantly, is not present in human biology.^{43,44} In this way, the activation of prodrugs at the tumor site when the chemical trigger has already accumulated may represent a major achievement. It may be conceivable for metal concentrations to reach 0.25 to 3.7 μg per g of tumor.^{41,45,46} For a 1 cm^3 tumor (approximately 1 g wet weight), the concentration of CisPt is estimated to be 0.83–12.3 μM .⁴⁷

Therefore, we were interested in investigating new bioorthogonal cleavage reactions catalyzed by platinum for applications in prodrug activation. Here, we demonstrate that pentynoyl tertiary amide and *N*-propargyl handles introduced into small-molecule drugs are successfully decaged in aqueous solution and cell media using nontoxic amounts of platinum salts (Scheme 1). This strategy was successfully applied to small molecule prodrug activation (MMAE and 5-FU) and further extended to drug release from a noninternalizing ADC in cancer cells. Finally, we show that CisPt-mediated bond

Scheme 1. Platinum-Mediated Bioorthogonal Bond Cleavage^a



^aSecondary amines protected in the form of a tertiary pentynoyl amide (top) or *N*-propargyl (bottom) can be selectively deprotected by platinum reagents like the chemotherapeutic drug CisPt. This strategy was explored for drug activation of the protected MMAE and 5-FU drugs and extended for drug release from an ADC in cancer cells. Ultimately, CisPt-mediated activation of a “5-FU-propargyl prodrug” was evaluated in a zebrafish xenograft model for treatment of colorectal cancer.

cleavage can be used to activate a 5-FU prodrug in a zebrafish xenograft model for treatment of colorectal cancer.

RESULTS AND DISCUSSION

Engineering of a Platinum-Mediated Decaging Reaction. From studies on the reactivity of platinum complexes, it is apparent that platinum shares many of its reactions with similar complexes of gold.⁴⁸ We therefore searched the literature for reactions with Au and Pt that would function at room temperature, in aqueous media, and with likely fast kinetics to adapt for CisPt-mediated bioorthogonal decaging reactions. The cyclization of 4-pentynoic acid is well-known to proceed quickly in aqueous media with reaction times ranging from minutes to a few hours^{49,50} and has even been demonstrated with platinum (II and IV) anticancer complexes (Figure 1a).⁵¹ Given the previous studies, a metal-catalyzed mechanism was devised whereby a carbamate carbonyl could be used as an internal nucleophile to cause carbocyclization followed by release of a secondary amine (Figure 1b). Working on this hypothesis, we synthesized the terminal propargyl carbamate 3a (Figure 1c) to verify if the carbonyl could act as a nucleophile and attack the alkyne to subsequently release morpholine 6a in the presence of K_2PtCl_4 . We observed conversions of 20% and 61% for reactions carried out in $\text{D}_2\text{O}/\text{CD}_3\text{OD}$ (3:1) with 0.1 and 2 equiv of metal salt, respectively (Figure 1d, Entries 1 and 2; Figures S1 and S2 of the Supporting Information, SI). Similar yields were found for the reaction with NaAuCl_4 (Figure S3). In contrast, if an aliphatic carbamate with no propargyl handle is used (compound SI S1) under the same decaging conditions the free amine is not released (Figures S4 and S5, respectively).

According to these observations, it should also be possible to decage tertiary amides to release secondary amines (Figure 1c). This was an attractive prospect because amides are often much more stable than their corresponding carbamates.⁵² Decaging of pentynoyl tertiary amide 4a was monitored by NMR spectroscopy over time and was proven to have comparable rates and yields to the corresponding carbamate 3a (Figure 1d, Entry 4; Figure 1e). Importantly, the reaction proceeds with substoichiometric amounts of the metal complex (Figure 1d, Entry 3; Figure S6). The reactions were also

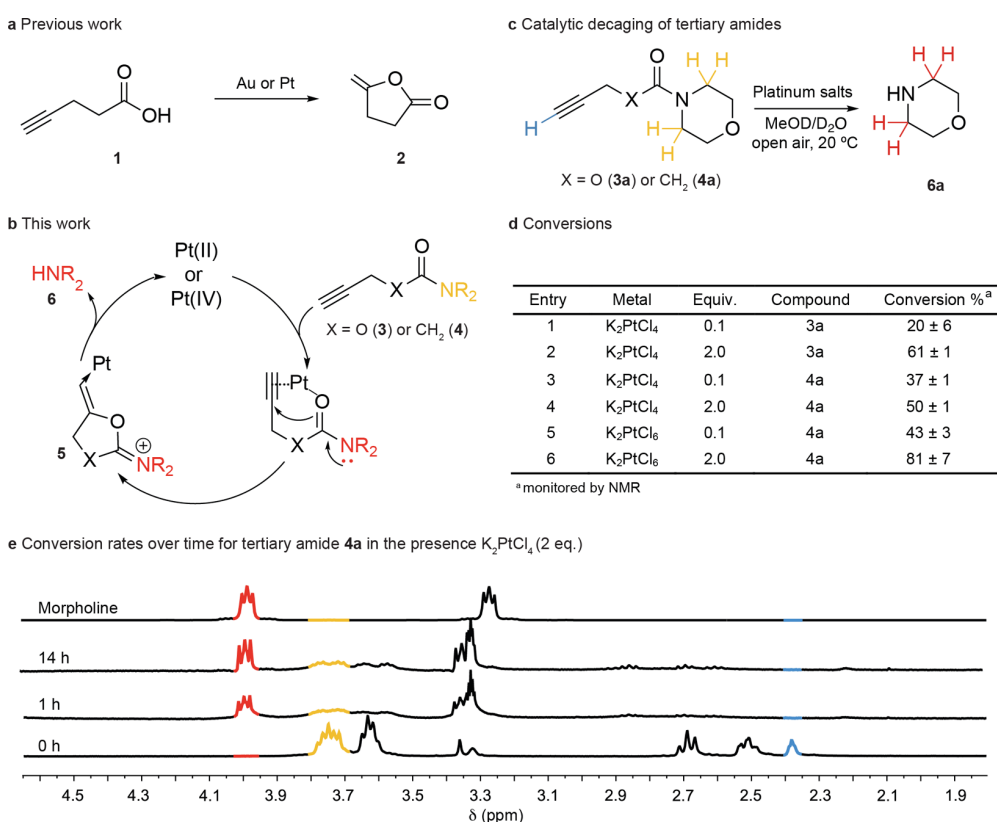


Figure 1. Platinum-mediated decaging reaction engineering. **a.** The cyclization of 4-pentyneoic acid is known to proceed rapidly in aqueous media with gold and platinum complexes. **b.** The proposed reaction uses a carboxamide as an internal nucleophile that cyclizes and displaces the secondary amine leaving group, which could be a drug or a fluorophore. **c.** Model compounds with alkyne amide or carbamate were used to survey the decaging reaction. **d.** Efficiency of the cleavage reaction under different conditions was assessed by ¹H NMR spectroscopy. **e.** ¹H NMR spectroscopy of the decaging of the tertiary amide **4a** in the presence of a catalytic amount of K_2PtCl_4 (2 eq.). The reaction generates a cyclized intermediate that undergoes hydrolysis to release morpholine **6a**. General procedure for determining decaging conversion by ¹H NMR spectroscopy: carbamate and amide compounds (10 mgs) were dissolved in MeOD (0.2 mL) and metal complexes (0.1 or 2 equiv) were added in D₂O (0.6 mL) at room temperature in an open vessel for 14 h. The reactions were transferred to an NMR spectroscopic tube and sealed. Conversion was calculated based on the relative ratios of methylene peaks resulting from the starting material and the released amine product. Numerical data are the mean of 2 or 3 replicates.

successfully trialed with K_2PtCl_6 as a representative Pt(IV) species (Figure 1d, Entries 5 and 6; Figure S7) and $NaAuCl_4$ (Figure S8) with good yields.

Overall, these results are important because they demonstrate a decaging reaction of stable protected tertiary amides by using substoichiometric amounts of platinum complexes that could function in water, open air, and without need of extreme temperatures or complex ligands. It is important to note that even after all of the starting material has been consumed (as evidenced by loss of terminal alkyne proton), not all of it has decomposed to release the amine (Figure 1e). This lack of conversion is likely due to side reactions, and nucleophilic attack on the alkyne, which seems the most plausible mechanism. To elucidate this a pentynoyl secondary amide (compound S2) was reacted with K_2PtCl_4 and $NaAuCl_4$ under similar conditions (Figures S9 and S10). We found that the reaction proceeds with much lower extents of decaging, likely due to the amide nitrogen competing as a nucleophile to yield a stable cyclized product, and thus a smaller yield of released amine.

Mechanistic and Kinetic Studies of the Platinum-Mediated Decaging Reaction. To further study the platinum decaging reaction, the pentynoyl tertiary amide was

conjugated to a naphthalimide-based fluorophore to generate fluorescent quenched probe **7** (Figure 2a, see SI for synthetic details).^{53,54} The reaction was then monitored by the increase in fluorescence upon removal of the protecting group to form fluorescent probe **8**. With 50 equiv of K_2PtCl_4 or CisPt, we found that the fluorescence was restored over a period of 200 min for K_2PtCl_4 and 300 min for CisPt (Figure 2b), with complete consumption of **7** and formation of corresponding “turned ON fluorophore”, as indicated by LC–MS analysis (Figure S11). For both metals the conversion was accompanied by an initial steady state followed by a marked increase of the fluorescence, which suggested the formation of an activated intermediate. Indeed, it is known that platinum complexes form a series of reactive intermediates by successive replacement of the chloro ligands by water or hydroxyl groups.^{55–57} We hypothesized that formation of such an aqua intermediate early on could be responsible for the activation of the platinum complexes. This hypothesis was verified using LC–MS studies to follow formation of K_2PtCl_4 – and CisPt–aqua complexes over time, which occurred within 6 h (Figures S12 and S13). Consistent with this hypothesis, platinum salts failed to form the aqua complexes when incubated in the presence of *N,N*-dimethylformamide (DMF). On the basis of

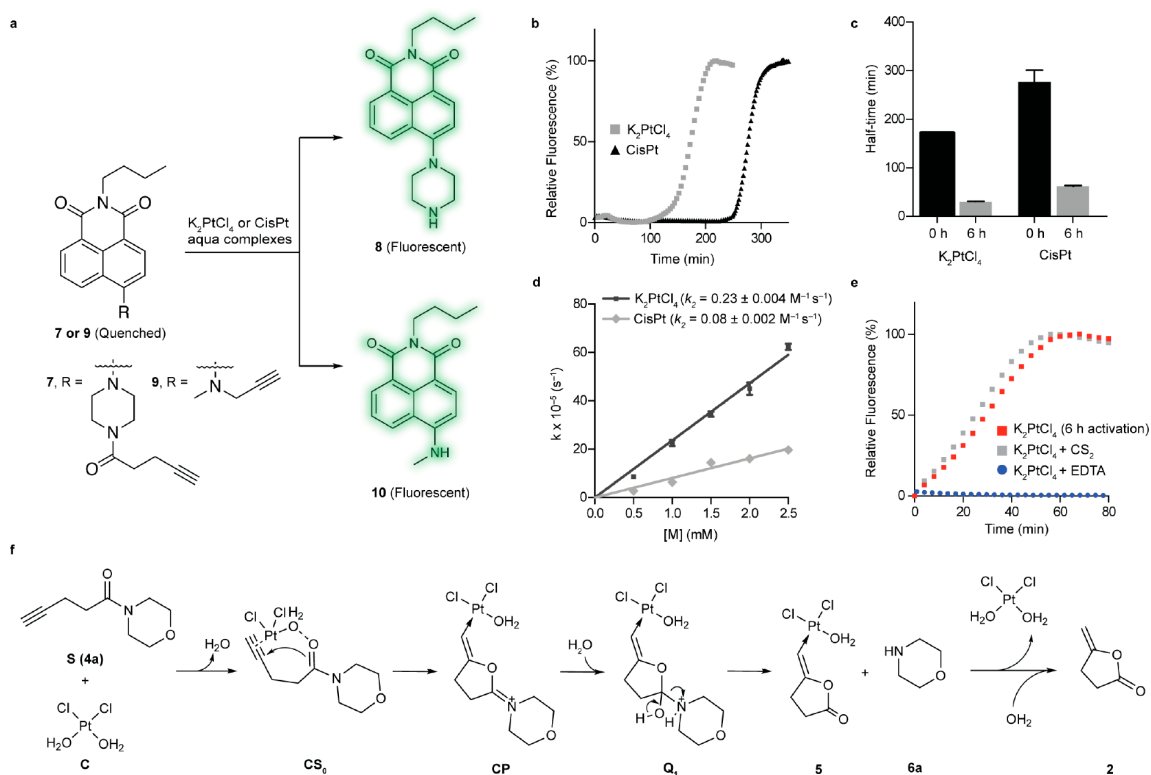


Figure 2. Examination of the platinum-catalyzed bioorthogonal cleavage reaction. a. Naphthalimide-based fluorogenic probes were used to study the cleavage efficiency of the platinum reaction for decaging alkyne-containing molecules. The caged naphthalimide derivatives exhibited high stability in solution and cell media and their quenched fluorescence could be reactivated upon removal of the caging group ($\lambda_{\text{ex}} = 445 \text{ nm}$, $\lambda_{\text{em}} = 545 \text{ nm}$). b. Changes in fluorescence intensity during the time course of the decaging reaction between fluorogenic probe 7 and platinum salts (K_2PtCl_4 /CisPt). c. Determined half-time for the reaction of 7 with activated and nonactivated platinum salts. d. Decaging kinetics for the pentynoyl amide fluorophore. Rate constants were determined under pseudo first order conditions with a $50 \mu\text{M}$ final concentration of probe 7 and 10–50 equiv of aqua platinum metals. e. Kinetics profiles of the decaging reaction in the presence of the metal poisons CS_2 and EDTA. Error bars represent \pm s.d. ($n = 3$). All experiments were repeated 3 independent times. f. Calculated mechanism for the depropargylation reaction catalyzed by Pt with model substrate 4a. Calculations were performed with an implicit solvent model for water. Geometries and frequencies were calculated with the functional revPBE and, to obtain very accurate energetics, single point energy calculations with DLPNO–CCSD(T) and counterpoise corrections were employed to suppress basis set superposition errors.

these observations, we further studied the kinetics of the releasing reaction after formation of the aqua complexes (6 h in water/DMF at 37°C). As expected, activation of the platinum salts significantly accelerated the turn-on half-time from $t_{1/2} = 171 \text{ min}$ to $t_{1/2} = 30 \text{ min}$ for K_2PtCl_4 and from $t_{1/2} = 276 \text{ min}$ to $t_{1/2} = 60 \text{ min}$ for “CisPt” (Figure 2c and Table S1). Accordingly, if the reaction was performed in pure DMF, then formation of the decaged probe was not observed (50 equiv of K_2PtCl_4 or CisPt for 14 h at 37°C). This result is in agreement with previous LC–MS studies that suggested the requirement of water to generate the active catalyst. The activation of metal chloride in aqueous solvents has few precedents but has been reported for gold complexes.⁵⁸ This effect is explained by facilitated ionization of the M–Cl bonds in water.⁵⁸

In terms of catalytic activity, the reaction of 7 with 0.3 equiv of activated K_2PtCl_4 complex yielded decaged probe 8 in 98% yield after 72 h at 37°C (catalyst turnover number 3.3). Upon moving to 2 equiv of the metal complex, the decaged product was obtained in quantitative yield after 4 h at 37°C (Figure S14). As a comparison, the same study was performed with $\text{Pd}(\text{OAc})_2$, a standard palladium complex for *N*-depropargylation.⁵⁹ Interestingly, the Pd-reaction proceeded with

comparable efficiency, although with slightly better rates of conversion (>98% yield in 1 h, LC–MS analysis). Of relevance, palladium decaging of alkyne amides has never been reported before. Finally, the compatibility and efficiency of the reactions were tested under physiological conditions. The activated aqua complexes were first shown to persist in complete DMEM cell media for at least 16 h at 37°C , as assessed by LC–MS analysis, although a significant decrease in their concentration was observed over time (Figure S15). Later, the reactions were shown to proceed in cell media with conversions of 69% for K_2PtCl_4 (50 equiv) and 17% for CisPt (150 equiv) after 14 h at 37°C (Figures S16 and S17). Similarly, the reaction was also trialed in high salt concentration buffers with high efficiency ($t_{1/2} = 36 \text{ min}$ for 50 equiv of K_2PtCl_4 and $t_{1/2} = 105 \text{ min}$ for 100 equiv of CisPt, 37°C in E3 medium, Figures S18 and S19).

Having found an efficient platinum complex for decaging pentynoyl tertiary amides, we turned our attention to the determination of the rate constant of the reaction (Figure 2d). By fitting the appearance of 8 in the presence of increasing amounts of metal complexes and by using pseudo-first order conditions, the reactions were found to have second order rate constants of $0.230 \pm 0.004 \text{ M}^{-1} \text{ s}^{-1}$ for K_2PtCl_4 and $0.080 \pm$

$0.002 \text{ M}^{-1} \text{ s}^{-1}$ for CisPt (Figure 2d). These reaction rates are similar to those reported for other metal-assisted decaging reactions.²⁷

To determine the nature of active species involved in the decaging reaction, we performed kinetic experiments with carbon disulfide (Figure 2e, Table S2). CS₂ acts as a catalyst poison for homogeneous and heterogeneous Pt(0) reactions, although Pt(II) species are unaffected. As seen in Figure 2e, the reaction rates are similar to those with or without CS₂. This result can be attributed to the noninvolvement of Pt(0) species in the reaction. However, the reaction rates were significantly affected by the addition of ethylenediamine tetraacetic acid (EDTA; Figure 2e), possibly due the participation of Pt(II) in the reaction.

We also performed computational studies to help understand the reaction mechanism (Figure 2f). These studies suggest that the most probable operating reaction pathway of substrate **4a** is a stepwise process involving the coordination of substrate molecule to Pt(II), followed by an intramolecular attack of the carbonyl oxygen of the Pt-coordinated substrate (CS₀) to the pentynoyl moiety, which gives five-membered ring intermediate **CP**. Different pathways to decomposition of **CP** were explored (Figure S20); the lowest energy one was the hydration of **CP** leading to formation of intermediate **Q₁**, which readily decomposes to liberate free amine **6a**. The metal complex is then recovered in a subsequent step by hydrolysis of **5** (Figure 2f). The complete calculation for the first reaction turnover of the main mechanism is depicted in Figure S21 and SI Movie. This mechanism is further supported by the identification of intermediate species CS₀ by LC–MS (Figures S22–S26). The main difference observed for the reaction with substrate **3a** relative to **4a** was the higher free energy of activation ($\Delta\Delta G^\# = 2.75 \text{ kcal mol}^{-1}$) for the intramolecular attack of the carbonyl oxygen at the pentynoyl moiety. However, both substrates share the same energy barrier for hydration of **CP** and release of **6a** (Figure S21).

Extending the Decaging Reaction to N-Propargyl Group. Following the discovery of a platinum-cleavable group, we hoped to extend the scope of handles that could be used for decaging. Metal-mediated decaging of *N*-propargyl handles has been widely explored to modulate the cytotoxic activity of antineoplastic drugs in a controlled manner.^{22,25} On this basis, we investigated the possibility of using *N*-propargyl groups introduced on drugs of interest for prodrug activation using platinum triggers. First, and similarly to the pentynoyl amide reaction, an *N*-propargyl group was used to protect a secondary amine on a naphthalimide derivative to generate fluorogenic probe **9** (Figure 2a). As described above, we tested the reactivity of K₂PtCl₄ and CisPt before and after formation of the aqua complexes (6 h incubation at 37 °C in DMF/water). Once again, dissociation of the chloride anions in water was found to be crucial for triggering the reactivity of platinum complexes. Indeed, we found that reactions with aqua complexes are faster according to the calculated half-time for the “fluorescent reactions” (from $t_{1/2} = 200 \pm 3 \text{ min}$ to $t_{1/2} = 27 \pm 3 \text{ min}$ for K₂PtCl₄ and from $t_{1/2} = 628 \pm 51 \text{ min}$ to $t_{1/2} = 303 \pm 34 \text{ min}$ for CisPt; Table S3). The fluorescence-based assay was also employed to calculate the second-order rate constant for the reaction. Accordingly, the calculated rate constant was $0.120 \pm 0.001 \text{ M}^{-1} \text{ s}^{-1}$ for K₂PtCl₄ and $0.0160 \pm 0.0004 \text{ M}^{-1} \text{ s}^{-1}$ for CisPt (Figure S27). These results show that *N*-propargyls decage slower than pentynoyl amides. As a reference, the same study was performed with palladium

complex Pd(OAc)₂, which behaved slightly better than the platinum salts, to promote formation of **10** with a second-order rate constant of $0.39 \pm 0.015 \text{ M}^{-1} \text{ s}^{-1}$ (Figure S28). The reaction was also subjected to CS₂ and EDTA poisoning. CS₂ had no effect but EDTA completely inhibited the reaction, which indicates the participation of Pt(II) species (Figure S29 and Table S4). On the basis of these results and LC–MS analysis after 2 h of reaction between K₂PtCl₄ and probe **9** (Figure S30), we propose that the first turnover of the reaction proceeds as recently disclosed for palladium depropargylation,⁵⁹ i.e., (i) co-ordination of Pt(II) to alkyne moiety, (ii) attack of a H₂O molecule at the propargyl terminal carbon to form an enol, (iii) tautomerization to a more stable Pt-aldehyde complex, and (iv) C–N bond cleavage by either hydrolysis or β -*N* elimination followed by hydration of Pt-complex (Figure S31). Finally, we investigated the ability of platinum salts to remove the propargyl protecting group in cells (DMEM) and zebrafish (E3) media. The reaction with the fluorogenic probe was monitored for K₂PtCl₄ and CisPt for 14 h at 37 °C. Efficiencies in E3 media were generally high with the reaction complete in 60 and 150 min for K₂PtCl₄ and CisPt, respectively (Figure S32). In DMEM, cleavage was less efficient with conversion yields of 67% for K₂PtCl₄ (50 equiv) and 30% for CisPt (150 equiv) after 14 h at 37 °C (Figure S33).

Platinum-Mediated Decaging in Living Cells. To verify whether platinum-mediated depropargylation would function in cell culture, a pentynoyl amide derivative of antineoplastic drug MMAE was synthesized. MMAE is the drug present in the ADC brentuximab vedotin that is in clinical use to treat patients with relapsed Hodgkin lymphoma and systemic anaplastic large-cell lymphoma,⁶⁰ and remains the drug of choice for antibody-targeted therapies. In addition, a *N*-propargyl 5-fluorouracil (pFU) derivative was also tested, which was found to be efficiently decaged and activated with gold nanoparticles³¹ and palladium complexes.²⁵ When MMAE-am was treated in DMF/water (1:1) for 4 h with 10 equiv of K₂PtCl₄, complete consumption of MMAE-am was seen by LC–MS with 37% release of MMAE along with the formation of the intermediate **Q_{1s}** (Figures S20 and S34). In a similar fashion, decaging of pFU proceeds with yields of $46\% \pm 2$ and $72\% \pm 2$ for K₂PtCl₄ and CisPt, after 14 h reaction with 2 equiv, at room temperature and 37 °C, respectively (Figures S35–S37). These prodrugs (MMAE-am **11** and pFU **12**, see the SI for synthetic details) were reacted with platinum salts in cell culture in the hope of observing a “turn-on” of toxicity. Unfortunately, the chemotherapeutic CisPt has a narrow window of nontoxic concentrations for efficient decaging in cells.⁶¹ Indeed, CisPt was demonstrated to be toxic in HeLa cells at concentrations as low as $2.5 \mu\text{M}$ (Figure S38). On the contrary, platinum salts K₂PtCl₄ and K₂PtCl₆ did not significantly influence the viability of HeLa cells at concentrations below $50 \mu\text{M}$ (Figure S38). With both prodrugs, an increase of about 2-fold in toxicity could be observed for some of the tested concentrations when reacted with K₂PtCl₄ over 3 days in cell culture (Figure 3a and 3b; e.g., 1 nM of MMAE-am and $50 \mu\text{M}$ of pFU). In contrast, no decrease of cytotoxicity was observed in cells treated independently with cFU **13**, a non-decaging control derivative, or in combination with K₂PtCl₄ (Figure 3b). These control studies indicate that 5-FU was not generated because the alkyl handle does not undergo decaging by K₂PtCl₄.

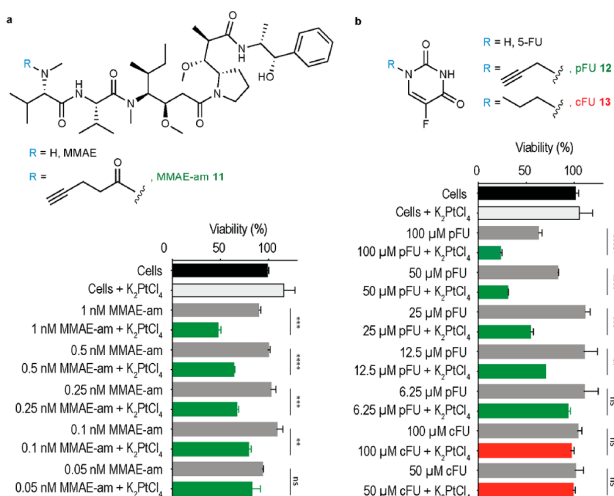
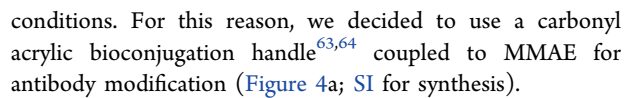


Figure 3. Platinum-mediated decaging in cells. HeLa cells were incubated with different concentrations of MMAE-am 11a or pFU 12b for 3 days with or without K_2PtCl_4 (20 μ M, twice a day). Compound 13, a nondecaging alkyl-FU derivative, was used as a negative control. Toxicity was determined by AlamarBlue assay. Error bars represent \pm s.d. ($n = 3$). Each experiment was repeated three times. The statistical significance of the differences between groups was evaluated with the unpaired t test. Statistical results: ns > 0.05, ** P < 0.01, *** P < 0.001 and **** P < 0.0001.

It is important to note that for both prodrugs the addition of K₂PtCl₄ did not restore their toxicity to the level observed for unmodified MMAE and 5-FU drugs (**Figures S39 and S40**). Although a 2-fold increase in toxicity for the prodrug activation may look modest, it is important to mention that this is considered relevant given the slow reaction rates possible at the low concentration of K₂PtCl₄ complex tolerated by cells. Indeed, this low reagent concentration was necessary to ensure the platinum complex remained nontoxic. On top of this, in vitro studies with probes 7 and 9 revealed that the presence of nucleophiles (e.g., glutathione) ends in lower conversions into the corresponding decaged products. It should be noted, however, that even in the presence of high concentrations of glutathione (e.g., 1.5 mM) the reaction still proceeds with moderate rates ($t_{1/2} = 197$ min for 7 + K₂PtCl₄; $t_{1/2} = 246$ min for 9 + K₂PtCl₄; **Table S5**). Regarding CisPt, we found that the reaction is more susceptible to the presence of nucleophiles (e.g., $t_{1/2} = 921$ min for 7 + CisPt in the presence of 0.5 mM of glutathione; **Table S6**). This deactivation of the metals in the presence of nucleophiles is in line with the modest decaging yields observed in the cell studies. This is an issue that could be further improved, for example, by using platinum-based nanoparticles known to have reduced toxicity and higher payload concentrations or by using platinum complexes stabilized with different organic ligands in a way to optimize the metal reactivity.⁶² Our data, however, demonstrate that decaging reactions with platinum complexes are possible in cell culture and could achieve release of sufficient amounts of the active drug in cells to induce cell death.

Platinum Decaging of ADC. Next, we decided to extend the tertiary amide caging group for chemically controlled drug-release from an ADC. The caging group of MMAE-am **11** was adapted for this purpose because MMAE is a common payload in ADC design.⁶⁰ Ideally a CisPt-cleavable ADC would be stable to cleavage by endogenous extra- or intracellular



To test the susceptibility of the conjugating linker to platinum decaging, compound **14** and K_2PtCl_4 (10 equiv) were incubated in DMF/water (1:1) at 37 °C for 18 h and analyzed by LC–MS (Figure S41). Release of MMAE was observed with complete consumption of **14** along with two potential

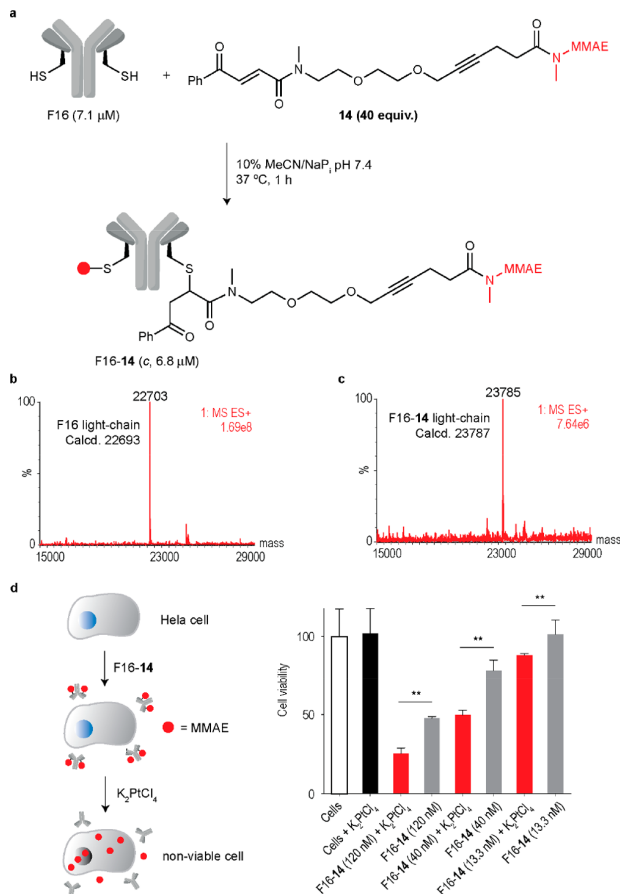


Figure 4. Platinum-mediated drug decaging from a noninternalizing ADC. a. Cysteine-selective and irreversible modification of the noninternalizing antibody F16 (anti tenascin-C) in IgG format with MMAE conjugating linker **14**. IgG(F16) contains a single reactive cysteine at the C-terminal extremity of the light chain ideal for cysteine-specific modification. Briefly, a solution of F16 (7.1 μ M) in sodium phosphate buffer (NaP_i) pH 7.4 was treated with **14** (40 equiv) in MeCN to a final concentration of 10% v/v. The reaction was heated to 37 °C for 1 h, and reaction progress was monitored by LC–MS. The ADC was purified by dialysis into fresh NaP_i buffer pH 7.4 with a 10 kDa MWCO overnight. b. Deconvoluted ESI–MS mass spectrum of the light-chain of F16. c. Deconvoluted ESI–MS mass spectrum of the light-chain of F16-**14** that shows an exact drug-to-light-chain ratio of 1. d. Schematic of the platinum-mediated decaging of MMAE from a noninternalizing ADC. e. Cell viability of HeLa cells after treatment with **F16-14** and subsequent decaging efficiency upon treatment with 20 μ M K_2PtCl_4 , twice daily. Cell viability was measured at day 3 by using AlamarBlue reagent. The statistical significance of the differences between groups was evaluated by using the unpaired *t* test. A *p* value <0.05 (**) was considered statistically significant. Error bars represent \pm s.d. (*n* = 3). Experiments were performed three times.

intermediates (Figure S41). We then went on and selected the noninternalizing F16 antibody for modification, which is specific to the alternatively spliced A1 domain of tenascin-C, found overexpressed in most solid tumors.⁶⁵ A noninternalizing ADC ensures that as little ADC as possible will be metabolized by the cells and that the maximum possible drug release is due to extracellular decaging with platinum complexes. Site-selective conjugation is expected to occur at the engineered cysteine residues in each light-chain of F16 enabling the construction of a chemically defined ADC. Furthermore, the newly formed C–S bond between the linker and the antibody is stable and does not undergo thiol-exchange reactions as in the case of frequently used maleimides.^{63,64} Complete conversion to a homogeneous ADC was achieved after reaction of F16 for 1 h at 37 °C with the carbonyl acrylic MMAE drug linker 14 in sodium phosphate buffer pH 7.4 as assessed by LC–MS (Figure 4b,c). Importantly, the heavy chain remained unmodified as expected considering the absence of reactive cysteines in the structure (Figures S42 and S43). Next, we performed the decaging in cells to release MMAE from the ADC (Figure 4d). With a cancer cell line (HeLa cells) as a model, we found F16-14 to be more toxic to cells at submicromolar concentrations in the presence of nontoxic amounts of the platinum complex K₂PtCl₄ (Figure 4d). This tertiary amide decaging reaction should stimulate platinum-mediated MMAE delivery from antibodies in the context of targeted cancer therapeutics. Furthermore, a small model protein (ubiquitin-K63C) engineered with a single cysteine residue⁶⁶ was modified with linker 14 for ease of analysis by LC–MS. When attempting decaging in vitro with CisPt, loss of MMAE followed by further degradation of the linker could be observed by LC–MS, which provides further evidence for the efficient release of the secondary amine drug from the protected tertiary amide protected conjugate (Figures S44–S47).

Cisplatin-Mediated Prodrug Decaging in Vivo. To test the *in vivo* efficacy of pFU and its combinatorial effect with CisPt, we used the zebrafish larvae xenograft model.⁶⁷ This model is a fast *in vivo* platform with resolution to analyze crucial hallmarks of cancer, such as metastatic and angiogenic potentials but it is also highly sensitive to discriminate differential anticancer therapy responses with single-cell resolution.^{68–71} We first attempted to visualize the CisPt reaction by decaging fluorogenic probe 9 in larval zebrafish (Figure 5). This probe shows an increase in fluorescence of 22-fold upon removal of the propargyl group (Figure S48). For *in vivo* imaging, a set of zebrafish larvae were incubated with probe 9 for 24 h, washed for 1 h in embryonic medium and

then further incubated with dimethyl sulfoxide (DMSO) or CisPt for 24 h (Figure 5a). Probe 9 and CisPt were used at the highest nontoxic concentration to the zebrafish embryos (9, 1 μM; CisPt, 34 μM; Figure S49). As shown in Figure 5b, the control group displays nearly no background fluorescence, but the CisPt-treated group showed an increased fluorescence (Figure 5c). This implies that probe 9 and CisPt are tissue-permeable and capable of reacting *in vivo*.

Before measuring efficacy of CisPt depropargylation, we assessed the maximum tolerated concentration for each compound: pFU 12, cFU 13, CisPt, pFU + CisPt, and cFU + CisPt in nontumor zebrafish larvae (Figure S49). Next, colorectal cancer (CRC) HCT116 zebrafish xenografts were generated as previously described.⁶⁷ Briefly, 24 h post injection (hpi), xenografts were randomly distributed into different treatments: DMSO (control), pFU (1.65 mM), cFU (1.65 mM), CisPt (0.034 mM), pFU + CisPt (1.65 mM + 0.034 mM), and cFU + CisPt (1.65 mM + 0.034 mM). Xenografts were analyzed at 4, 6, and 7 days post injection (dpi), i.e., 3, 5, and 6 days post treatment (dpt), respectively (Figure 6). At 3dpt (4dpi) (Figure 6 I), in the single treatments with pFU or CisPt, we could not observe any significant reduction of mitotic index (Figure 6 I, m), induction of apoptosis (activated caspase 3, Figure 6 I, n) or reduction of tumor size (Figure 6 I, o). In contrast, the combinatorial treatment—pFU + CisPt—induced a significant antitumoral synergistic effect manifested by a ~2 fold increase in apoptosis (Figure 6 I, n; DMSO versus pFU + CisPt **P = 0.0033; pFU versus pFU + CisPt ***P = 0.0006) accompanied by 25% reduction of tumor size (Figure 6 I, o; DMSO versus pFU + CisPt *P = 0.0279; Figure 6 I, a versus d). However, if the duration of the treatment is increased 2 (Figure 6 II) or 3 (Figure 6 III) additional days, then we could detect some toxicity in single treatment (Figure 6 II, p–r; Figure 6 III, s–u). Nevertheless, the combination of pFU with CisPt induced a clear pronounced antitumor synergistic effect. At 5 dpt (6 dpi), the combinatorial treatment led to a reduction of proliferation (Figure 6 II, p; DMSO versus pFU + CisPt ****P < 0.0001; pFU versus pFU + CisPt *P = 0.0104), a ~4 fold increase in cell death by apoptosis (Figure 6 II, q; DMSO versus pFU + CisPt ****P < 0.0001; pFU versus pFU + CisPt ****P < 0.0001) and a ~38% reduction of tumor size (Figure 6 II, r; DMSO versus pFU + CisPt ****P < 0.0001; Figure 6 II, e versus h). Finally, the 6 days of treatment (7 dpi) culminates in a ~45% tumor shrinkage (Figure 6 III, u; DMSO versus pFU + CisPt **P = 0.0010; Figure 6 III, i versus l).

Importantly, by comparing the combined treatment of the nondecaging compound cFU with CisPt to the prodrug pFU with CisPt, it is clear that pFU was able to induce a more significant cytostatic (block proliferation) and cytotoxic effect (apoptosis and reduction of tumor size) than the control cFU at both 5 dpf (6 dpi) and 6 dpt (7 dpi; Figures S50 and S51). Also, the combined effect of pFU + CisPt was more pronounced than the combination of 5-FU + CisPt, regarding proliferation (DMSO versus pFU + CisPt ****P < 0.0001; DMSO versus FU + CisPt *P = 0.0104; Figure S50i) and tumor size (DMSO versus pFU + CisPt ****P < 0.0001; DMSO versus FU + CisPt *P = 0.0273; Figure S50k). This might be related with the increased permeability of pFU (versus FU), which results in a more efficient intracellular delivery of FU after Pt decaging. In conclusion, our results show the efficient activation of the anticancer pFU in the

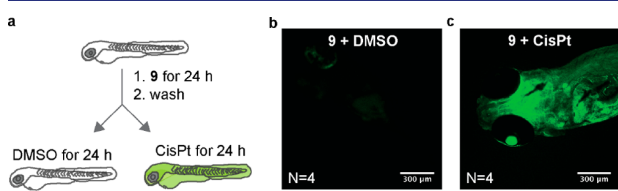


Figure 5. CisPt Decages the Fluorogenic Probe 9 *in vivo*. Zebrafish larvae were exposed to 9 diluted in embryonic medium for 24 h, followed by a 1 h wash in embryonic medium. Larvae were randomly distributed into two conditions: DMSO or CisPt for 24 h (a). Confocal image of zebrafish larvae exposed to 9 + DMSO (b) and 9 + CisPt (c).

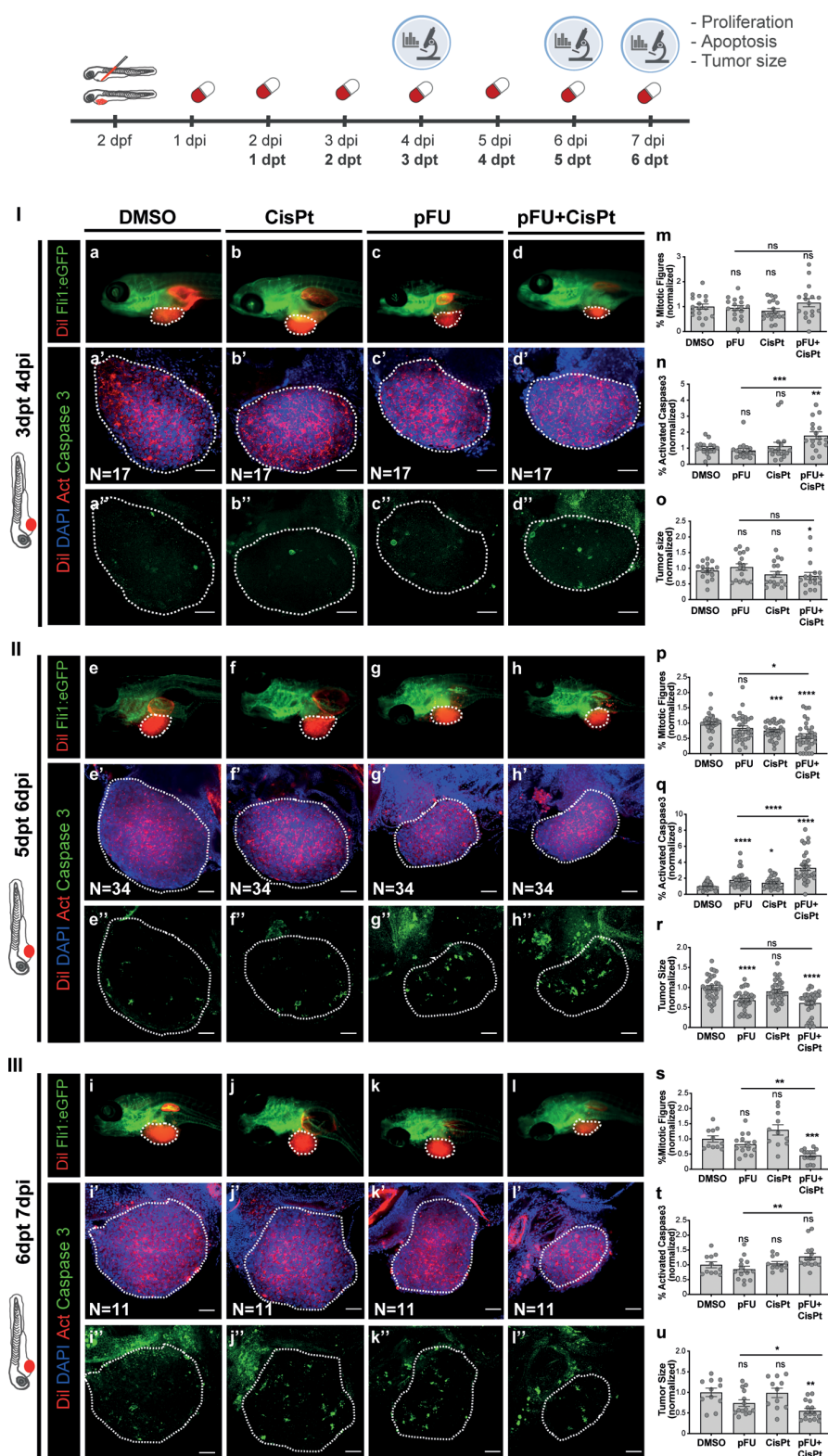


Figure 6. CisPt-mediated prodrug decaging in zebrafish xenografts. HCT116 human CRC cells were fluorescently labeled with lipophilic CM-Dil (shown in red) and injected into the perivitelline space (PVS) 2 days post fertilization (dpf) *Tg(Fli1:eGFP)* zebrafish larvae. Zebrafish xenografts were randomly distributed into treatment groups, daily treated with DMSO, CisPt, pFU, and pFU+CisPt and analyzed at 4, 6, or 7 dpi for proliferation, apoptosis and tumor size. At 4 dpi, 6 dpi, and 7 dpi, zebrafish xenografts were imaged by stereoscope (a–l) and by confocal microscopy (a''–l'' DAPI plus Dil, a''–l'' maximum projection of activated caspase 3). Proliferation (mitotic figures: m; p, *P = 0.0104, ***P = 0.0004, ****P < 0.0001; s, **P = 0.0023, ***P = 0.0002), apoptosis (activated caspase 3: n, **P = 0.0033, ***P = 0.0006; q, *P = 0.0126, ****P < 0.0001; t, **P = 0.0068) and tumor size (n° of tumor cells: o, *P = 0.0279; r, ****P < 0.0001; u, *P = 0.0411, **P = 0.0010) were analyzed and

Figure 6. continued

quantified. Graphs represent fold induction (normalized values to controls) of Avg \pm SEM. The number of xenografts analyzed is indicated in the representative images and each dot represents one zebrafish xenograft. Statistical analysis was performed using an unpaired test. Statistical results: ns > 0.05, *P ≤ 0.05, **P ≤ 0.01, ***P ≤ 0.001, and ****P ≤ 0.0001. All images are anterior to the left, posterior to right, dorsal up, and ventral down. Scale bar 50 μ m.

presence of nontherapeutic amounts of the anticancer drug CisPt in an *in vivo* setting.

CONCLUSIONS

In summary, we present a new decaging reaction of alkynes with platinum complexes for the release of secondary amines from otherwise stable tertiary amides, both in mammalian cell culture and in living organisms. This reaction was shown to proceed by platinum-mediated intramolecular cyclization mechanism. Our data suggest that water, a necessary solvent in chemical biology applications, is working as a metal-activating agent. Molecular electronic structure calculations further corroborated the mechanism of the reaction which was also supported by LC–MS characterization of the intermediates. The reaction can proceed catalytically under certain conditions and was later extended to *N*-propargyl groups with comparable efficacies to that of palladium-mediated deprotection. The caging group was adapted for the synthesis of a noninternalizing ADC, which results in drug release upon treatment with platinum complexes in cancer cells. The reaction was also adapted and demonstrated to function in a colorectal cancer zebrafish xenograft model with nontoxic amounts of CisPt to activate a prodrug of anticancer agent 5-FU, which led to a significant tumor reduction *in vivo*.

The work disclosed here represents a significant addition to the toolbox of decaging strategies for chemical biology applications. Indeed, the platinum-mediated cleavable reaction can be accomplished in aqueous systems having high concentrations of salts with high yields and reaction rates, similar to those observed for the standard palladium decaging metal. The reaction is, however, susceptible to the presence of nucleophiles resulting in slower rates (~6–15 times slower). We further demonstrate the compatibility of the reaction in cellular environments. Although the reaction is suitable for drug activation on cells inducing cytotoxicity, the presence of a range of biomolecules/nucleophiles significantly reduces the overall yield. These results are suggestive of instability of the Pt complexes, probably by formation of bioinorganic complexes. Although the active aqua Pt species have a limited lifetime in cell media, they persist long enough to be partially effective.

Our work was conceived on the hypothesis that platinum complexes could be used for prodrug activation on tumors during CisPt chemotherapy. The instability of the platinum complexes in physiological/biological conditions preclude the application envisioned. Further studies are needed to obtain Pt complexes compatible for such *in vivo* applications, but these results set the stage for future developments on platinum-mediated decaging reactions.

ASSOCIATED CONTENT

Supporting Information

The Supporting Information is available free of charge at <https://pubs.acs.org/doi/10.1021/jacs.0c01622>.

Detailed methods, characterization data and additional figures ([PDF](#))

Movie with metadynamics calculations ([MOV](#))

AUTHOR INFORMATION

Corresponding Authors

Gonçalo J. L. Bernardes — Department of Chemistry, University of Cambridge, Cambridge CB2 1EW, United Kingdom; Instituto de Medicina Molecular, Faculdade de Medicina, Universidade de Lisboa, 1649-028 Lisboa, Portugal;  orcid.org/0000-0001-6594-8917; Email: gb453@cam.ac.uk

Rita Fior — Champalimaud Centre for the Unknown, Champalimaud Foundation, 1400-038 Lisboa, Portugal; Email: rita.fior@research.fchampalimaud.org

Bruno L. Oliveira — Department of Chemistry, University of Cambridge, Cambridge CB2 1EW, United Kingdom; Instituto de Medicina Molecular, Faculdade de Medicina, Universidade de Lisboa, 1649-028 Lisboa, Portugal; Email: bruno.oliveira@medicina.ulisboa.pt

Authors

Benjamin J. Stenton — Department of Chemistry, University of Cambridge, Cambridge CB2 1EW, United Kingdom

V. B. Unnikrishnan — Department of Chemistry, University of Cambridge, Cambridge CB2 1EW, United Kingdom

Cátia Rebelo de Almeida — Champalimaud Centre for the Unknown, Champalimaud Foundation, 1400-038 Lisboa, Portugal

João Conde — Instituto de Medicina Molecular, Faculdade de Medicina, Universidade de Lisboa, 1649-028 Lisboa, Portugal;  orcid.org/0000-0001-8422-6792

Magda Negrão — Champalimaud Centre for the Unknown, Champalimaud Foundation, 1400-038 Lisboa, Portugal

Felipe S. S. Schneider — Department of Chemistry, Federal University of Santa Catarina—UFSC, Florianópolis, Santa Catarina 88040-900, Brazil;  orcid.org/0000-0001-8090-2976

Carlos Cordeiro — Laboratório de FT-ICR e Espectrometria de Massa Estrutural, Faculdade de Ciências da Universidade de Lisboa, Campo-Grande 1749-016, Lisboa, Portugal

Miguel Godinho Ferreira — Champalimaud Centre for the Unknown, Champalimaud Foundation, 1400-038 Lisboa, Portugal; Institute for Research on Cancer and Aging of Nice (IRCAN), Université Côte d'Azur, UMR7284 U1081 UNS, 06107 Nice, France

Giovanni F. Caramori — Department of Chemistry, Federal University of Santa Catarina—UFSC, Florianópolis, Santa Catarina 88040-900, Brazil;  orcid.org/0000-0002-6455-7831

Josiel B. Domingos — Department of Chemistry, Federal University of Santa Catarina—UFSC, Florianópolis, Santa Catarina 88040-900, Brazil;  orcid.org/0000-0002-6001-4522

Complete contact information is available at:

<https://pubs.acs.org/10.1021/jacs.0c01622>

Author Contributions

These authors contributed equally to this work.

Notes

The authors declare no competing financial interest.

ACKNOWLEDGMENTS

This project has received funding from the European Union's Horizon 2020 research and innovation programme under the Marie Skłodowska-Curie grant agreement Nos 675007 and 702574. We also thank the EPSRC (doctoral studentship to B.S.), FCT Portugal (FCT Investigator to G.J.L.B., IF/00624/2015; FCT Stimulus to B.L.O., CEECIND/02335/2017; LISBOA-01-0145-FEDER-022170 and FCT-PTDC/MEC-ONC/31627/2017 to R.F.), CNPq (PhD scholarship to F.S.S.S., 140485/2017-1; research grant to G.F.C., 311963/2017-0), the Champalimaud Foundation and Congento (R.F.), H2020 (EU_FT-ICR_MS, GA 731077, C.C.) and CAPES (Print call 88887.310560-00 to J.B.D. and G.J.L.B.) for funding. We also thank Prof. Dario Neri's laboratory for the generous gift of F16 antibody, Dr Ester Jiménez-Moreno for providing ubiquitin, the Champalimaud Fish and Rodents Facility for their excellent animal care, the Portuguese Mass Spectrometry Network (LISBOA-01-0145- FEDER-022125), SeTIC/UFSC, special staff members (Bruno Amattos, Guilherme Arthur Geronimo and Stephanie Andreon) for supercomputing resources, infrastructure and assistance, and Dr Vikki Cantrill for her help with the editing of this manuscript. G.J.L.B. is a Royal Society University Research Fellow (URF\R\180019) and the recipient of a European Research Council Starting Grant (TagIt, GA 676832).

REFERENCES

- (1) Hanahan, D.; Weinberg, R. A. Hallmarks of cancer: the next generation. *Cell* **2011**, *144* (5), 646–674.
- (2) Beck, A.; Goetsch, L.; Dumontet, C.; Corvaia, N. Strategies and challenges for the next generation of antibody-drug conjugates. *Nat. Rev. Drug Discovery* **2017**, *16* (5), 315–337.
- (3) Chudasama, V.; Maruani, A.; Caddick, S. Recent advances in the construction of antibody-drug conjugates. *Nat. Chem.* **2016**, *8* (2), 114–119.
- (4) Caculian, N. G.; dela Cruz Chuh, J.; Ma, Y.; Zhang, D.; Kozak, K. R.; Liu, Y.; Pillow, T. H.; Sadowsky, J.; Cheung, T. K.; Phung, Q.; Haley, B.; Lee, B.-C.; Akita, R. W.; Sliwkowski, M. X.; Polson, A. G. Cathepsin B Is Dispensable for Cellular Processing of Cathepsin B-Cleavable Antibody–Drug Conjugates. *Cancer Res.* **2017**, *77* (24), 7027–7037.
- (5) Dorywalska, M.; Dushin, R.; Moine, L.; Farias, S. E.; Zhou, D.; Navaratnam, T.; Lui, V.; Hasa-Moreno, A.; Casas, M. G.; Tran, T.-T.; et al. Molecular Basis of Valine-Citrulline-PABC Linker Instability in Site-Specific ADCs and Its Mitigation by Linker Design. *Mol. Cancer Ther.* **2016**, *15* (5), 958–970.
- (6) Rodrigues, T.; Bernardes, G. J. L. Development of Antibody-Directed Therapies: Quo Vadis? *Angew. Chem., Int. Ed.* **2018**, *57* (8), 2032–2034.
- (7) Bargh, J. D.; Isidro-Llobet, A.; Parker, J. S.; Spring, D. R. Cleavable linkers in antibody–drug conjugates. *Chem. Soc. Rev.* **2019**, *48* (16), 4361–4374.
- (8) Li, J.; Chen, P. R. Development and application of bond cleavage reactions in bioorthogonal chemistry. *Nat. Chem. Biol.* **2016**, *12* (3), 129–137.
- (9) Rossin, R.; van Duijnhoven, S. M.; Ten Hoeve, W.; Janssen, H. M.; Kleijn, L. H.; Hoeben, F. J.; Versteegen, R. M.; Robillard, M. S. Triggered Drug Release from an Antibody-Drug Conjugate Using Fast "Click-to-Release" Chemistry in Mice. *Bioconjugate Chem.* **2016**, *27* (7), 1697–1706.
- (10) Rossin, R.; Versteegen, R. M.; Wu, J.; Khasanov, A.; Wessels, H. J.; Steenbergen, E. J.; Ten Hoeve, W.; Janssen, H. M.; van Onzen, A.; Hudson, P. J.; et al. Chemically triggered drug release from an antibody-drug conjugate leads to potent antitumour activity in mice. *Nat. Commun.* **2018**, *9* (1), 1484.
- (11) Oliveira, B. L.; Guo, Z.; Bernardes, G. J. L. Inverse electron demand Diels-Alder reactions in chemical biology. *Chem. Soc. Rev.* **2017**, *46* (16), 4895–4950.
- (12) Mondal, M.; Liao, R.; Xiao, L.; Eno, T.; Guo, J. Highly Multiplexed Single-Cell In Situ Protein Analysis with Cleavable Fluorescent Antibodies. *Angew. Chem., Int. Ed.* **2017**, *56* (10), 2636–2639.
- (13) Nani, R. R.; Gorka, A. P.; Nagaya, T.; Kobayashi, H.; Schnermann, M. J. Near-IR Light-Mediated Cleavage of Antibody-Drug Conjugates Using Cyanine Photocages. *Angew. Chem., Int. Ed.* **2015**, *54* (46), 13635–13638.
- (14) Ji, X.; Pan, Z.; Yu, B.; De La Cruz, L. K.; Zheng, Y.; Ke, B.; Wang, B. Click and release: bioorthogonal approaches to "on-demand" activation of prodrugs. *Chem. Soc. Rev.* **2019**, *48* (4), 1077–1094.
- (15) Davies, S.; Stenton, B. J.; Bernardes, G. J. L. Bioorthogonal Decaging Reactions for Targeted Drug Activation. *Chimia* **2018**, *72* (11), 771–776.
- (16) Zhang, D. A.-O.; Dragovich, P. S.; Yu, S. F.; Ma, Y.; Pillow, T. H.; Sadowsky, J. D.; Su, D.; Wang, W.; Polson, A.; Khojasteh, S. C.; Hop, C. Exposure-Efficacy Analysis of Antibody-Drug Conjugates Delivering an Excessive Level of Payload to Tissues. *Drug Metab. Dispos.* **2019**, *47* (10), 1146–1155.
- (17) Durbin, K. R.; Phipps, C.; Liao, X. Mechanistic Modeling of Antibody-Drug Conjugate Internalization at the Cellular Level Reveals Inefficient Processing Steps. *Mol. Cancer Ther.* **2018**, *17* (6), 1341–1351.
- (18) Yang, M.; Li, J.; Chen, P. R. Transition metal-mediated bioorthogonal protein chemistry in living cells. *Chem. Soc. Rev.* **2014**, *43* (18), 6511–6526.
- (19) Soldevila-Barreda, J. J.; Metzler-Nolte, N. Intracellular Catalysis with Selected Metal Complexes and Metallic Nanoparticles: Advances toward the Development of Catalytic Metallodrugs. *Chem. Rev.* **2019**, *119* (2), 829–869.
- (20) Völker, T.; Meggers, E. Transition-metal-mediated uncaging in living human cells—an emerging alternative to photolabile protecting groups. *Curr. Opin. Chem. Biol.* **2015**, *25*, 48–54.
- (21) Miller, M. A.; Askevold, B.; Mikula, H.; Kohler, R. H.; Pirovich, D.; Weissleder, R. Nano-palladium is a cellular catalyst for in vivo chemistry. *Nat. Commun.* **2017**, *8* (1), 15906.
- (22) Yusop, R. M.; Unciti-Broceta, A.; Johansson, E. M.; Sanchez-Martin, R. M.; Bradley, M. Palladium-mediated intracellular chemistry. *Nat. Chem.* **2011**, *3* (3), 239–243.
- (23) Martinez-Calvo, M.; Couceiro, J. R.; Destito, P.; Rodriguez, J.; Mosquera, J.; Mascarenas, J. L. Intracellular Deprotection Reactions Mediated by Palladium Complexes Equipped with Designed Phosphine Ligands. *ACS Catal.* **2018**, *8* (7), 6055–6061.
- (24) Bray, T. L.; Salji, M.; Brombin, A.; Perez-Lopez, A. M.; Rubio-Ruiz, B.; Galbraith, L. C. A.; Patton, E. E.; Leung, H. Y.; Unciti-Broceta, A. Bright insights into palladium-triggered local chemotherapy. *Chem. Sci.* **2018**, *9* (37), 7354–7361.
- (25) Weiss, J. T.; Dawson, J. C.; Macleod, K. G.; Rybski, W.; Fraser, C.; Torres-Sanchez, C.; Patton, E. E.; Bradley, M.; Carragher, N. O.; Unciti-Broceta, A. Extracellular palladium-catalysed dealkylation of 5-fluoro-1-propargyl-uracil as a bioorthogonally activated prodrug approach. *Nat. Commun.* **2014**, *5*, 3277.
- (26) Weiss, J. T.; Carragher, N. O.; Unciti-Broceta, A. Palladium-mediated dealkylation of N-propargyl-flouxuridine as a bioorthogonal oxygen-independent prodrug strategy. *Sci. Rep.* **2015**, *5* (1), 9329.
- (27) Stenton, B. J.; Oliveira, B. L.; Matos, M. J.; Sinatra, L.; Bernardes, G. J. L. A thioether-directed palladium-cleavable linker for targeted bioorthogonal drug decaging. *Chem. Sci.* **2018**, *9* (17), 4185–4189.

- (28) Streu, C.; Meggers, E. Ruthenium-induced allylcarbamate cleavage in living cells. *Angew. Chem., Int. Ed.* **2006**, *45* (34), 5645–5648.
- (29) Volker, T.; Dempwolff, F.; Graumann, P. L.; Meggers, E. Progress towards bioorthogonal catalysis with organometallic compounds. *Angew. Chem., Int. Ed.* **2014**, *53* (39), 10536–10540.
- (30) Tomas-Gamasa, M.; Martinez-Calvo, M.; Couceiro, J. R.; Mascarenas, J. L. Transition metal catalysis in the mitochondria of living cells. *Nat. Commun.* **2016**, *7* (1), 12538.
- (31) Perez-Lopez, A. M.; Rubio-Ruiz, B.; Sebastian, V.; Hamilton, L.; Adam, C.; Bray, T. L.; Irusta, S.; Brennan, P. M.; Lloyd-Jones, G. C.; Sieger, D.; Santamaria, J.; Unciti-Broceta, A. Gold-Triggered Uncaging Chemistry in Living Systems. *Angew. Chem., Int. Ed.* **2017**, *56* (41), 12548–12552.
- (32) Tsubokura, K.; Vong, K. K.; Pradipta, A. R.; Ogura, A.; Urano, S.; Tahara, T.; Nozaki, S.; Onoe, H.; Nakao, Y.; Sibgatullina, R.; Kurbangalieva, A.; Watanabe, Y.; Tanaka, K. In Vivo Gold Complex Catalysis within Live Mice. *Angew. Chem., Int. Ed.* **2017**, *56* (13), 3579–3584.
- (33) Wang, X.; Liu, Y.; Fan, X.; Wang, J.; Ngai, W. S. C.; Zhang, H.; Li, J.; Zhang, G.; Lin, J.; Chen, P. R. Copper-Triggered Bioorthogonal Cleavage Reactions for Reversible Protein and Cell Surface Modifications. *J. Am. Chem. Soc.* **2019**, *141* (43), 17133–17141.
- (34) Labinger, J. A. Platinum-Catalyzed C–H Functionalization. *Chem. Rev.* **2017**, *117* (13), 8483–8496.
- (35) Basu, U.; Banik, B.; Wen, R.; Pathak, R. K.; Dhar, S. The Platinum X series: activation, targeting, and delivery. *Dalton Trans.* **2016**, *45* (33), 12992–13004.
- (36) Johnstone, T. C.; Suntharalingam, K.; Lippard, S. J. The Next Generation of Platinum Drugs: Targeted Pt(II) Agents, Nanoparticle Delivery, and Pt(IV) Prodrugs. *Chem. Rev.* **2016**, *116* (5), 3436–3486.
- (37) Ivanov, A. I.; Christodoulou, J.; Parkinson, J. A.; Barnham, K. J.; Tucker, A.; Woodrow, J.; Sadler, P. J. Cisplatin binding sites on human albumin. *J. Biol. Chem.* **1998**, *273* (24), 14721–14730.
- (38) Florea, A.-M.; Büsselfberg, D. Cisplatin as an anti-tumor drug: cellular mechanisms of activity, drug resistance and induced side effects. *Cancers* **2011**, *3* (1), 1351–1371.
- (39) Kenny, R. G.; Marmion, C. J. Toward Multi-Targeted Platinum and Ruthenium Drugs—A New Paradigm in Cancer Drug Treatment Regimens? *Chem. Rev.* **2019**, *119* (2), 1058–1137.
- (40) Dasari, S.; Tchounwou, P. B. Cisplatin in cancer therapy: molecular mechanisms of action. *Eur. J. Pharmacol.* **2014**, *740*, 364–378.
- (41) Stewart, D. J.; Molepo, J. M.; Green, R. M.; Montpetit, V. A.; Hugenholtz, H.; Lamothe, A.; Mikhael, N. Z.; Redmond, M. D.; Gadla, M.; Goel, R. Factors affecting platinum concentrations in human surgical tumour specimens after cisplatin. *Br. J. Cancer* **1995**, *71* (3), 598–604.
- (42) van Hennik, M. B.; van der Vijgh, W. J.; Klein, I.; Elferink, F.; Vermorken, J. B.; Winograd, B.; Pinedo, H. M. Comparative pharmacokinetics of cisplatin and three analogues in mice and humans. *Cancer Res.* **1987**, *47* (23), 6297–6301.
- (43) Jacobs, S.; McCully, C. L.; Murphy, R. F.; Bacher, J.; Balis, F. M.; Fox, E. Extracellular fluid concentrations of cisplatin, carboplatin, and oxaliplatin in brain, muscle, and blood measured using microdialysis in nonhuman primates. *Cancer Chemother. Pharmacol.* **2010**, *65* (5), 817–824.
- (44) Klein, A. V.; Hambley, T. W. Platinum Drug Distribution in Cancer Cells and Tumors. *Chem. Rev.* **2009**, *109* (10), 4911–4920.
- (45) Holding, J. D.; Lindup, W. E.; Bowdler, D. A.; Siodlak, M. Z.; Stell, P. M. Disposition and tumour concentrations of platinum in hypoalbuminaemic patients after treatment with cisplatin for cancer of the head and neck. *Br. J. Clin. Pharmacol.* **1991**, *32* (2), 173–179.
- (46) Pujol, J. L.; Cupissol, D.; Gestin-Boyer, C.; Bres, J.; Serrou, B.; Michel, F. B. Tumor-tissue and plasma concentrations of platinum during chemotherapy of non-small-cell lung cancer patients. *Cancer Chemother. Pharmacol.* **1990**, *27* (1), 72–75.
- (47) Del Monte, U. Does the cell number 10(9) still really fit one gram of tumor tissue? *Cell Cycle* **2009**, *8* (3), 505–506.
- (48) Abu Sohel, S. M.; Liu, R.-S. Carbocyclisation of alkynes with external nucleophiles catalysed by gold, platinum and other electrophilic metals. *Chem. Soc. Rev.* **2009**, *38* (8), 2269–2281.
- (49) Tomás-Mendivil, E.; Toullec, P. Y.; Díez, J.; Conejero, S.; Michelet, V.; Cadierno, V. Cycloisomerization versus Hydration Reactions in Aqueous Media: A Au(III)-NHC Catalyst That Makes the Difference. *Org. Lett.* **2012**, *14* (10), 2520–2523.
- (50) Belger, K.; Krause, N. Smaller, faster, better: modular synthesis of unsymmetrical ammonium salt-tagged NHC–gold(i) complexes and their application as recyclable catalysts in water. *Org. Biomol. Chem.* **2015**, *13* (31), 8556–8560.
- (51) Alemán, J.; del Solar, V.; Navarro-Ranninger, C. Anticancer platinum complexes as non-innocent compounds for catalysis in aqueous media. *Chem. Commun.* **2010**, *46* (3), 454–456.
- (52) Ghosh, A. K.; Brindisi, M. Organic Carbamates in Drug Design and Medicinal Chemistry. *J. Med. Chem.* **2015**, *58* (7), 2895–2940.
- (53) Tu, J.; Xu, M.; Parvez, S.; Peterson, R. T.; Franzini, R. M. Bioorthogonal Removal of 3-Isocyanopropyl Groups Enables the Controlled Release of Fluorophores and Drugs in Vivo. *J. Am. Chem. Soc.* **2018**, *140* (27), 8410–8414.
- (54) Morihiro, K.; Ankenbruck, N.; Lukasak, B.; Deiters, A. Small Molecule Release and Activation through DNA Computing. *J. Am. Chem. Soc.* **2017**, *139* (39), 13909–13915.
- (55) Corinti, D.; Coletti, C.; Re, N.; Piccirillo, S.; Giampà, M.; Crestoni, M. E.; Fornarini, S. Hydrolysis of cis- and transplatin: structure and reactivity of the aqua complexes in a solvent free environment. *RSC Adv.* **2017**, *7* (26), 15877–15884.
- (56) Berners-Price, S. J.; Appleton, T. G. The Chemistry of Cisplatin in Aqueous Solution. In *Platinum-Based Drugs in Cancer Therapy*; Kelland, L. R., Farrell, N. P., Eds.; Humana Press: Totowa, NJ, 2000; pp 3–35.
- (57) Dolezel, P.; Kuban, V. Mass spectrometric study of platinum complexes based on cisplatin. *Chem. Zvesti* **2002**, *56* (4), 236–240.
- (58) Vidal, C.; Tomás-Gamasa, M.; Destito, P.; López, F.; Mascareñas, J. L. Concurrent and orthogonal gold(I) and ruthenium(II) catalysis inside living cells. *Nat. Commun.* **2018**, *9* (1), 1913.
- (59) Coelho, S. E.; Schneider, F. S. S.; de Oliveira, D. C.; Tripodi, G. L.; Eberlin, M. N.; Caramori, G. F.; de Souza, B.; Domingos, J. B. Mechanism of Palladium(II)-Mediated Uncaging Reactions of Propargylic Substrates. *ACS Catal.* **2019**, *9* (5), 3792–3799.
- (60) Senter, P. D.; Sievers, E. L. The discovery and development of brentuximab vedotin for use in relapsed Hodgkin lymphoma and systemic anaplastic large cell lymphoma. *Nat. Biotechnol.* **2012**, *30* (7), 631–637.
- (61) Kelland, L. R.; Abel, G.; McKeage, M. J.; Jones, M.; Goddard, P. M.; Valenti, M.; Murrer, B. A.; Harrap, K. R. Preclinical Antitumor Evaluation of Bis-acetato-ammine-dichloro-cyclohexylamine Platinum(IV): an Orally Active Platinum Drug. *Cancer Res.* **1993**, *53* (11), 2581–2586.
- (62) Cheng, Q.; Liu, Y. Multifunctional platinum-based nanoparticles for biomedical applications. *Wiley Interdiscip. Rev. Nanomed. Nanobiotechnol.* **2017**, *9* (2), No. e1410.
- (63) Bernardim, B.; Cal, P. M. S. D.; Matos, M. J.; Oliveira, B. L.; Martínez-Sáez, N.; Albuquerque, I. S.; Perkins, E.; Corzana, F.; Burtoloso, A. C. B.; Jiménez-Osés, G.; et al. Stoichiometric and irreversible cysteine-selective protein modification using carbonylacrylic reagents. *Nat. Commun.* **2016**, *7* (1), 13128.
- (64) Bernardim, B.; Matos, M. J.; Ferhati, X.; Compañón, I.; Guerreiro, A.; Akkapeddi, P.; Burtoloso, A. C. B.; Jiménez-Osés, G.; Corzana, F.; Bernardes, G. J. L. Efficient and irreversible antibody–cysteine bioconjugation using carbonylacrylic reagents. *Nat. Protoc.* **2019**, *14* (1), 86–99.
- (65) Gébleux, R.; Stringhini, M.; Casanova, R.; Soltermann, A.; Neri, D. Non-internalizing antibody-drug conjugates display potent anti-cancer activity upon proteolytic release of monomethyl auristatin E in the subendothelial extracellular matrix. *Int. J. Cancer* **2017**, *140* (7), 1670–1679.

- (66) Lee, B.; Sun, S.; Jiménez-Moreno, E.; Neves, A. A.; Bernardes, G. J. L. Site-selective installation of an electrophilic handle on proteins for bioconjugation. *Bioorg. Med. Chem.* **2018**, *26* (11), 3060–3064.
- (67) Fior, R.; Póvoa, V.; Mendes, R. V.; Carvalho, T.; Gomes, A.; Figueiredo, N.; Ferreira, M. G. Single-cell functional and chemosensitive profiling of combinatorial colorectal therapy in zebrafish xenografts. *Proc. Natl. Acad. Sci. U. S. A.* **2017**, *114* (39), No. E8234.
- (68) Fazio, M.; Ablain, J.; Chuan, Y.; Langenau, D. M. Zebrafish patient avatars in cancer biology and precision cancer therapy. *Nat. Rev. Cancer* **2020**, *20* (9), 263–273.
- (69) Fazio, M.; Zon, L. I. Fishing for answers in precision cancer medicine. *Proc. Natl. Acad. Sci. U. S. A.* **2017**, *114* (39), 10306.
- (70) Yan, C.; Brunson, D. C.; Tang, Q.; Do, D.; Iftimia, N. A.; Moore, J. C.; Hayes, M. N.; Welker, A. M.; Garcia, E. G.; Dubash, T. D.; et al. Visualizing Engrafted Human Cancer and Therapy Responses in Immunodeficient Zebrafish. *Cell* **2019**, *177* (7), 1903–1914.
- (71) Costa, B.; Ferreira, S.; Póvoa, V.; Cardoso, M. J.; Vieira, S.; Stroom, J.; Fidalgo, P.; Rio-Tinto, R.; Figueiredo, N.; Parés, O.; Greco, C.; Ferreira, M. G.; Fior, R. Developments in zebrafish avatars as radiotherapy sensitivity reporters — towards personalized medicine. *EBioMedicine* **2020**, *51*, 102578.

6 Paper III: Overreact, an in silico lab: automatic quantum chemical microkinetic simulations for complex chemical reactions

SCHNEIDER, F. S. S.; CARAMORI, G. F. Overreact, an in silico lab: Automatic quantum chemical microkinetic simulations for complex chemical reactions. *Journal of Computational Chemistry*, Wiley, Apr 2022. ISSN 1096-987x. Disponível em: <<http://dx.doi.org/10.1002/jcc.26861>>.

`overreact` is a software package for microkinetic modelling using data from first-principles quantum chemical calculations [1, 2]. It is an improvement on a first attempt to build a chemical kinetics simulator that uses first-principles quantum chemical calculations [72] (for a list of other software contributions that have taken place during the course of the PhD, see Appendix A). Lessons learned from this first iteration, as well as the methodology underlying `overreact`, can be found in Section 3.4.

6.1 Paper

The publication can be read in full next.

Overreact, an *in silico* lab: Automative quantum chemical microkinetic simulations for complex chemical reactions

Felipe S. S. Schneider | Giovanni F. Caramori

Department of Chemistry, Federal University of Santa Catarina, Florianópolis, Santa Catarina, Brazil

Correspondence

Giovanni F. Caramori, Department of Chemistry, Federal University of Santa Catarina, Florianópolis, SC 88040-900, Brazil.
 Email: giovanni.caramori@ufsc.br

Funding information

National Council for Scientific and Technological Development, Grant/Award Numbers: 140485/2017-1, 311132/2020-0

Abstract

Today's demand for precisely predicting chemical reactions from first principles requires research to go beyond Gibbs' free energy diagrams and consider other effects such as concentrations and quantum tunneling. The present work introduces overreact, a novel Python package for propagating chemical reactions over time using data from computational chemistry only. The overreact code infers all differential equations and parameters from a simple input that consists of a set of chemical equations and quantum chemistry package outputs for each chemical species. We evaluate some applications from the literature: gas-phase eclipsed-staggered isomerization of ethane, gas-phase umbrella inversion of ammonia, gas-phase degradation of methane by chlorine radical, and three solvation-phase reactions. Furthermore, we comment on a simple solvation-phase acid-base equilibrium. We show how it is possible to achieve reaction profiles and information matching experiments.

KEY WORDS

chemical reactions, concentration effects, *in silico* experiments, microkinetic modeling, overreact, Python3

1 | INTRODUCTION

Many of the challenges of this century, such as producing fuels and chemicals from biomass^{1–4} and greenhouse gases,^{5–8} as well as developing greener synthetic protocols,^{9–12} encompass problems related with both chemical kinetics and catalysis. Improving the understanding of reaction mechanisms is mandatory to meet the demand in designing efficient catalysts and molecular machines of increasingly complex behavior, needed to overcome such challenges in a sustainable and efficient manner.^{4,13–15}

The demand for rational design of reactions, catalysts, and chemical devices is leading our community towards the development of accurate and efficient computational modeling tools and methodologies.^{13,16–18} Despite the challenges in predicting observed reaction rate constants correctly, by using first principle calculations, the recent growth¹⁹ of computing resources and methodological developments have made the calculation of complex reaction mechanisms almost routine.^{16,18,20–26} This has uniquely aided both the elucidation of experiments and the comprehension of complex chemical phenomena.^{13,16}

Notwithstanding, feasible mechanistic propositions must be calculated with adequate levels of theory²⁷ and take into account all the relevant physics of the problem. The computational modeling of chemical reactions is a complex topic due to the overwhelming set of physical considerations that are required,²⁸ and the quest for mechanistic understandings actually requires a significant amount of automation,^{16,18} being therefore necessary to consider effects such as pre-equilibrium and concentration,²³ dispersion corrections,^{29,30} solvation,^{30–32} molecular symmetry,³⁰ proper treatment of Gibbs energy contributions,^{29,30,32,33} standard state corrections,^{30–32} tunneling and others.^{28,30}

Even so, most of the modeling of chemical reactions based on first-principles calculations is done using reaction rate constants alone, which is oftentimes not enough. Comparison with the experiment requires reaction rates, which depend on concentrations. For instance, the outcome and selectivity of two competing second-order reactions such as $R + A \rightarrow P_A$ and $R + B \rightarrow P_B$, whose kinetic equations are given by $d[P_A]/dt = k_1 [R][A]$ and $d[P_B]/dt = k_2 [R][B]$, are undoubtedly dependent not only on the rate constants k_1 and k_2 , but also on the concentrations $[A]$ and $[B]$.²³ Furthermore, it is well known that a

TABLE 1 Comparison of programs in the literature for theoretical chemical kinetics. Partially adapted from Dzib et al.³⁸ (only available software indicated).

Program	Theory	Molecularity	Phase	Tunnel effect	Language
overreact	TST	Any	Gas, solution	Wigner, Eckart	Python
Eyringpy	TST, MT, CKT	Uni/bi	Gas, solution	Wigner, Eckart	Python
Polyrate	TST, VTST, RRKM	Uni/bi	Gas, solid, gas-solid	ZCT, SCT, LCT	Fortran
MultiWell	ME, RRKM	Uni	Gas	-	Fortran
TAMkin	TST	Uni/bi	Gas	Wigner, Eckart	Python
MESMER	ME, RRKM	Uni/bi	Gas, solution	Eckart	C++
KiSThelp	TST, VTST, RRKM	Uni/bi	Gas	Wigner, Eckart	Java
RMG	TST, CKT	Uni/bi	Gas, solution	Wigner, Eckart	Python
APUAMA	TST	Uni/bi	Gas	Wigner, Eckart, SCT	C++
Pilgrim ⁵⁹	TST, VTST, CVT	Uni/bi	Gas	SCT	Python

Abbreviations: CKT, Collins–Kimball Theory; CVT, canonical variational transition state theory; LCT, large curvature tunneling; ME, master equation; MT, Marcus theory; RRKM, Rice–Ramsperger–Kassel–Marcus; SCT, small curvature tunneling; VTST, variational transition state theory; ZCT, zero curvature tunneling.

single reaction step may not be enough to determine a whole chemical reaction path or catalytic cycle,^{34–36} bringing ambiguity in the general concept of “rate-determining step.”³⁵ The reasoning becomes still more entangled when a single observed reaction rate law is taken into consideration, such as when two steps with similar barriers within a single mechanism exist or when concurrent mechanisms coexist with an equal probability of occurring. Those problems have led to the development of new analytical tools, broadening the interpretation of reactions and, in particular, catalytic processes.^{34,36,37}

A useful solution to these issues is to simulate reaction models whose parameters are taken from computational chemistry calculations. For instance, modeling reactions using microkinetic simulations has become increasingly important, especially when it is essential to take concentration effects into account.²³ First-principle calculations have allowed us to calculate binding free energies³⁰ and reaction rate constants³⁸ reasonably close to experimental values, as long as the correct physical phenomena are appropriately addressed. This idea is not new in the experimental laboratory: Blackmond have advocated using full-blown kinetics simulations to elucidate experimentally observed reaction mechanisms through model exploration.^{34,36} This analysis protocol has been shown to be crucial for elucidating many mechanisms of industrial importance. Similarly, microkinetic models provide time-resolved kinetic analysis that allows one to consolidate, analyze and test hypotheses in catalysis and chemical kinetics in general,^{34,36} and it has extensively used in computational heterogeneous catalysis,^{15,39–55} experimental biology⁵⁶ and mechanism validation.⁵⁷ It is thus possible to accurately perform first-principles microkinetic simulations on rather complex reaction phenomena over time, which allows one to better comprehend tricky aspects not revealed by more simplistic models.^{34,36} Even with possible systematic errors brought by first-principle calculations, insights are warranted.^{35,37,58}

Unfortunately, there is currently no general solution for first-principles microkinetic modeling that, simultaneously, (1) calculates all the required thermochemical quantities and corrections from first-principles, (2) automatically calculates reaction rate constants, including

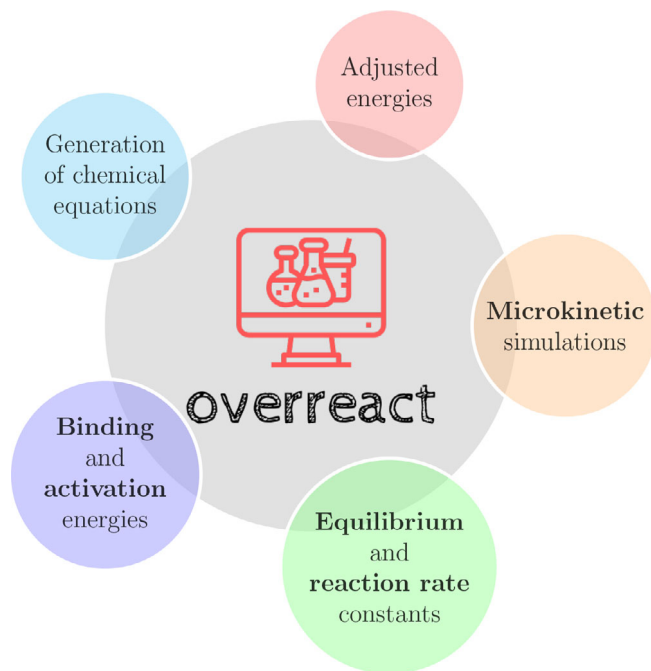
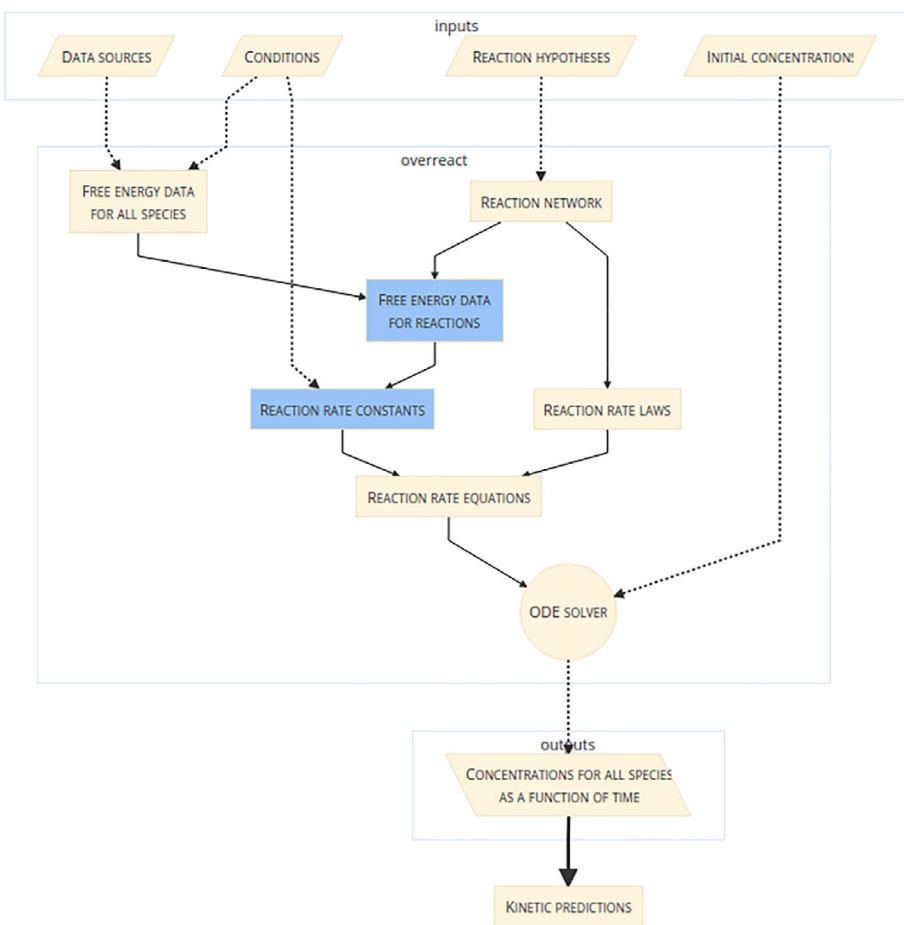


FIGURE 1 Visual depiction of some of the capabilities of overreact, a Python library and command-line tool for building and analyzing homogeneous microkinetic models from first-principles calculations. Instructions on how to install and use can be found at <https://geem-lab.github.io/overreact-guide>

quantum tunneling approximations, for all reactions, (3) generates an (usually non-linear) ordinary differential equation (ODE) system from an arbitrary reaction scheme automatically, (4) produces a Jacobian for the ODE system using automatic differentiation for improved accuracy and performance, and (5) propagates the chemical kinetic processes generating concentrations for all compounds as a function of time and initial concentrations. Table 1 compares the capabilities of overreact with some other known microkinetic software in the literature.

FIGURE 2 A simplified diagram featuring the overreact dataflow. Computational chemistry logfiles are taken as data sources. Together with temperature conditions, a chemical reaction network and initial concentrations, overreact calculates Gibbs' free energies for all species. From this information, reaction rate constants and a system of ordinary differential equations (ODEs) are devised. This ODE system is solved, yielding concentrations for all species over time. Further details can be found in the supporting information



The present work presents a simple yet robust software that treats all the five points listed above in an automated way, starting from the outputs of ab initio calculations of numerous levels of theory (Density Functional Theory, Hartree-Fock, post-Hartree-Fock or any other where Hessian calculations are available).⁶⁰ It is able to solve any chemical reaction network, including parallel and concurrent reactions, from elementary steps at constant temperature in the well-stirred approximation. The key features of the proposed code, called overreact, are highlighted in Figure 1. It has been developed as a user-friendly, open-source (MIT license) Python program and library that does simple and automatic microkinetic modeling of complex reaction networks in solution and gas-phase using only the user description of the reactions to be considered in the model, the corresponding computational chemistry output files, initial concentrations, and a set of reaction conditions such as temperature. Only the converged geometries, electronic energies, and vibrational frequencies of each species in the model are required from the outputs. Overreact is freely available, simple to install and use, well tested, well documented, and encompasses an easy-to-use command-line application (<https://geem-lab.github.io/overreact-guide/>). Although only thoroughly tested with ORCA⁶¹ and Gaussian 09⁶² output files at the moment, it employs the Python library cclib⁶³ for parsing computational chemistry outputs, which is actually known to work with 14 different computational chemistry packages. Overreact not only

generates and solves arbitrary chemical kinetic ODE problems, but also allows the user to fix the concentration of one or more compounds, which is useful for simulating reactions in neat or buffered conditions. Furthermore, the user can adjust systematic first-principle absolute Gibbs energy errors by comparison with experiments automatically, which are expected to be up to 4 kcal mol⁻¹ even when suitable density functional are employed.^{26,64-67}

2 | METHODOLOGY

The overreact code attempts to make the process of building precise chemical microkinetic models from first principle calculations as automatic as possible. It takes data from computational chemistry logfiles and uses them to calculate thermodynamic and kinetic properties, as shown in the dataflow diagram in Figure 2. This information gives rise to reaction rate constants and a system of ordinary differential equations, which, together with initial concentrations, yields concentrations of all species over time.

The dataflow diagram of Figure 2 is simplification of the whole process, not a complete description of the system. A detailed description of the library's core functionalities can be found in the Supporting Information, where automated procedures, methodologies and capabilities implemented in overreact are highlighted.

3 | RESULTS AND DISCUSSION

Representative results of overreact usage are available in the following subsections. Defaults are used when not otherwise specified.

3.1 | Examples in the gas phase

3.1.1 | Simple gas-phase autoisomerizations

In order to demonstrate that overreact can estimate precise reaction rate constants from ab initio calculations, we first consider some simple gas-phase autoisomerization reactions.

Ethane

We estimated the rate of autoisomerization of the ethane from staggered to eclipsed back to staggered again. At B97-3c,⁶⁸ the rate calculated was found to be $8.2 \times 10^{10} \text{ s}^{-1}$ (including tunneling coefficient of 1.11). Higher levels of theory gave similar results (4.8×10^{10} and $6.3 \times 10^{10} \text{ s}^{-1}$, including tunneling coefficients of 1.13 and 1.12, for 6-311G(d,p) and UMP2/6-311G(3df,3pd), respectively). There is overall good agreement with the experimental estimate of $8.3 \times 10^{10} \text{ s}^{-1}$.⁶⁹

Ammonia

The reaction rate constant for the umbrella inversion of ammonia was estimated to be $1.3 \times 10^{10} \text{ s}^{-1}$ at MP2/ma-def2-TZVP (tunneling coefficient $\kappa = 2.00$), which agrees with the experimental value of $4 \times 10^{10} \text{ s}^{-1}$.⁷⁰ On the other hand, the barrier at MP2/ma-def2-TZVP was found to be 4.1 kcal mol⁻¹, lower than the experimental one (5.8 kcal mol⁻¹).⁷⁰ A calculation at CCSD(T)/cc-pVTZ better agrees with the thermodynamical barrier (6.0 kcal mol⁻¹), but degrades the reaction rate constant ($5.9 \times 10^8 \text{ s}^{-1}$, with $\kappa = 2.37$). Similar results were found using DFT ($\Delta G^\ddagger = 5.4 \text{ kcal mol}^{-1}$ and $k = 3.6 \times 10^9 \text{ s}^{-1}$ with $\kappa = 4.88$ at ω B97X-D4-gCP/def2-TZVP), suggesting that the Eckart approximation is not enough to get quantitative results in this particular case, as one of the key assumptions of the model is that the reaction takes place through a linear path in the potential energy surface.

3.1.2 | $\text{CH}_4 + \text{Cl} \rightarrow \text{CH}_3 + \text{HCl}$

Tanaka et al. studied the degradation of methane by chlorine radical gas in the context of the global methane cycle in the atmosphere.⁷¹ In line with the results reported by Dzib et al.,³⁸ we obtained a reaction rate constant of $9.3 \times 10^{-14} \text{ cm}^3 \text{ molecule}^{-1} \text{ s}^{-1}$ ($\kappa = 3.64$) at UMP2/cc-pVTZ for this bimolecular reaction, in line with previous computational results of Tanaka et al.⁷¹ ($2.2 \times 10^{-13} \text{ cm}^3 \text{ molecule}^{-1} \text{ s}^{-1}$) and the current recommended experimental value of $1.0 \times 10^{-13} \text{ cm}^3 \text{ molecule}^{-1} \text{ s}^{-1}$.⁷² Overall, the calculated reaction rate constants using the Eckart tunneling approximation fall in the lower range of the experimental 95% confidence interval in the range 181–300 K (Figure 3A), in excellent agreement with experimental results in that range ($r^2 = 0.9984$, Figure 3B). Furthermore, a one-second

microkinetic modeling of this fast gas-phase reaction example (using as initial concentrations 250, 100, and 25 nM for CH₄, Cl, and HCl, respectively) is shown in Figure 3c, where the concentrations of all species are obtained as a function of time.

3.2 | Examples in solution

3.2.1 | Constrained equilibria: acetic acid-acetate equilibrium concentrations versus pH

overreact is able to calculate simple equilibrium systems without knowledge of reaction rate constants by producing them such that equilibrium constants are satisfied. When used together in a reaction network, the algorithm ensures that the fictitious, calculated forward and backwards reaction rate constants are larger than any other reaction rate constant in the system by a factor of eight. Although it makes equations stiffer, this allows investigating systems containing both equilibria and fast reactions together, as is indicated in the following sections.

On the other hand, pure equilibria can still be useful. Even though it is not possible to obtain quantitative kinetic profiles with equilibria alone, it is perfectly reasonable to obtain final Boltzmann populations from them. In fact, together with a simple constraint optimizer implemented in overreact, it is possible to fix the concentrations of any part of the system and check how this would affect the final populations.

In order to assess the correctness of pure equilibria calculations in overreact, as well as the concentration constraining feature, we estimated the final concentrations in solution of the acetic acid-acetate, acid-base equilibrium system. For that, we employed a combination of ab initio calculations and experimental pK_a values to account for systematic errors.^{31,73} Different values of pH were fixed by constraining the H⁺ concentration.

Optimizations and frequencies for the AcOH(aq) ⇌ AcO⁻(aq) + H⁺(aq) system were performed at UM06-2X/6-311++G(d,p)/SMD (water).^{31,74,75} All data for H⁺ was inserted directly in the overreact input. For comparison, two distinct energies for the proton solvation energy were separately employed: -265.9 kcal mol⁻¹, as used in the parameterization process of SMD,³¹ and -277.2 kcal mol⁻¹, which is the value that correctly predicts the experimental pK_a of 4.756 for this system.⁷⁶ The final calculated concentrations as a function of pH for both proton solvation energies can be seen in Figure 4. As can be seen, although errors are very sensitive to the energy values provided, overreact produces the expected result if precise energy values are provided.

3.2.2 | Hickel (1992)

We compared the applicability of overreact for reactions in solvation using the well-known radical reaction NH_{3(w)} + OH_(w) → NH_{2(w)} + H₂O_(w) at M06-2X-D3(0)/6-311++G(d,p)/SMD(water)^{31,74,75} (using ORCA 4.2.1⁶¹). The calculated reaction rate constant can be seen in Figure 5, together with a comparison with experimental and theoretical results available in the literature (exact figures are available in

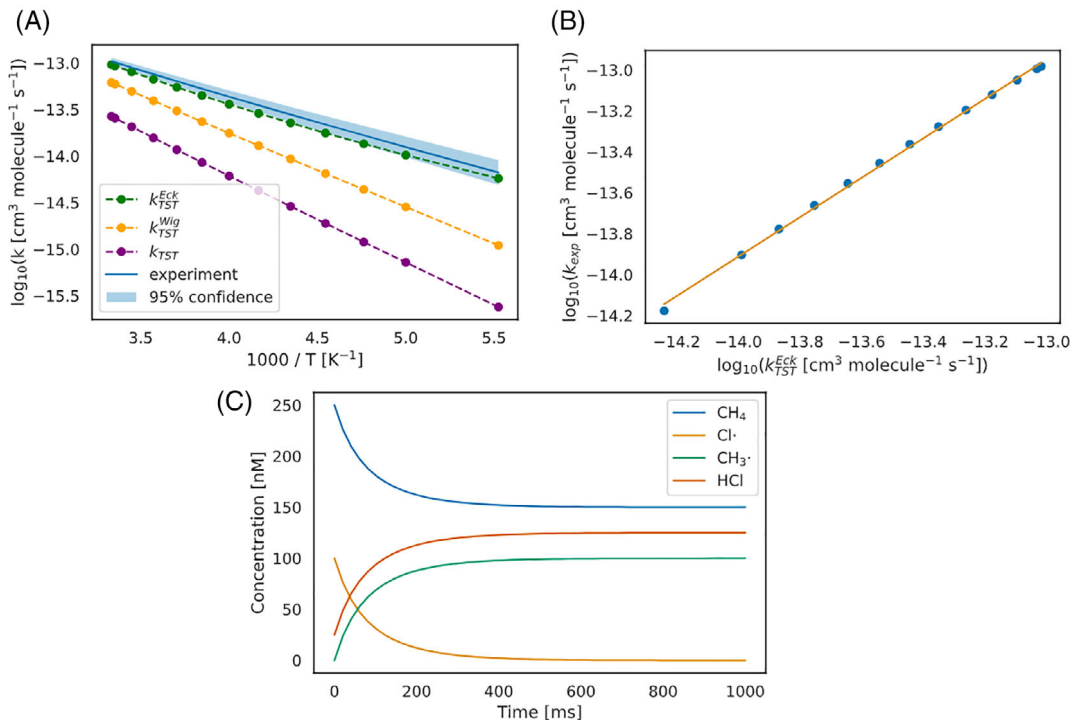


FIGURE 3 Computed chemical kinetics of $\text{CH}_4 + \text{Cl} \rightarrow \text{CH}_3 + \text{HCl}$ in the gas phase. (A) Arrhenius plots in the range 181–300 K with different tunneling approximations compared against the recommended experimental fit of Burkholder et al. and its 95% confidence interval.⁷² Compare to Figures 1 and 2 of Dzib et al.³⁸ and Tanaka et al.,⁷¹ respectively. (B) Linear regression between the calculated, Eckart-corrected reaction rate constants against the experimental results, in logarithmic scale ($\log_{10}\left(\frac{k^{\text{Eck}}}{k_{\text{TST}}}\right) = 0.9633 \times \log_{10}(k_{\text{exp}}) + 0.4256, r^2 = 0.9984$). (C) Microkinetic simulation of the gas-phase reaction $\text{CH}_4 + \text{Cl} \rightarrow \text{CH}_3 + \text{HCl}$ (using 250, 100, and 25 nM as initial concentrations of CH_4 , Cl^- , and HCl , respectively)

FIGURE 4 Computed acid-base equilibrium for $\text{AcOH}(\text{aq}) \rightleftharpoons \text{AcO}^-(\text{aq}) + \text{H}^+(\text{aq})$ at UM06-2X/6-311++G(d,p)/SMD(water)^{31,74,75} for a series of pH values

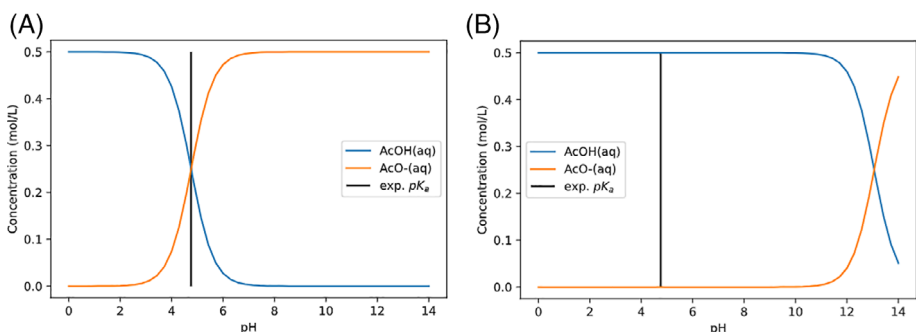


Table S1). The experimental results were all measured at high pH and, since the effect of the ammonia-ammonium equilibrium is negligible in those conditions,^{38,77} the phenomenon was not considered in this case for simplicity.

3.2.3 | Pérez-Soto (2020)

Pérez-Soto et al. have applied computer experiments to a well-studied imine formation reaction using techniques very similar to the ones in the present work.⁶⁷ Since those reactions encompass a proton transfer, they suffer from effects of residual water, as water can facilitate proton shuttling. Even though the reaction happens in dichloromethane, water is found as

an impurity in the commercially-available solvent and, most importantly, it is produced as a by-product in the second, dehydrating step.⁶⁷

Such cases are not uncommon and can hardly be properly rationalized by simple free energy diagrams, requiring microkinetics or other techniques that take into account changes of concentration throughout the reaction.^{24,25}

The work of Pérez-Soto et al. is particularly important due to their investigation on systematic errors in bimolecular reaction barriers.⁶⁷ This takes place due to the impossibility, for bimolecular reactions, of the common error cancellation found in monomolecular reactions. They not only showed the systematicity of such errors, but also that they could be reduced, for a given reaction, by properly adjusting all Gibbs' free energies with a single tunable parameter.⁶⁷

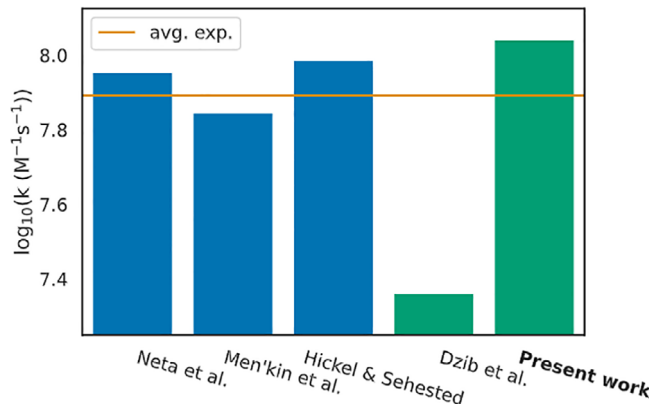


FIGURE 5 Comparison of experimental and computational results from the literature for the reaction rate constant of the reaction $\text{NH}_{3(w)} + \text{OH}_{(w)} \rightarrow \text{NH}_{2(w)} + \text{H}_2\text{O}_{(w)}$ at M06-2X-D3(0)/6-311++G(d,p)/SMD (water)^{31,74,75} (using ORCA 4.2.1⁶¹). All values indicated are in logarithmic scale. Blue and green bars represent experimental and computational results, respectively. The orange line is the \log_{10} value of the average of experimental values. The exact values can be found in Table S1

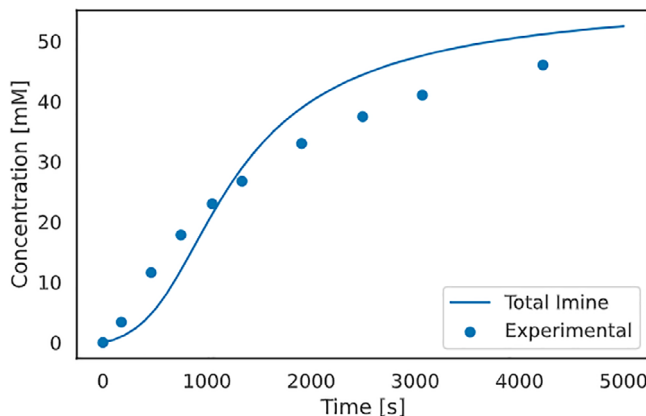


FIGURE 6 Predicted kinetic profile for the reaction of Pérez-Soto et al.⁶⁷ experimental data taken from the supporting information of Pérez-Soto et al.⁶⁷ is also shown. A systematic bias of 3.2 kcal mol⁻¹ was employed in agreement with the original work,⁶⁷ which translates to a root-mean-squared deviation (RMSD) of 4.97 mM. The summed concentration of the imine product is shown, as it is found in association with different amine and water quantities. A detailed profile with all relevant species can be found in Figure S3

In Figure 6 a reproduction of their work is shown and compared against experimental concentration data points. The exact same Gibb's free energy adjustment of 3.2 kcal mol⁻¹ as employed in the original work was used by us, which is equivalent to a root-mean-squared error of 4.97 mM when compared against the experimental data points. Apart from that, the present results differ from Pérez-Soto et al. in that we employed all additional approximations implemented in overreact: Eckart tunneling corrections for all reaction steps and the quasi-rigid rotor-harmonic approximation for both enthalpies and entropies. The fact that a systematic energy correction

was still required to attain experimental-grade quality suggests yet another source of error.

A systematic study on the effect of the tunable parameter can be seen in Figure S2, which shows a flat region around 2–3 kcal mol⁻¹. This suggests that, even though such energy adjustments might be seen as arbitrary, they may make little influence on the final result as long as the chosen value is reasonable. Due to DFT errors in general, fitting systematic deviations in first-principles reaction schemes seems to be warranted and, in the future, this could be performed automatically using available experimental data. Progress is currently being made in this respect in our laboratory.

3.2.4 | Intramolecular amide hydrolysis of N-alkyl maleamic acids

We have looked into intramolecular amide hydrolysis initially investigated by Kirby and Lancaster⁷⁸ and subsequently studied by others.^{79–81} We employed calculations using ωB97XD/6-311++G**/SMD(water)^{31,74,82} and used Gaussian 09 (Revision C.01).⁶² As before, the proton energy was adjusted in order to reproduce the experimental pK_a of 4.756 for acetic acid.⁷⁶ Three distinct mechanisms proposed in the literature can be seen in Figure 7. One thing that is worth of note in Figure 7 is the step going through I[‡], which presents a proton transfer in a four-membered ring transition state. While its bare barrier is around 28.8 kcal mol⁻¹, this can be reduced to 13.6 kcal mol⁻¹ by the use of a single-water-molecule proton shuttle. Furthermore, while the facilitated transfer shows only an 8% reaction rate constant increase due to tunneling (using the Eckart approximation), the bare reaction step shows a 960 times (!) increase, even at room temperature. Notwithstanding, the product M is not formed during simulation if the facilitated I[‡] step is removed from the system. All this, together with the indication that the tetrahedral intermediate J appears to be an important rest state, strongly suggests that the step passing through I[‡] is the rate-determining one, and that it includes active participation of the solvent.

One key feature of this reaction is its strong dependency on pH: as early shown by Kirby and Lancaster, the reaction takes place on acidity environments only.⁷⁸ In order to access its behavior in different acidic environments, we employed a series of short (0.5 s) simulations at different pH values, always starting with 0.1 M of the maleamic acid A (Figure 8A). We kept the concentration of H⁺ at a different value for each simulation (corresponding to pH 0–7), but we employed pseudo-first order conditions with respect to the solvent in each of them, constraining the water concentration to stay at 55.6 M. In total, the presented system encompasses 25 simultaneous and automatically simulated reactions and 17 distinct species. As can be seen in Figure 8A, the results corroborate with initial velocity essays worked by Kirby and Lancaster for closely-related systems,⁷⁸ where reaction ceases to happen around pH 5.

By simulating the whole system for an hour at pH 2, we could obtain the kinetic profile in Figure 8B. Observing the concentration over time of different intermediates leads us to conclude that, under

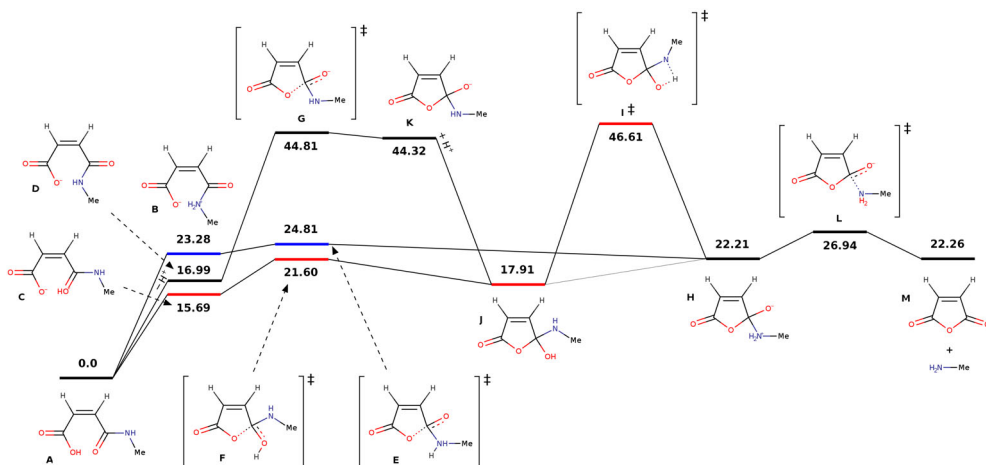
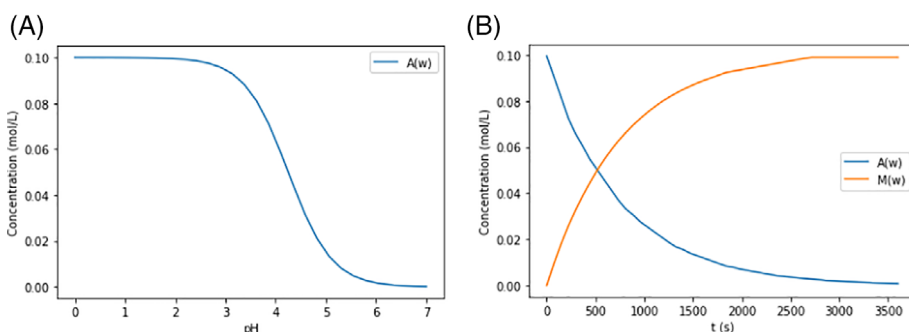


FIGURE 7 Proposed reaction mechanisms for the amide hydrolysis of N-alkyl maleamic acids, as previously proposed in the literature.^{78–81} Three possible mechanisms are indicated with distinct colors. The black bars denote the path starting with proton dissociation, followed by an intramolecular attack on the amide carbon. The red bars indicate a path where the attack happens concomitant to a proton transfer to the amide carbonyl. In addition, the blue bars indicate a similar path, but the proton is transferred to the amide nitrogen upon attack on the carbon. Subsequent dissociation of the product complex is worth $\Delta G^\circ = -4.74 \text{ kcal mol}^{-1}$. In the current work, we investigate the base case where $R_1 = -\text{CH}_3$ and $R_2 = R_3 = \text{H}$

FIGURE 8 (A) Short (0.5 s) simulations at different pH values (pH 0–7). (B) Kinetic profile for the reaction at pH 2, as simulated for an hour (3600 s). In all cases, pseudo-first order conditions with respect to water were maintained (55.6 M) and the initial concentration of the maleamic acid A (Figure 7) was 0.1 M. All reactions presented so far were included in the simulations (25 in total, see text and Figure 7)



these conditions, the reaction seems to happen mostly through equilibrium-state C and rest-state J: as J starts to build up, it gradually transitions, with the help of the solvent, to H, whose C–N bond has been elongated at this point. Finally, after the production of both M and the primary amine leaving group, actual separation further steers the reaction forward due to entropy ($\Delta S^\circ = 27 \text{ cal mol}^{-1} \text{ K}^{-1}$).

4 | SUMMARY AND OUTLOOK

We applied an automatic process for obtaining reaction kinetic profiles of increasingly complex reactions from first principles. The presented method allows for direct comparison with experimentally obtained results, which are often indispensable when studying chemical reactions.¹⁶ Known disparities can be systematically adjusted using energetic biases if the computational model is known to deliver systematic errors, which is particularly important in systems involving bimolecular reactions.

Although not a magic blackbox, overreact offers a hopefully complete but simple predictive computational environment for hypothesis

testing in first-principles homogeneous chemical kinetics and catalysis. In fact, from the calculated concentrated curves using microkinetic simulations, observed reaction rate constants can be inferred using the same mathematical techniques employed in common experimental data treatments.^{34,36}

The open-source package presented in this article is already available to explore and analyze reaction mechanisms. Detailed instructions on how to install and use can be found at <https://geem-lab.github.io/overreact-guide/>. In the future, we will investigate the applicability of overreact to more complex, catalytic systems,^{83,84} extend the present work to heterogeneous reactions, and attempt to fully predict the outcome of reactors by coupling computational fluid dynamics with first-principles microkinetic modeling.⁸⁵ All this would, in principle, allow us to design catalysts that work well in the scale they are meant to.

ACKNOWLEDGMENTS

The authors Felipe S. S. Schneider and Giovanni F. Caramori thank the National Council for Scientific and Technological Development, CNPq for their PhD (140485/2017-1) and research (311132/2020-0) grants, respectively.

DATA AVAILABILITY STATEMENT

Data that supports the findings of this study are available in the supplementary material of this article. A complete data set is openly available in <https://github.com/geem-lab/overreact-data>. The source code of overreact is also openly available at <https://github.com/geem-lab/overreact>. A user guide can be found at <https://geem-lab.github.io/overreact-guide/>.

ORCID

Felipe S. S. Schneider  <https://orcid.org/0000-0001-8090-2976>
Giovanni F. Caramori  <https://orcid.org/0000-0002-6455-7831>

REFERENCES

- [1] D. Klass, *Biomass for Renewable Energy, Fuels, and Chemicals*, Academic Press, Cambridge, Massachusetts **1998**.
- [2] A. Demirbaş, *Energy Convers. Manag.* **2001**, 42, 1357.
- [3] J. B. Binder, R. T. Raines, *J. Am. Chem. Soc.* **2009**, 131, 1979.
- [4] R. Šivec, M. Grilc, M. Huš, B. Likozar, *Ind. Eng. Chem. Res.* **2019**, 58, 16018.
- [5] M. Auffhammer, V. Ramanathan, J. R. Vincent, *Proc. Natl. Acad. Sci.* **2006**, 103, 19668.
- [6] H. V. M. Hamelers, O. Schaetzle, J. M. Paz-García, P. M. Biesheuvel, C. J. N. Buisman, *Environ. Sci. Technol. Lett.* **2013**, 1, 31.
- [7] V. Barbarossa, G. Vanga, R. Visconti, D. M. Gattia, *Energy Procedia* **2014**, 45, 1325.
- [8] J. Fanchi, C. Fanchi, *Energy IN THe 21st Century*, 4th ed., World Scientific Publishing Company, Hackensack, NJ **2016**.
- [9] P. Raveendran, J. Fu, S. L. Wallen, *J. Am. Chem. Soc.* **2003**, 125, 13940.
- [10] A. Arcadi, *Chem. Rev.* **2008**, 108, 3266.
- [11] P. Anastas, N. Eghbali, *Chem. Soc. Rev.* **2010**, 39, 301.
- [12] O. V. Kharissova, B. I. Kharisov, C. M. Oliva González, Y. P. Méndez, I. López, *R. Soc. Open Sci.* **2019**, 6, 191378.
- [13] D. J. Tantillo, C. Jiangang, K. N. Houk, *Curr. Opin. Chem. Biol.* **1998**, 2, 743.
- [14] K. N. Houk, F. Liu, *Acc. Chem. Res.* **2017**, 50, 539.
- [15] Y. Wang, L. Xiao, Y. Qi, M. Mahmoodinia, X. Feng, J. Yang, Y.-A. Zhu, D. Chen, *Phys. Chem. Chem. Phys.* **2019**, 21, 19269.
- [16] S. Ahn, M. Hong, M. Sundararajan, D. H. Ess, M.-H. Baik, *Chem. Rev.* **2019**, 119, 6509.
- [17] J. W. Kim, Y. Kim, K. Y. Baek, K. Lee, W. Y. Kim, *Chem. A Eur. J.* **2019**, 123, 4796.
- [18] I. Funes-Ardoiz, F. Schoenebeck, *Chem* **2020**, 6, 1904.
- [19] M. S. Gordon, G. Barca, S. S. Leang, D. Poole, A. P. Rendell, J. L. Galvez Vallejo, B. Westheimer, *Chem. A Eur. J.* **2020**, 124, 4557.
- [20] N. Nikbin, S. Caratzoulas, D. G. Vlachos, *ChemCatChem* **2012**, 4, 504.
- [21] J. Jover, *Phys. Chem. Chem. Phys.* **2017**, 19, 29344.
- [22] W. Guo, R. Kuniyil, J. E. Gómez, F. Maseras, A. W. Kleij, *J. Am. Chem. Soc.* **2018**, 140, 3981.
- [23] M. Besora, F. Maseras, *Wiley Interdiscip. Rev.: Comput. Mol. Sci.* **2018**, 8, e1372.
- [24] Y. Yu, Y. Zhu, M. N. Bhagat, A. Raghuraman, K. F. Hirsekorn, J. M. Notestein, S. T. Nguyen, L. J. Broadbelt, *ACS Catal.* **2018**, 8, 11119.
- [25] M. Jaraíz, J. E. Rubio, L. Enríquez, R. Pinacho, J. L. López-Pérez, A. Lesarri, *ACS Catal.* **2019**, 9, 4804.
- [26] A. Ishikawa, Y. Tateyama, *J. Comput. Chem.* **2019**, 40, 1866.
- [27] P. Morgante, R. Peverati, *Int. J. Quantum Chem.* **2020**, 120, e26332.
- [28] H. Ryu, J. Park, H. K. Kim, J. Y. Park, S.-T. Kim, M.-H. Baik, *Organometallics* **2018**, 37, 3228.
- [29] S. Grimme, *Chem. Eur. J.* **2012**, 18, 9955.
- [30] J. H. Jensen, *Phys. Chem. Chem. Phys.* **2015**, 17, 12441.
- [31] A. V. Marenich, C. J. Cramer, D. G. Truhlar, *J. Phys. Chem. B* **2009**, 113, 6378.
- [32] R. F. Ribeiro, A. V. Marenich, C. J. Cramer, D. G. Truhlar, *J. Phys. Chem. B* **2011**, 115, 14556.
- [33] Y.-P. Li, J. Gomes, S. Mallikarjun Sharada, A. T. Bell, M. Head-Gordon, *J. Phys. Chem. C* **2015**, 119, 1840.
- [34] D. G. Blackmond, *Angew. Chem. Int. Ed.* **2005**, 44, 4302.
- [35] S. Kozuch, J. M. L. Martin, *ChemPhysChem* **2011**, 12, 1413.
- [36] D. G. Blackmond, *J. Am. Chem. Soc.* **2015**, 137, 10852.
- [37] E. Solel, N. Tarannam, S. Kozuch, *Chem. Commun.* **2019**, 55, 5306.
- [38] E. Dzib, J. L. Cabelllos, F. Ortiz-Chi, S. Pan, A. Galano, G. Merino, *Int. J. Quantum Chem.* **2018**, 119, e25686.
- [39] J. A. Dumesic, D. F. Rudd, D. F. Rudd, L. M. Aparicio, J. E. Rekoske, A. A. Trevino, *The microkinetics of heterogeneous catalysis*, American Chemical Society, **1993**.
- [40] A. van de Runstraat, J. van Grondelle, R. A. van Santen, *Ind. Eng. Chem. Res.* **1997**, 36, 3116.
- [41] M. Neurock, E. W. Hansen, *Comput. Chem. Eng.* **1998**, 22, S1045.
- [42] A. B. Mhadeshwar, H. Wang, D. G. Vlachos, *J. Phys. Chem. B* **2003**, 107, 12721.
- [43] A. Bhan, S. Hsu, G. Blau, J. Caruthers, V. Venkatasubramanian, W. Delgass, *J. Catal.* **2005**, 235, 35.
- [44] L. C. Grabow, A. A. Gokhale, S. T. Evans, J. A. Dumesic, M. Mavrikakis, *J. Phys. Chem. C* **2008**, 112, 4608.
- [45] G. Novell-Leruth, J. M. Ricart, J. Pérez-Ramírez, *J. Phys. Chem. C* **2008**, 112, 13554.
- [46] S. C. Ammal, A. Heyden, *J. Phys. Chem. Lett.* **2012**, 3, 2767.
- [47] R. A. van Santen, A. J. Markvoort, I. A. W. Filot, M. M. Ghouri, E. J. M. Hensen, *Phys. Chem. Chem. Phys.* **2013**, 15, 17038.
- [48] A. J. Medford, C. Shi, M. J. Hoffmann, A. C. Lausche, S. R. Fitzgibbon, T. Bligaard, J. K. Nørskov, *Catal. Lett.* **2015**, 145, 794.
- [49] C. F. Goldsmith, R. H. West, *J. Phys. Chem. C* **2017**, 121, 9970.
- [50] Y. Mao, H. Wang, P. Hu, *WIREs* **2017**, 7, e1321.
- [51] Z. Chen, H. Wang, N. Q. Su, S. Duan, T. Shen, X. Xu, *ACS Catal.* **2018**, 8, 5816.
- [52] L. Foppa, K. Larmier, A. Comas-Vives, *CHIMIA Int. J. Chem.* **2019**, 73, 239.
- [53] J. Park, J. Cho, Y. Lee, M.-J. Park, W. B. Lee, *Ind. Eng. Chem. Res.* **2019**, 58, 8663.
- [54] H. Liu, J. Liu, B. Yang, *Phys. Chem. Chem. Phys.* **2019**, 21, 9876.
- [55] M. Huš, M. Grilc, A. Pavlišič, B. Likozar, A. Hellman, *Catal. Today* **2019**, 338, 128.
- [56] A. L. Slusarczyk, A. Lin, R. Weiss, *Nat. Rev. Genet.* **2012**, 13, 406.
- [57] M. O. Miranda, Y. DePorre, H. Vazquez-Lima, M. A. Johnson, D. J. Marell, C. J. Cramer, W. B. Tolman, *Inorg. Chem.* **2013**, 52, 13692.
- [58] R. Christensen, H. A. Hansen, T. Vegge, *Cat. Sci. Technol.* **2015**, 5, 4946.
- [59] Ferro-Costas, D.; Truhlar, D. G.; Fernández-Ramos, A. Pilgrim: A thermal rate constant calculator and kinetics Monte Carlo Simulator (version 1.0). <https://github.com/daferro/Pilgrim>, **2019**; Accessed: March 2022.
- [60] Schneider, F. S. S. geem-lab/overreact: v1.0.2. **2021**; <https://zenodo.org/record/5730603>.
- [61] F. Neese, *WIREs Comput. Mol. Sci.* **2017**, 8, e1327.
- [62] M. J. Frisch, G. W. Trucks, H. B. Schlegel, G. E. Scuseria, M. A. Robb, J. R. Cheeseman, G. Scalmani, V. Barone, G. A. Petersson, H. Nakatsuji, X. Li, M. Caricato, A. V. Marenich, J. Bloino, B. G. Janesko, R. Gomperts, B. Mennucci, H. P. Hratchian, J. V. Ortiz, A. F. Izmaylov, J. L. Sonnenberg, D. Williams-Young, F. Ding, F. Lipparini, F. Egidi, J. Goings, B. Peng, A. Petrone, T. Henderson, D. Ranasinghe, V. G. Zakrzewski, J. Gao, N. Rega, G. Zheng, W. Liang, M. Hada, M. Ehara, K. Toyota, R. Fukuda, J. Hasegawa, M. Ishida, T. Nakajima, Y. Honda, O. Kitao, H. Nakai, T. Vreven, K. Throssell, J. A. Montgomery Jr., J. E. Peralta, F. Ogliaro, M. J. Bearpark, J. J. Heyd, E. N. Brothers, K. N. Kudin, V. N. Staroverov, T. A. Keith, R. Kobayashi, J. Normand, K. Raghavachari, A. P. Rendell, J. C. Burant, S. S. Iyengar, J. Tomasi, M. Cossi, J. M. Millam, M. Klene, C. Adamo, R. Cammi, J. W. Ochterski,

- R. L. Martin, K. Morokuma, O. Farkas, J. B. Foresman, D. J. Fox, *Gaussian ~09 Revision C.01*, Gaussian Inc., Wallingford, CT **2010**.
- [63] N. M. O'boyle, A. L. Tenderholt, K. M. Langner, *J. Comput. Chem.* **2008**, *29*, 839.
- [64] L. Goerigk, S. Grimme, *Phys. Chem. Chem. Phys.* **2011**, *13*, 6670.
- [65] N. Mardirossian, M. Head-Gordon, *Mol. Phys.* **2017**, *115*, 2315.
- [66] L. Goerigk, A. Hansen, C. Bauer, S. Ehrlich, A. Najibi, S. Grimme, *Phys. Chem. Chem. Phys.* **2017**, *19*, 32184.
- [67] R. Pérez-Soto, M. Besora, F. Maseras, *Org. Lett.* **2020**, *22*, 2873.
- [68] J. G. Brandenburg, C. Bannwarth, A. Hansen, S. Grimme, *J. Chem. Phys.* **2018**, *148*, 064104.
- [69] J. Zheng, *Science* **2006**, *313*, 1951.
- [70] J. M. Lehn, *Dynamic Stereochemistry*, Springer, Berlin, Heidelberg **1970**, p. 311.
- [71] N. Tanaka, Y. Xiao, A. C. Lasaga, *J. Atmos. Chem.* **1996**, *23*, 37.
- [72] J. Burkholder, S. Sander, J. Abbatt, J. Barker, C. Cappa, J. Crounse, T. Dibble, R. Huie, C. Kolb, M. Kurylo, V. Orkin, *Chemical kinetics and photochemical data for use in atmospheric studies; evaluation number, 19*, JPL Publication, Jet Propulsion Laboratory, Pasadena **2020**.
- [73] P. Pracht, S. Grimme, *Chem. A Eur. J.* **2021**, *125*, 5681.
- [74] R. Krishnan, J. S. Binkley, R. Seeger, J. A. Pople, *J. Chem. Phys.* **1980**, *72*, 650.
- [75] Y. Zhao, D. G. Truhlar, *Theor. Chem. Acc.* **2007**, *120*, 215.
- [76] R. N. Goldberg, N. Kishore, R. M. Lennen, *J. Phys. Chem. Ref. Data* **2002**, *31*, 231.
- [77] P. Neta, P. Maruthamuthu, P. M. Carton, R. W. Fessenden, *J. Phys. Chem.* **1978**, *82*, 1875.
- [78] A. J. Kirby, P. W. Lancaster, *J. Chem. Soc., Perkin Trans. 2* **1972**, *1206*.
- [79] R. Karaman, *Comput. Theor. Chem.* **2011**, *974*, 133.
- [80] B. S. Souza, J. R. Mora, E. H. Wanderlind, R. M. Clementin, J. C. Gesser, H. D. Fiedler, F. Nome, F. M. Menger, *Angew. Chem. Int. Ed.* **2017**, *56*, 5345.
- [81] S. Su, F.-S. Du, Z.-C. Li, *Org. Biomol. Chem.* **2017**, *15*, 8384.
- [82] J.-D. Chai, M. Head-Gordon, *Phys. Chem. Chem. Phys.* **2008**, *10*, 6615.
- [83] S. E. Coelho, F. S. S. Schneider, D. C. de Oliveira, G. L. Tripodi, M. N. Eberlin, G. F. Caramori, B. de Souza, J. B. Domingos, *ACS Catal.* **2019**, *9*, 3792.
- [84] B. L. Oliveira, B. J. Stenton, V. B. Unnikrishnan, C. R. de Almeida, J. Conde, M. Negrão, F. S. S. Schneider, C. Cordeiro, M. G. Ferreira, G. F. Caramori, J. B. Domingos, R. Fior, G. J. L. Bernardes, *J. Am. Chem. Soc.* **2020**, *142*, 10869.
- [85] B. Partopour, A. G. Dixon, *Ind. Eng. Chem. Res.* **2019**, *58*, 5733.

SUPPORTING INFORMATION

Additional supporting information may be found in the online version of the article at the publisher's website.

How to cite this article: F. S. S. Schneider, G. F. Caramori, *J. Comput. Chem.* **2022**, *1*. <https://doi.org/10.1002/jcc.26861>

7 Concluding remarks and closing

The present thesis described approaches to the elucidation of reaction mechanisms in general and the elucidation of specific reaction mechanisms in particular. Two computational-experimental collaborations have been presented and a third purely computational publication detailed the development of an open-source library and command-line application for automating the investigation of reaction mechanisms.

One could inspect steady-state conditions, in which the concentrations and rates have converged to some final value, search for the most predominant species under catalytic conditions, computationally estimate the overall turn-over frequency, an essential measure of catalytic activity, and understand selectivity of a catalysts towards particular products. Not only it provides insight into concentration dependencies and comparison with experiment, such framework would serve as a benchmark for hypothesis testing, allowing the prediction of chemical behaviour in a computationally affordable and precise way. Kinetic models in such a framework can be progressively constructed, with a single pathway added at a time until a match with the experiment, simplifying the workflow, easing the computational burden and increasing efficiency, as was recommended elsewhere [??]. Such an incremental modeling protocol is arguably maximally efficient, as a minimal set of reactions lead to more easily rationalisable and “probably less wrong” models [????].

Bibliography

- 1 SCHNEIDER, F. S. S.; CARAMORI, G. F. Overreact, an in silico lab: Automatic quantum chemical microkinetic simulations for complex chemical reactions. *Journal of Computational Chemistry*, Wiley, Apr 2022. ISSN 1096-987x. Disponível em: <<http://dx.doi.org/10.1002/jcc.26861>>. Cited 6 times in pages 27, 31, 38, 71, 96, and 97.
- 2 SCHNEIDER, F. S. S. *geem-lab/overreact: overreact v1.0.2*. Zenodo, 2021. <<https://doi.org/10.5281/ZENODO.5730603>>. Accessed: 2022-07-29. Disponível em: <<https://zenodo.org/record/5730603>>. Cited 5 times in pages 27, 38, 71, 96, and 97.
- 3 COELHO, S. E. et al. Mechanism of palladium(ii)-mediated uncaging reactions of propargylic substrates. *ACS Catalysis*, American Chemical Society (ACS), v. 9, n. 5, p. 3792–3799, Mar 2019. ISSN 2155-5435. Disponível em: <<http://dx.doi.org/10.1021/acscatal.9b00210>>. Cited 6 times in pages 27, 47, 48, 57, 58, and 96.
- 4 OLIVEIRA, B. L. et al. Platinum-triggered bond-cleavage of pentynoyl amide and n-propargyl handles for drug-activation. *Journal of the American Chemical Society*, American Chemical Society (ACS), v. 142, n. 24, p. 10869–10880, May 2020. ISSN 1520-5126. Disponível em: <<http://dx.doi.org/10.1021/jacs.0c01622>>. Cited 3 times in pages 27, 57, and 97.
- 5 BERTOZZI, C. R. et al. Grand challenges in chemistry for 2016 and beyond. *ACS Central Science*, American Chemical Society (ACS), v. 2, n. 1, p. 1–3, Jan 2016. ISSN 2374-7951. Disponível em: <<http://dx.doi.org/10.1021/acscentsci.6b00010>>. Cited in page 31.
- 6 RECOGNIZING the Best in Innovation: Breakthrough Catalyst. 2005. 20 p. R&D Magazine. Cited in page 31.
- 7 MARKET Report: Global Catalyst Market. Third. [S.l.]: Acmite Market Intelligence, 2015. 542 p. Cited in page 31.
- 8 CAO, Y. et al. Reinforcement learning supercharges redox flow batteries. *Nature Machine Intelligence*, Springer Science and Business Media LLC, Aug 2022. ISSN 2522-5839. Disponível em: <<http://dx.doi.org/10.1038/S42256-022-00523-2>>. Cited in page 31.
- 9 JENCKS, W. P. *Catalysis in Chemistry and Enzymology*. [S.l.]: Dover Publications, 1987. ISBN 0486654605. Cited 2 times in pages 31 and 37.
- 10 HOHENBERG, P.; KOHN, W. Inhomogeneous electron gas. *Physical Review*, American Physical Society (APS), v. 136, n. 3b, p. B864–b871, Nov 1964. ISSN 0031-899x. Disponível em: <<http://dx.doi.org/10.1103/PhysRev.136.B864>>. Cited in page 33.
- 11 KOHN, W.; SHAM, L. J. Self-consistent equations including exchange and correlation effects. *Physical Review*, American Physical Society (APS),

- v. 140, n. 4a, p. A1133–a1138, Nov 1965. ISSN 0031-899x. Disponível em: <<http://dx.doi.org/10.1103/PhysRev.140.A1133>>. Cited in page 33.
- 12 PERDEW, J. P. et al. Gedanken densities and exact constraints in density functional theory. *The Journal of Chemical Physics*, AIP Publishing, v. 140, n. 18, p. 18a533, May 2014. ISSN 1089-7690. Disponível em: <<http://dx.doi.org/10.1063/1.4870763>>. Cited in page 33.
- 13 KRYACHKO, E. S.; nA, E. V. L. Density functional theory: Foundations reviewed. *Physics Reports*, Elsevier BV, v. 544, n. 2, p. 123–239, Nov 2014. ISSN 0370-1573. Disponível em: <<http://dx.doi.org/10.1016/j.physrep.2014.06.002>>. Cited in page 33.
- 14 YU, H. S.; LI, S. L.; TRUHLAR, D. G. Perspective: Kohn-sham density functional theory descending a staircase. *The Journal of Chemical Physics*, AIP Publishing, v. 145, n. 13, p. 130901, Oct 2016. ISSN 1089-7690. Disponível em: <<http://dx.doi.org/10.1063/1.4963168>>. Cited in page 33.
- 15 SZABO, A.; OSTLUND, N. S. *Modern Quantum Chemistry: Introduction to Advanced Electronic Structure Theory (Dover Books on Chemistry)*. [S.l.]: Dover Publications, 1996. ISBN 0486691861. Cited 2 times in pages 33 and 34.
- 16 MARENICH, A. V.; CRAMER, C. J.; TRUHLAR, D. G. Universal solvation model based on solute electron density and on a continuum model of the solvent defined by the bulk dielectric constant and atomic surface tensions. *The Journal of Physical Chemistry B*, American Chemical Society (ACS), v. 113, n. 18, p. 6378–6396, May 2009. ISSN 1520-5207. Disponível em: <<http://dx.doi.org/10.1021/jp810292n>>. Cited 2 times in pages 33 and 35.
- 17 MARENICH, A. V. et al. Resolution of a challenge for solvation modeling: Calculation of dicarboxylic acid dissociation constants using mixed discrete-continuum solvation models. *The Journal of Physical Chemistry Letters*, American Chemical Society (ACS), v. 3, n. 11, p. 1437–1442, May 2012. ISSN 1948-7185. Disponível em: <<http://dx.doi.org/10.1021/jz300416r>>. Cited in page 33.
- 18 CHAI, J.-D.; HEAD-GORDON, M. Systematic optimization of long-range corrected hybrid density functionals. *The Journal of Chemical Physics*, AIP Publishing, v. 128, n. 8, p. 084106, Feb 2008. ISSN 1089-7690. Disponível em: <<http://dx.doi.org/10.1063/1.2834918>>. Cited in page 34.
- 19 CHAI, J.-D.; HEAD-GORDON, M. Long-range corrected hybrid density functionals with damped atom-atom dispersion corrections. *Physical Chemistry Chemical Physics*, Royal Society of Chemistry (RSC), v. 10, n. 44, p. 6615, 2008. ISSN 1463-9084. Disponível em: <<http://dx.doi.org/10.1039/B810189B>>. Cited in page 34.
- 20 GOERIGK, L.; GRIMME, S. A thorough benchmark of density functional methods for general main group thermochemistry, kinetics, and noncovalent interactions. *Physical Chemistry Chemical Physics*, Royal Society of Chemistry (RSC), v. 13, n. 14, p. 6670, 2011. ISSN 1463-9084. Disponível em: <<http://dx.doi.org/10.1039/C0CP02984J>>. Cited in page 34.
- 21 ARAGÓ, J. et al. Ab initio modeling of donor-acceptor interactions and charge-transfer excitations in molecular complexes: The case of terthiophene-tetracyanoquinodimethane. *Journal of Chemical Theory and Computation*, American

- Chemical Society (ACS), v. 7, n. 7, p. 2068–2077, Jul 2011. ISSN 1549-9626. Disponível em: <<http://dx.doi.org/10.1021/ct200203k>>. Cited in page 34.
- 22 SALZNER, U.; AYDIN, A. Improved prediction of properties of π -conjugated oligomers with range-separated hybrid density functionals. *Journal of Chemical Theory and Computation*, American Chemical Society (ACS), v. 7, n. 8, p. 2568–2583, Aug 2011. ISSN 1549-9626. Disponível em: <<http://dx.doi.org/10.1021/ct2003447>>. Cited in page 34.
- 23 BURNS, L. A. et al. Density-functional approaches to noncovalent interactions: A comparison of dispersion corrections (dft-d), exchange-hole dipole moment (xdm) theory, and specialized functionals. *The Journal of Chemical Physics*, AIP Publishing, v. 134, n. 8, p. 084107, Feb 2011. ISSN 1089-7690. Disponível em: <<http://dx.doi.org/10.1063/1.3545971>>. Cited in page 34.
- 24 MINENKOV, Y. et al. The accuracy of dft-optimized geometries of functional transition metal compounds: a validation study of catalysts for olefin metathesis and other reactions in the homogeneous phase. *Dalton Transactions*, Royal Society of Chemistry (RSC), v. 41, n. 18, p. 5526, 2012. ISSN 1477-9234. Disponível em: <<http://dx.doi.org/10.1039/c2dt12232d>>. Cited in page 34.
- 25 SWART, M.; BICKELHAUPT, F. M.; DURAN, M. *DFT2016 poll*. 2016. <<http://www.marcelswart.eu/dft-poll/news2016.pdf>>. Accessed: 2017-06-10. Cited in page 34.
- 26 HELGAKER, T. et al. The prediction of molecular equilibrium structures by the standard electronic wave functions. *The Journal of Chemical Physics*, AIP Publishing, v. 106, n. 15, p. 6430–6440, Apr 1997. ISSN 1089-7690. Disponível em: <<http://dx.doi.org/10.1063/1.473634>>. Cited in page 34.
- 27 JENSEN, F. Atomic orbital basis sets. *Wiley Interdisciplinary Reviews: Computational Molecular Science*, Wiley, v. 3, n. 3, p. 273–295, Oct 2012. ISSN 1759-0876. Disponível em: <<http://dx.doi.org/10.1002/wcms.1123>>. Cited in page 34.
- 28 HILL, J. G. Gaussian basis sets for molecular applications. *International Journal of Quantum Chemistry*, Wiley, v. 113, n. 1, p. 21–34, Oct 2012. ISSN 0020-7608. Disponível em: <<http://dx.doi.org/10.1002/qua.24355>>. Cited in page 34.
- 29 DITCHFIELD, R.; HEHRE, W. J.; POPLE, J. A. Self-consistent molecular-orbital methods. ix. an extended gaussian-type basis for molecular-orbital studies of organic molecules. *The Journal of Chemical Physics*, AIP Publishing, v. 54, n. 2, p. 724–728, Jan 1971. ISSN 1089-7690. Disponível em: <<http://dx.doi.org/10.1063/1.1674902>>. Cited in page 34.
- 30 HEHRE, W. J.; DITCHFIELD, R.; POPLE, J. A. Self-consistent molecular orbital methods. xii. further extensions of gaussian-type basis sets for use in molecular orbital studies of organic molecules. *The Journal of Chemical Physics*, AIP Publishing, v. 56, n. 5, p. 2257–2261, Mar 1972. ISSN 1089-7690. Disponível em: <<http://dx.doi.org/10.1063/1.1677527>>. Cited in page 34.
- 31 HARIHARAN, P. C.; POPLE, J. A. The influence of polarization functions on molecular orbital hydrogenation energies. *Theoretica Chimica Acta*, Springer

- Nature, v. 28, n. 3, p. 213–222, 1973. ISSN 1432-2234. Disponível em: <<http://dx.doi.org/10.1007/BF00533485>>. Cited in page 34.
- 32 HARIHARAN, P.; POPLE, J. Accuracy of ahnequilibrium geometries by single determinant molecular orbital theory. *Molecular Physics*, Informa UK Limited, v. 27, n. 1, p. 209–214, Jan 1974. ISSN 1362-3028. Disponível em: <<http://dx.doi.org/10.1080/00268977400100171>>. Cited in page 34.
- 33 GORDON, M. S. The isomers of silacyclopropane. *Chemical Physics Letters*, Elsevier BV, v. 76, n. 1, p. 163–168, Nov 1980. ISSN 0009-2614. Disponível em: <[http://dx.doi.org/10.1016/0009-2614\(80\)80628-2](http://dx.doi.org/10.1016/0009-2614(80)80628-2)>. Cited in page 34.
- 34 FRANCL, M. M. et al. Self-consistent molecular orbital methods. xxiii. a polarization-type basis set for second-row elements. *The Journal of Chemical Physics*, AIP Publishing, v. 77, n. 7, p. 3654–3665, Oct 1982. ISSN 1089-7690. Disponível em: <<http://dx.doi.org/10.1063/1.444267>>. Cited in page 34.
- 35 CLARK, T. et al. Efficient diffuse function-augmented basis sets for anion calculations. iii. the 3-21+g basis set for first-row elements, li-f. *Journal of Computational Chemistry*, Wiley-Blackwell, v. 4, n. 3, p. 294–301, 1983. ISSN 1096-987x. Disponível em: <<http://dx.doi.org/10.1002/jcc.540040303>>. Cited in page 34.
- 36 FRISCH, M. J.; POPLE, J. A.; BINKLEY, J. S. Self-consistent molecular orbital methods 25. supplementary functions for gaussian basis sets. *The Journal of Chemical Physics*, AIP Publishing, v. 80, n. 7, p. 3265–3269, Apr 1984. ISSN 1089-7690. Disponível em: <<http://dx.doi.org/10.1063/1.447079>>. Cited in page 34.
- 37 BINNING, R. C.; CURTISS, L. A. Compact contracted basis sets for third-row atoms: Ga-kr. *Journal of Computational Chemistry*, Wiley-Blackwell, v. 11, n. 10, p. 1206–1216, Nov 1990. ISSN 1096-987x. Disponível em: <<http://dx.doi.org/10.1002/jcc.540111013>>. Cited in page 34.
- 38 BLAUDEAU, J.-P. et al. Extension of gaussian-2 (g2) theory to molecules containing third-row atoms k and ca. *The Journal of Chemical Physics*, AIP Publishing, v. 107, n. 13, p. 5016–5021, Oct 1997. ISSN 1089-7690. Disponível em: <<http://dx.doi.org/10.1063/1.474865>>. Cited in page 34.
- 39 RASSOLOV, V. A. et al. 6-31g*basis set for atoms k through zn. *The Journal of Chemical Physics*, AIP Publishing, v. 109, n. 4, p. 1223–1229, Jul 1998. ISSN 1089-7690. Disponível em: <<http://dx.doi.org/10.1063/1.476673>>. Cited in page 34.
- 40 RASSOLOV, V. A. et al. 6-31g*basis set for third-row atoms. *Journal of Computational Chemistry*, Wiley-Blackwell, v. 22, n. 9, p. 976–984, 2001. ISSN 1096-987x. Disponível em: <<http://dx.doi.org/10.1002/jcc.1058>>. Cited in page 34.
- 41 BANERJEE, A. et al. Search for stationary points on surfaces. *The Journal of Physical Chemistry*, American Chemical Society (ACS), v. 89, n. 1, p. 52–57, Jan 1985. ISSN 1541-5740. Disponível em: <<http://dx.doi.org/10.1021/j100247a015>>. Cited in page 34.
- 42 SCHLEGEL, H. B. Optimization of equilibrium geometries and transition structures. In: *Ab Initio Methods in Quantum Chemistry, Part 1 (Advances in Chemical*

- Physics*). Wiley-Interscience, 1987. p. 249–286. ISBN 9780471909002. Disponível em: <<http://dx.doi.org/10.1002/9780470142936.ch4>>. Cited in page 34.
- 43 MAURO, J. C.; LOUCKS, R. J.; BALAKRISHNAN, J. A simplified eigenvector-following technique for locating transition points in an energy landscape. *The Journal of Physical Chemistry A*, American Chemical Society (ACS), v. 109, n. 42, p. 9578–9583, Oct 2005. ISSN 1520-5215. Disponível em: <<http://dx.doi.org/10.1021/jp053581t>>. Cited in page 34.
- 44 PENG, C.; SCHLEGEL, H. B. Combining synchronous transit and quasi-newton methods to find transition states. *Israel Journal of Chemistry*, Wiley-Blackwell, v. 33, n. 4, p. 449–454, 1993. ISSN 0021-2148. Disponível em: <<http://dx.doi.org/10.1002/ijch.199300051>>. Cited in page 34.
- 45 PENG, C. et al. Using redundant internal coordinates to optimize equilibrium geometries and transition states. *Journal of Computational Chemistry*, Wiley-Blackwell, v. 17, n. 1, p. 49–56, Jan 1996. ISSN 1096-987X. Disponível em: <[http://dx.doi.org/10.1002/\(SICI\)1096-987X\(19960115\)17:1<49::AID-JCC5>3.0.CO;2-0](http://dx.doi.org/10.1002/(SICI)1096-987X(19960115)17:1<49::AID-JCC5>3.0.CO;2-0)>. Cited in page 34.
- 46 TRANSITION state theory. *IUPAC Compendium of Chemical Terminology*, Iupac, fev. 2014. Accessed: 2017-05-27. Disponível em: <<http://dx.doi.org/10.1351/goldbook.T06470>>. Cited 2 times in pages 35 and 38.
- 47 DING, F.; SMITH, J. M.; WANG, H. First-principles calculation of *pKa* values for organic acids in nonaqueous solution. *The Journal of Organic Chemistry*, American Chemical Society (ACS), v. 74, n. 7, p. 2679–2691, Apr 2009. ISSN 1520-6904. Disponível em: <<http://dx.doi.org/10.1021/jo802641r>>. Cited 2 times in pages 35 and 36.
- 48 SUMON, K. Z.; HENNI, A.; EAST, A. L. L. Predicting *pKa* of amines for CO₂ capture: Computer versus pencil-and-paper. *Industrial & Engineering Chemistry Research*, American Chemical Society (ACS), v. 51, n. 37, p. 11924–11930, Sep 2012. ISSN 1520-5045. Disponível em: <<http://dx.doi.org/10.1021/ie301033p>>. Cited in page 35.
- 49 TISSANDIER, M. D. et al. The proton's absolute aqueous enthalpy and gibbs free energy of solvation from cluster-ion solvation data. *The Journal of Physical Chemistry A*, American Chemical Society (ACS), v. 102, n. 40, p. 7787–7794, Oct 1998. ISSN 1520-5215. Disponível em: <<http://dx.doi.org/10.1021/jp982638r>>. Cited in page 35.
- 50 YANG, C. et al. Theoretical study on the acidities of chiral phosphoric acids in dimethyl sulfoxide: Hints for organocatalysis. *The Journal of Organic Chemistry*, American Chemical Society (ACS), v. 78, n. 14, p. 7076–7085, Jul 2013. ISSN 1520-6904. Disponível em: <<http://dx.doi.org/10.1021/jo400915f>>. Cited in page 35.
- 51 PLIEGO, J. R.; RIVEROS, J. M. Theoretical calculation of *pKa* using the cluster-continuum model. *The Journal of Physical Chemistry A*, American Chemical Society (ACS), v. 106, n. 32, p. 7434–7439, Aug 2002. ISSN 1520-5215. Disponível em: <<http://dx.doi.org/10.1021/jp025928n>>. Cited in page 35.
- 52 GOLDBERG, R. N.; KISHORE, N.; LENNEN, R. M. Thermodynamic quantities for the ionization reactions of buffers. *Journal of Physical and Chemical Reference Data*,

- AIP Publishing, v. 31, n. 2, p. 231–370, Jun 2002. ISSN 1529-7845. Disponível em: <<http://dx.doi.org/10.1063/1.1416902>>. Cited in page 35.
- 53 BRESLOW, R. Biomimetic chemistry and artificial enzymes: Catalysis by design. *Accounts of Chemical Research*, American Chemical Society (ACS), v. 28, n. 3, p. 146–153, Mar 1995. ISSN 1520-4898. Disponível em: <<http://dx.doi.org/10.1021/ar00051a008>>. Cited in page 37.
- 54 THE Nobel Prize in Chemistry 1929. 1929. <http://www.nobelprize.org/nobel_prizes/chemistry/laureates/1929/>. Accessed: 2017-05-16. Cited in page 37.
- 55 THE Nobel Prize in Chemistry 1946. 1946. <http://www.nobelprize.org/nobel_prizes/chemistry/laureates/1946/>. Accessed: 2017-05-16. Cited in page 37.
- 56 THE Nobel Prize in Chemistry 1957. 1957. <http://www.nobelprize.org/nobel_prizes/chemistry/laureates/1957/>. Accessed: 2017-05-16. Cited in page 37.
- 57 THE Nobel Prize in Chemistry 1975. 1975. <http://www.nobelprize.org/nobel_prizes/chemistry/laureates/1975/>. Accessed: 2017-05-16. Cited in page 37.
- 58 THE Nobel Prize in Chemistry 1997. 1997. <http://www.nobelprize.org/nobel_prizes/chemistry/laureates/1997/>. Accessed: 2017-05-16. Cited in page 37.
- 59 THE Nobel Prize in Chemistry 2013. 2013. <http://www.nobelprize.org/nobel_prizes/chemistry/laureates/2013/>. Accessed: 2017-05-16. Cited 2 times in pages 37 and 104.
- 60 FISCHER, E. Ueber die optischen isomeren des traubenzuckers, der gluconsäure und der zuckersäure. *Berichte der deutschen chemischen Gesellschaft*, Wiley-Blackwell, v. 23, n. 2, p. 2611–2624, Jul 1890. ISSN 1099-0682. Disponível em: <<http://dx.doi.org/10.1002/cber.189002302157>>. Cited in page 37.
- 61 FISCHER, E. Einfluss der configuration auf die wirkung der enzyme. *Berichte der deutschen chemischen Gesellschaft*, Wiley-Blackwell, v. 27, n. 3, p. 2985–2993, Oct 1894. ISSN 1099-0682. Disponível em: <<http://dx.doi.org/10.1002/cber.18940270364>>. Cited in page 37.
- 62 KOSHLAND, D. Application of a theory of enzyme specificity to protein synthesis. *Proceedings of the National Academy of Sciences*, National Academy of Sciences, v. 44, n. 2, p. 98–104, 1958. Cited in page 37.
- 63 DAFFORN, A.; KOSHLAND, D. E. Theoretical aspects of orbital steering. *Proceedings of the National Academy of Sciences*, v. 68, n. 10, p. 2463–2467, 1971. Disponível em: <<http://www.pnas.org/content/68/10/2463.abstract>>. Cited in page 37.
- 64 KIRBY, A. J. Enzyme mechanisms, models, and mimics. *Angewandte Chemie International Edition in English*, Wiley-Blackwell, v. 35, n. 7, p. 706–724, Apr 1996. ISSN 1521-3773. Disponível em: <<http://dx.doi.org/10.1002/anie.199607061>>. Cited in page 37.
- 65 NILSSON, H.; SMITH, L. Die bildungsweise der chlorhydrine. *Zeitschrift für Physikalische Chemie*, Walter de Gruyter GmbH, v. 166a, n. 1, Jan 1933. ISSN 0942-9352. Disponível em: <<http://dx.doi.org/10.1515/zpch-1933-16615>>. Cited in page 37.

- 66 BRUICE, T. C.; PANDIT, U. K. Intramolecular models depicting the kinetic importance of „fit” in enzymatic catalysis. *Proceedings of the National Academy of Sciences*, v. 46, n. 4, p. 402–404, 1960. Disponível em: <<http://www.pnas.org/content/46/4/402.short>>. Cited 2 times in pages 37 and 103.
- 67 JUNG, M. E. Substituent and solvent effects in intramolecular diets-alder reactions. *Synlett*, Thieme Publishing Group, v. 1990, n. 04, p. 186–190, 1990. ISSN 1437-2096. Disponível em: <<http://dx.doi.org/10.1055/s-1990-21028>>. Cited in page 37.
- 68 KIRBY, A. J.; LANCASTER, P. W. Structure and efficiency in intramolecular and enzymic catalysis. catalysis of amide hydrolysis by the carboxy-group of substituted maleamic acids. *Journal of the Chemical Society, Perkin Transactions 2*, Royal Society of Chemistry (RSC), n. 9, p. 1206, 1972. ISSN 1364-5471. Disponível em: <<http://dx.doi.org/10.1039/P29720001206>>. Cited 4 times in pages 37, 103, 104, and 105.
- 69 BECKE, A. D. Perspective: Fifty years of density-functional theory in chemical physics. *The Journal of Chemical Physics*, AIP Publishing, v. 140, n. 18, p. 18a301, May 2014. ISSN 1089-7690. Disponível em: <<http://dx.doi.org/10.1063/1.4869598>>. Cited in page 39.
- 70 BOGOJESKI, M. et al. Quantum chemical accuracy from density functional approximations via machine learning. *Nature Communications*, Springer Science and Business Media LLC, v. 11, n. 1, Oct 2020. ISSN 2041-1723. Disponível em: <<http://dx.doi.org/10.1038/s41467-020-19093-1>>. Cited in page 39.
- 71 BÍM, D. et al. Beyond the classical thermodynamic contributions to hydrogen atom abstraction reactivity. *Proceedings of the National Academy of Sciences*, Proceedings of the National Academy of Sciences, v. 115, n. 44, Sep 2018. ISSN 1091-6490. Disponível em: <<http://dx.doi.org/10.1073/pnas.1806399115>>. Cited 2 times in pages 39 and 100.
- 72 SCHNEIDER, F. S. S. *schneiderfelipe/pyrrole: pyrrole 0.2.1*. Zenodo, 2019. <<https://doi.org/10.5281/zenodo.3242195>>. Accessed: 2022-07-29. Disponível em: <<https://zenodo.org/record/3242196>>. Cited 3 times in pages 40, 71, and 96.
- 73 GROSS, I. P. et al. Polylactic acid, maleic anhydride and dicumyl peroxide: Nmr study of the free-radical melt reaction product. *Polymer Degradation and Stability*, Elsevier BV, v. 155, p. 1–8, Sep 2018. ISSN 0141-3910. Disponível em: <<http://dx.doi.org/10.1016/j.polymdegradstab.2018.06.016>>. Cited 2 times in pages 45 and 95.
- 74 SCHNEIDER, F. S. et al. A theoretical investigation on the aminolysis of pyromellitic and 1,4,5,8-naphthalenetetracarboxylic dianhydrides. *Computational and Theoretical Chemistry*, Elsevier BV, v. 1147, p. 13–19, Jan 2019. ISSN 2210-271x. Disponível em: <<http://dx.doi.org/10.1016/j.comptc.2018.11.008>>. Cited 2 times in pages 45 and 96.
- 75 ALMERINDO, G. I. et al. Kinetics and adsorption calculations: insights into the mgo-catalyzed detoxification of simulants of organophosphorus biocides. *Journal of Materials Chemistry A*, Royal Society of Chemistry (RSC), v. 8, n. 36, p. 19011–19021, 2020. ISSN 2050-7496. Disponível em: <<http://dx.doi.org/10.1039/C9TA14028J>>. Cited 2 times in pages 45 and 96.

- 76 VIDAL, C. et al. Concurrent and orthogonal gold(i) and ruthenium(ii) catalysis inside living cells. *Nature Communications*, Springer Science and Business Media LLC, v. 9, n. 1, May 2018. ISSN 2041-1723. Disponível em: <<http://dx.doi.org/10.1038/s41467-018-04314-5>>. Cited in page 57.
- 77 KAR, T. et al. Solvation enhances the distinction between carboxylated armchair and zigzag single-wall carbon nanotubes (swnt-cooh). *The Journal of Physical Chemistry C*, American Chemical Society (ACS), v. 121, n. 17, p. 9516–9527, Apr 2017. ISSN 1932-7455. Disponível em: <<http://dx.doi.org/10.1021/acs.jpcc.6b10676>>. Cited in page 95.
- 78 SCHNEIDER, F. S. S. et al. Bond analysis in dihalogen-halide and dihalogen-dimethylchalcogenide systems. *European Journal of Inorganic Chemistry*, Wiley, v. 2018, n. 8, p. 1007–1015, Feb 2018. ISSN 1099-0682. Disponível em: <<http://dx.doi.org/10.1002/ejic.201701337>>. Cited in page 95.
- 79 ØSTRØM, I. et al. Quest for insight into ultrashort c-h···π proximities in molecular “iron maidens”. *The Journal of Organic Chemistry*, American Chemical Society (ACS), v. 83, n. 9, p. 5114–5122, Apr 2018. ISSN 1520-6904. Disponível em: <<http://dx.doi.org/10.1021/acs.joc.8b00461>>. Cited in page 95.
- 80 SCHNEIDER, F. S. S. et al. How do secondary phosphine oxides interact with silver nanoclusters? insights from computation. *The Journal of Physical Chemistry C*, American Chemical Society (ACS), v. 122, n. 37, p. 21449–21461, Aug 2018. ISSN 1932-7455. Disponível em: <<http://dx.doi.org/10.1021/acs.jpcc.8b06244>>. Cited in page 95.
- 81 SCHNEIDER, F. S. S. *schniederfelipe/pnictogen: Lightweight generation of input files*. Zenodo, 2019. <<https://doi.org/10.5281/zenodo.3380593>>. Accessed: 2022-07-29. Disponível em: <<https://zenodo.org/record/3380594>>. Cited in page 96.
- 82 MELO, C. E. de et al. Solvatochromism of new substituted 4-[(e)-(4-nitrophenyl)diazenyl]phenolate dyes. *Journal of Molecular Liquids*, Elsevier BV, v. 301, p. 112330, Mar 2020. ISSN 0167-7322. Disponível em: <<http://dx.doi.org/10.1016/j.molliq.2019.112330>>. Cited in page 96.
- 83 ORENHA, R. P. et al. On the recognition of chloride, bromide and nitrate anions by anthracene-squaramide conjugated compounds: a computational perspective. *New Journal of Chemistry*, Royal Society of Chemistry (RSC), v. 44, n. 41, p. 17831–17839, 2020. ISSN 1369-9261. Disponível em: <<http://dx.doi.org/10.1039/D0NJ03685D>>. Cited in page 96.
- 84 SCHNEIDER, F. S. S. *schniederfelipe/doi2bib: doi2bib v1.1*. Zenodo, 2021. <<https://doi.org/10.5281/ZENODO.4625655>>. Accessed: 2022-07-29. Disponível em: <<https://zenodo.org/record/4625655>>. Cited in page 97.
- 85 BEESLEY, R. M.; INGOLD, C. K.; THORPE, J. F. Cxix.—the formation and stability of spiro-compounds. part i. spiro-compounds from cyclohexane. *J. Chem. Soc., Trans.*, Royal Society of Chemistry (RSC), v. 107, n. 0, p. 1080–1106, 1915. ISSN 0368-1645. Disponível em: <<http://dx.doi.org/10.1039/CT9150701080>>. Cited in page 103.

- 86 ALLINGER, N. L.; ZALKOW, V. Conformational analysis. ix. the gem-dimethyl effect^{1,2}. *The Journal of Organic Chemistry*, American Chemical Society (ACS), v. 25, n. 5, p. 701–704, May 1960. ISSN 1520-6904. Disponível em: <<http://dx.doi.org/10.1021/jo01075a006>>. Cited in page 103.
- 87 BRUICE, T. C.; PANDIT, U. K. The effect of geminal substitution ring size and rotamer distribution on the intramolecular nucleophilic catalysis of the hydrolysis of monophenyl esters of dibasic acids and the solvolysis of the intermediate anhydrides. *Journal of the American Chemical Society*, American Chemical Society (ACS), v. 82, n. 22, p. 5858–5865, Nov 1960. ISSN 1520-5126. Disponível em: <<http://dx.doi.org/10.1021/ja01507a023>>. Cited in page 103.
- 88 CAPON, B. Neighbouring group participation. *Quarterly Reviews, Chemical Society*, Royal Society of Chemistry, v. 18, n. 1, p. 45–111, 1964. Cited in page 103.
- 89 BRUICE, T. C.; BRADBURY, W. C. The gem effect. i. the influence of 3-substituents on the rates of solvolysis of glutaric anhydride. a conformational analysis. *Journal of the American Chemical Society*, American Chemical Society (ACS), v. 87, n. 21, p. 4838–4845, Nov 1965. ISSN 1520-5126. Disponível em: <<http://dx.doi.org/10.1021/ja00949a030>>. Cited in page 103.
- 90 GALLI, C. et al. Ring-closure reactions. 12. gem-dimethyl effect in some medium and large rings. *The Journal of Organic Chemistry*, American Chemical Society (ACS), v. 44, n. 8, p. 1258–1261, Apr 1979. ISSN 1520-6904. Disponível em: <<http://dx.doi.org/10.1021/jo01322a015>>. Cited in page 103.
- 91 KIRBY, A. J. Effective molarities for intramolecular reactions. *Advances in Physical Organic Chemistry*, Elsevier, p. 183–278, 1980. ISSN 0065-3160. Disponível em: <[http://dx.doi.org/10.1016/S0065-3160\(08\)60129-X](http://dx.doi.org/10.1016/S0065-3160(08)60129-X)>. Cited in page 103.
- 92 LIGHTSTONE, F. C.; BRUICE, T. C. Geminal dialkyl substitution, intramolecular reactions, and enzyme efficiency. *Journal of the American Chemical Society*, American Chemical Society (ACS), v. 116, n. 23, p. 10789–10790, Nov 1994. ISSN 0002-7863. Disponível em: <<http://dx.doi.org/10.1021/ja00102a056>>. Cited in page 103.
- 93 KANETI, J. et al. Thorpe-ingold effects in cyclizations to five-membered and six-membered rings containing planar segments. the rearrangement of n(1)-alkyl-substituted dihydroorotic acids to hydantoinacetic acids in base. *Org. Biomol. Chem.*, Royal Society of Chemistry (RSC), v. 2, n. 7, p. 1098–1103, 2004. ISSN 1477-0539. Disponível em: <<http://dx.doi.org/10.1039/B400248B>>. Cited in page 103.
- 94 JUNG, M. E.; PIIZZI, G. gem-disubstituent effect: theoretical basis and synthetic applications. *Chemical Reviews*, American Chemical Society (ACS), v. 105, n. 5, p. 1735–1766, May 2005. ISSN 1520-6890. Disponível em: <<http://dx.doi.org/10.1021/cr940337h>>. Cited 2 times in pages 103 and 105.
- 95 KARAMAN, R. Analyzing the efficiency in intramolecular amide hydrolysis of kirby's n-alkylmaleamic acids - a computational approach. *Computational and Theoretical Chemistry*, Elsevier BV, v. 974, n. 1-3, p. 133–142, Nov 2011. ISSN 2210-271x. Disponível em: <<http://dx.doi.org/10.1016/j.comptc.2011.07.025>>. Cited 2 times in pages 103 and 105.

- 96 NELSON, D. L.; COX, M. M. *Lehninger Principles of Biochemistry*. [S.l.]: Freeman/Worth, 2012. Cited in page 104.
- 97 FESIK, S. W. Structural biology: Controlling the caspases. *Science*, American Association for the Advancement of Science (AAAS), v. 294, n. 5546, p. 1477–1478, Nov 2001. ISSN 1095-9203. Disponível em: <<http://dx.doi.org/10.1126/science.1062236>>. Cited in page 104.
- 98 KENNY, A.; O'HARE, M.; GUSTERSON, B. Cell-surface peptidases as modulators of growth and differentiation. *The Lancet*, Elsevier BV, v. 334, n. 8666, p. 785–787, Sep 1989. ISSN 0140-6736. Disponível em: <[http://dx.doi.org/10.1016/S0140-6736\(89\)90841-6](http://dx.doi.org/10.1016/S0140-6736(89)90841-6)>. Cited in page 104.
- 99 KAPUST, R. B.; WAUGH, D. S. Controlled intracellular processing of fusion proteins by tev protease. *Protein Expression and Purification*, Elsevier BV, v. 19, n. 2, p. 312–318, Jul 2000. ISSN 1046-5928. Disponível em: <<http://dx.doi.org/10.1006/prep.2000.1251>>. Cited in page 104.
- 100 BORISOFF, J. I. et al. Is thrombin a key player in the “coagulation-atherogenesis” maze? *Cardiovascular Research*, Oxford University Press (OUP), v. 82, n. 3, p. 392–403, Feb 2009. ISSN 0008-6363. Disponível em: <<http://dx.doi.org/10.1093/cvr/cvp066>>. Cited in page 104.
- 101 SOUZA, B. S. et al. Transforming a stable amide into a highly reactive one: Capturing the essence of enzymatic catalysis. *Angewandte Chemie*, Wiley, v. 129, n. 19, p. 5429–5432, Apr 2017. ISSN 0044-8249. Disponível em: <<http://dx.doi.org/10.1002/ange.201701306>>. Cited in page 104.

Appendices

Appendix A – List of Works

The following list presents all the papers that I have co-authored and published during my PhD (after March 2017), together with open-source software that I have developed or contributed to. The ones relevant to the current topic are highlighted and referenced to the relevant chapters¹.

2017

- KAR, T. et al. Solvation enhances the distinction between carboxylated armchair and zigzag single-wall carbon nanotubes (swnt-cooh). *The Journal of Physical Chemistry C*, American Chemical Society (ACS), v. 121, n. 17, p. 9516–9527, Apr 2017. ISSN 1932-7455. Disponível em: <<http://dx.doi.org/10.1021/acs.jpcc.6b10676>>.
- SCHNEIDER, F. S. S. et al. Bond analysis in dihalogen-halide and dihalogen-dimethylchalcogenide systems. *European Journal of Inorganic Chemistry*, Wiley, v. 2018, n. 8, p. 1007–1015, Feb 2018. ISSN 1099-0682. Disponível em: <<http://dx.doi.org/10.1002/ejic.201701337>>.

2018

- ØSTRØM, I. et al. Quest for insight into ultrashort c-h···π proximities in molecular “iron maidens”. *The Journal of Organic Chemistry*, American Chemical Society (ACS), v. 83, n. 9, p. 5114–5122, Apr 2018. ISSN 1520-6904. Disponível em: <<http://dx.doi.org/10.1021/acs.joc.8b00461>>.
- GROSS, I. P. et al. Polylactic acid, maleic anhydride and dicumyl peroxide: Nmr study of the free-radical melt reaction product. *Polymer Degradation and Stability*, Elsevier BV, v. 155, p. 1–8, Sep 2018. ISSN 0141-3910. Disponível em: <<http://dx.doi.org/10.1016/j.polymdegradstab.2018.06.016>>. (**Minor contribution**, see Section 3.9.1.)
- SCHNEIDER, F. S. S. et al. How do secondary phosphine oxides interact with silver nanoclusters? insights from computation. *The Journal of Physical Chemistry C*, American Chemical Society (ACS), v. 122, n. 37, p. 21449–21461, Aug 2018. ISSN 1932-7455. Disponível em: <<http://dx.doi.org/10.1021/acs.jpcc.8b06244>>.

¹ *Minor contributions* are publications tangentially relevant to this thesis’ topic, while *major contributions* encompass publications described in the present work.

2019

- SCHNEIDER, F. S. et al. A theoretical investigation on the aminolysis of pyromellitic and 1,4,5,8-naphthalenetetracarboxylic dianhydrides. *Computational and Theoretical Chemistry*, Elsevier BV, v. 1147, p. 13–19, Jan 2019. ISSN 2210-271x. Disponível em: <<http://dx.doi.org/10.1016/j.comptc.2018.11.008>>. (Minor contribution, see Section 3.9.1.)
- COELHO, S. E. et al. Mechanism of palladium(ii)-mediated uncaging reactions of propargylic substrates. *ACS Catalysis*, American Chemical Society (ACS), v. 9, n. 5, p. 3792–3799, Mar 2019. ISSN 2155-5435. Disponível em: <<http://dx.doi.org/10.1021/acscatal.9b00210>>. (Major contribution, see Section 3.9.2 and Chapter 4.)

Software

- SCHNEIDER, F. S. S. *schneiderfelipe/pyrrole: pyrrole 0.2.1*. Zenodo, 2019. <<https://doi.org/10.5281/zenodo.3242195>>. Accessed: 2022-07-29. Disponível em: <<https://zenodo.org/record/3242196>>. (A first iteration on `overreact` [1, 2], see Section 3.9.2 and Chapter 6.)
- SCHNEIDER, F. S. S. *schneiderfelipe/pnictogen: Lightweight generation of input files*. Zenodo, 2019. <<https://doi.org/10.5281/zenodo.3380593>>. Accessed: 2022-07-29. Disponível em: <<https://zenodo.org/record/3380594>>.

2020

- MELO, C. E. de et al. Solvatochromism of new substituted 4-[(e)-(4-nitrophenyl)diazenyl]phenolate dyes. *Journal of Molecular Liquids*, Elsevier BV, v. 301, p. 112330, Mar 2020. ISSN 0167-7322. Disponível em: <<http://dx.doi.org/10.1016/j.molliq.2019.112330>>.
- ORENHA, R. P. et al. On the recognition of chloride, bromide and nitrate anions by anthracene-squaramide conjugated compounds: a computational perspective. *New Journal of Chemistry*, Royal Society of Chemistry (RSC), v. 44, n. 41, p. 17831–17839, 2020. ISSN 1369-9261. Disponível em: <<http://dx.doi.org/10.1039/D0NJ03685D>>.
- ALMERINDO, G. I. et al. Kinetics and adsorption calculations: insights into the mgo-catalyzed detoxification of simulants of organophosphorus biocides. *Journal of Materials Chemistry A*, Royal Society of Chemistry (RSC), v. 8, n. 36, p. 19011–19021, 2020. ISSN 2050-7496. Disponível em: <<http://dx.doi.org/10.1039/C9TA14028J>>. (Minor contribution, see Section 3.9.1.)

-
- OLIVEIRA, B. L. et al. Platinum-triggered bond-cleavage of pentynoyl amide and n-propargyl handles for drug-activation. *Journal of the American Chemical Society*, American Chemical Society (ACS), v. 142, n. 24, p. 10869–10880, May 2020. ISSN 1520-5126. Disponível em: <<http://dx.doi.org/10.1021/jacs.0c01622>>. (**Major contribution**, see Section 3.9.2 and Chapter 5.)

2021

Software

- SCHNEIDER, F. S. S. *schneiderfelipe/doi2bib: doi2bib v1.1*. Zenodo, 2021. <<https://doi.org/10.5281/ZENODO.4625655>>. Accessed: 2022-07-29. Disponível em: <<https://zenodo.org/record/4625655>>.
- SCHNEIDER, F. S. S. *geem-lab/overreact: overreact v1.0.2*. Zenodo, 2021. <<https://doi.org/10.5281/ZENODO.5730603>>. Accessed: 2022-07-29. Disponível em: <<https://zenodo.org/record/5730603>>. (**Major contribution**, see Section 3.9.2 and Chapter 6.)

2022

- SCHNEIDER, F. S. S.; CARAMORI, G. F. Overreact, an in silico lab: Automative quantum chemical microkinetic simulations for complex chemical reactions. *Journal of Computational Chemistry*, Wiley, Apr 2022. ISSN 1096-987x. Disponível em: <<http://dx.doi.org/10.1002/jcc.26861>>. (**Major contribution**, see Section 3.9.2 and Chapter 6.)

Appendix B – Practical computational chemistry for the investigation of reaction mechanisms and transition state searches

This appendix is an account of techniques used and hard tested during my PhD. Most of them are of practical value and might be useful for other researchers to use.

B.1 General remarks about transition state structures

Obtaining transition state structures is not an easy task, at least not as easy as optimizing structures to minima. One core reason is that, although we have a good understanding about how minimum energy structures look like, it is not so easy with transition states, as they necessarily are in *between* observed minima (in the sense of potential energy surface).

One could imagine that bond lengths, angles and dihedrals be exactly at the middle between reactants and products, but reality is more complicated than that. As suggested by Hammond's postulate (and more generally the Bell-Evans-Polanyi principle), a transition state will more closely resemble the reactant structure if the reaction is exothermic (early transition state), and more the product if endothermic (late transition state).

CITE THE SECTION ABOUT BEP AND HAMMOND.

As such, it is reasonable to assume that the transition state structure can only be exactly at the middle if the reaction is thermoneutral, i.e., reactants and products sharing the same energy. This occurs, for example, in the umbrella effect of amines, or in enantiomeric interconversions.

B.1.1 Using Hammond's postulate for estimating transition state structures

RELEVANT PAPERS FOR THE DISCUSSION ARE <<https://doi.org/10.19142/rpq.v6i11.152>> AND CITATIONS 4–6 THEREIN.

The rate at which the reaction complex changes in the start of a reaction, as it walks along the reaction path, is related to the curvature of energy in the reaction valley along this path. It is worth mentioning that, since reactions tend to go along the least energy path, this curvature is most likely to be wide (i.e., less steep) when compared with

the other directions in the reaction valley. The reason is that molecular vibrations that don't lead to the reaction are normally stiffer than the reaction direction.

Along the lines of Hammond's postulate and the Bell-Evans-Polanyi principle, there is evidence (REF 14 OF THE PAPER ABOVE) that the reaction energy is proportional to the difference in position between the transition state and the exact midpoint of the reaction path. Although this requires knowledge of the reaction path and its midpoint position, and approximation for the linear path with a single changing degree of freedom is useful for guessing the transition state:

$$\Delta E^\circ \propto \Delta s = s_{\text{TS}} - s_{\text{midpoint}} \approx d_{\text{TS}} - \frac{d_{\text{P}} + d_{\text{R}}}{2} \quad (\text{B.1})$$

where s stands for the actual distance in some respect (e.g., root mean squared deviation), d is the distance in a single degree of freedom, and R, TS, and P correspond the reactant, transition state and product, respectively. We are also setting d_{midpoint} to $\frac{d_{\text{P}} + d_{\text{R}}}{2}$. As such, using a linear approximation,

$$d_{\text{TS}} \approx d_{\text{midpoint}} + \frac{\Delta E^\circ - b}{a} \quad (\text{B.2})$$

where a and b are constants to be determined. By making the reasonable assumption that the transition state should be at the midpoint for thermoneutral reactions, we learn that b is zero. Furthermore, if we consider $\Delta d < 0$ to be an early transition state, we determine that a is positive, since the reaction is exothermic ($\Delta E^\circ < 0$) in this case due to the BEP principle. A typical value for $|a|$ is around $1.5 \times 10^{-2} \sqrt{\text{amu}} \cdot \text{Bohr}/\text{kcal}\cdot\text{mol}^{-1}$ (JUSTIFY??).

Partial evidence for this can be found in the literature on hydrogen abstraction reactions (HAA) [71]. Bím et al.[71] suggest a relationship between Marcus' reorganization energy λ and an asynchronicity parameter ν that can empirically rationalize the concertedness of HAA reactions as whether the proton or the electron is transferred first. The ν factor is, conceptually, a decomposition between the effective redox and effective acidobasic contributions to the reaction. A perfectly synchronous HAA reaction would have $\nu = 0$, whereas positive values favor electron transfer (ET) and negative values favor proton transfer (PT). They showed that λ reaches its maximum where $|\nu|$ is lowest. This implies that, for this particular class of reactions, among systems with similar reaction free energies, the highest barrier is to be expected for the most synchronous proton-coupled electron transfer [71].

B.2 Some methods for obtaining transition states

The general idea is that the technique will depend on the information you have. If you have

1. only reasonable reactants or only reasonable products, start with conformational search, metadynamics and scans. Chemical knowledge can help in finding candidates, though.
2. both reasonable reactants and products, but no idea about the transition state, you can use all of the above, plus QST2 and NEB. Chemical knowledge plus simple estimates above can help on finding a transition state estimate, though.
3. reasonable reactants and products, but crude transition state estimate, use QST3, NEB, and the above. The goal here is validate your transition state structure candidate as a *true* transition state.
4. reasonable transition state, use an eigenvector following method. Good ones provide normal mode projection so that you can better control de optimization direction. Furthermore, a good initial hessian is also nice to have.

If have structures for both reactants and products, you can use techniques such as quadratic synchronous transit (QST2) or nudge-elastic band (NEB) to obtain a good guess on the transition state.

In such calculations, it is normally mandatory that the atom numbering match between atoms in both reactants and products.

In case you already have a reasonable guess for the transition state, both methods above (QST3 and NEB) can take advantage of that.

B.2.1 What if this don't work?

Sometimes you end up with an unconverged calculation. In other words, the calculation has performed some cycles, but then crashed. Changes are the final state of the calculation already has a better guess for the transition state. This structure can be used for further calculations.

B.3 What to do once you found a transition state candidate

Once you got a transition state candidate, both with its structure optimized and calculated frequencies, you should check that:

- only a single frequency appears, and
- that it corresponds to the expected bond breaking and forming.

B.3.1 If you are finding a set of homologous transition states

Focus on finding the simplest one first, then use it as a template for the other ones.

Appendix C – *gem*- and *vic* disubstitutions

The source of kinetic effect in the geminal substitution is similar to the one commonly involved in enzyme catalysis: the intramolecular reaction rate can be increased by rearranging the substrate reactive centers in a way similar to the steric configuration corresponding to the transition state, which is itself a consequence of the Bells-Evans-Polanyi (BEP) principle.

This steric compression can be obtained by the introduction of geminal disubstitutions (*gem*-) in the chain connecting two reaction centers (Figure 2): when *cis* reacting groups are held close in a rigid system, those reactions take place faster than otherwise [85, 86, 87, 66, 88, 89, 68, 90, 91, 92, 93, 94, 95]. The alkyl *gem*-disubstitution effect,

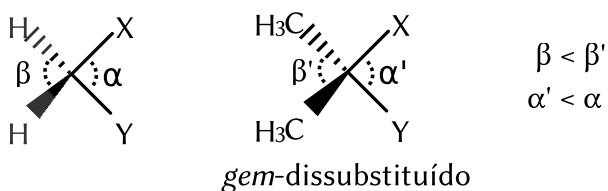


Figure 2 – *Gem*-dimethyl substitution (center), a kind of *gem*-disubstitution. According to Beesley, Thorpe and Ingold [85, 94], such substitutions promote the increase of the β angle and the decrease of the α angle (so called “Beesley-Thorpe-Ingold” effect, or “geminal dimethyl effect”), when compared to the non-substituted structure (left), which brings the reactive centers X and Y closer together. The reactive centers X and Y can consist of carbonic chains, which allow the formation of rings of arbitrary size.

already known and studied for more than a century, is the name given to the increase in cyclization rate due to the substitution of hydrogen atoms by alkyl groups in carbons in the tethering chain that connects two reactive centers (X and Y in Figure 2, for example) [88, 91, 93, 94].

The present of vicinal alkyl groups in the chain undergoing cyclization indices a similar kinetic effect (*vic*-disubstitution) to the *gem*-dialkyl one. One example that allows a comparison between the two involves the anhydride formation from monoesters of many diacid succinates [91, 87, 66, 89, 92] (Figure 3), whose relative reaction rates k_{rel} span one order of magnitude. In this case, the cyclization rate of the *vic*-dimethyl substituted succinate is significantly higher than the *gem*-dimethyl substituted one (Figure 3).

Another staggering example of the vicinal effect is found in *N*-alkyl substituted maleamic acids [68, 95] (Figure 4), whose structures are more rigid than the ones of the

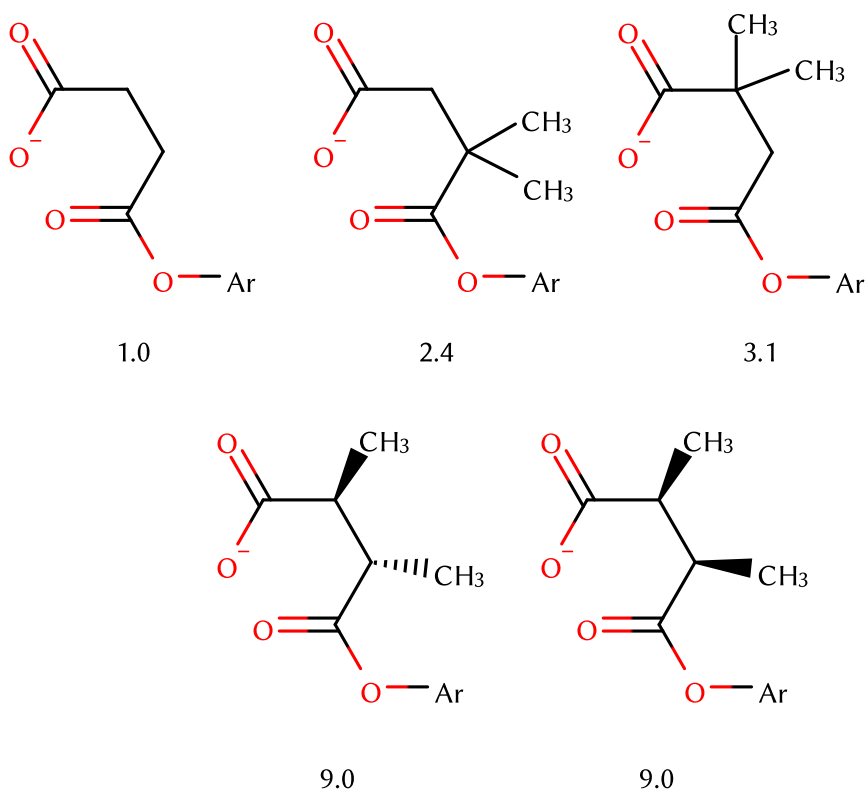


Figure 3 – Kinetic effect of geminal disubstitution when compared to the vicinal disubstitution. The relative cyclization rate (k_{rel}) is shown under each compound.

succinates mentioned above. In fact, the substituent effect in this class of reactions span *ten* orders of magnitude in k_{rel} (10^{-6} – 10^4 , Figure 4). Such structures undergo cyclization and intramolecular hydrolysis of the amidic bond, resulting in the formation of maleamic anhydride derivatives (Figure 4). The breakdown of the amidic bond allows us to classify the reaction as mimetic to the one catalytic promoted by peptidases [68], which are of great importance in many biological processes such as digestion [96], programmed cell death [97], cancer cell development [98], the widespread of crop diseases [99], and biochemical signaling in living organisms [96, 100]. Being more rigid, it is expected that those compounds present higher reaction rates, as evidenced by fact that substrates closer to the active site of enzymes is enough for the enzymatic behavior [101], although such view in general has been questioned by other authors [59]; it is not reasonable, on the other hand, to believe that the distance between reactive centers is not a key factor in catalysis.

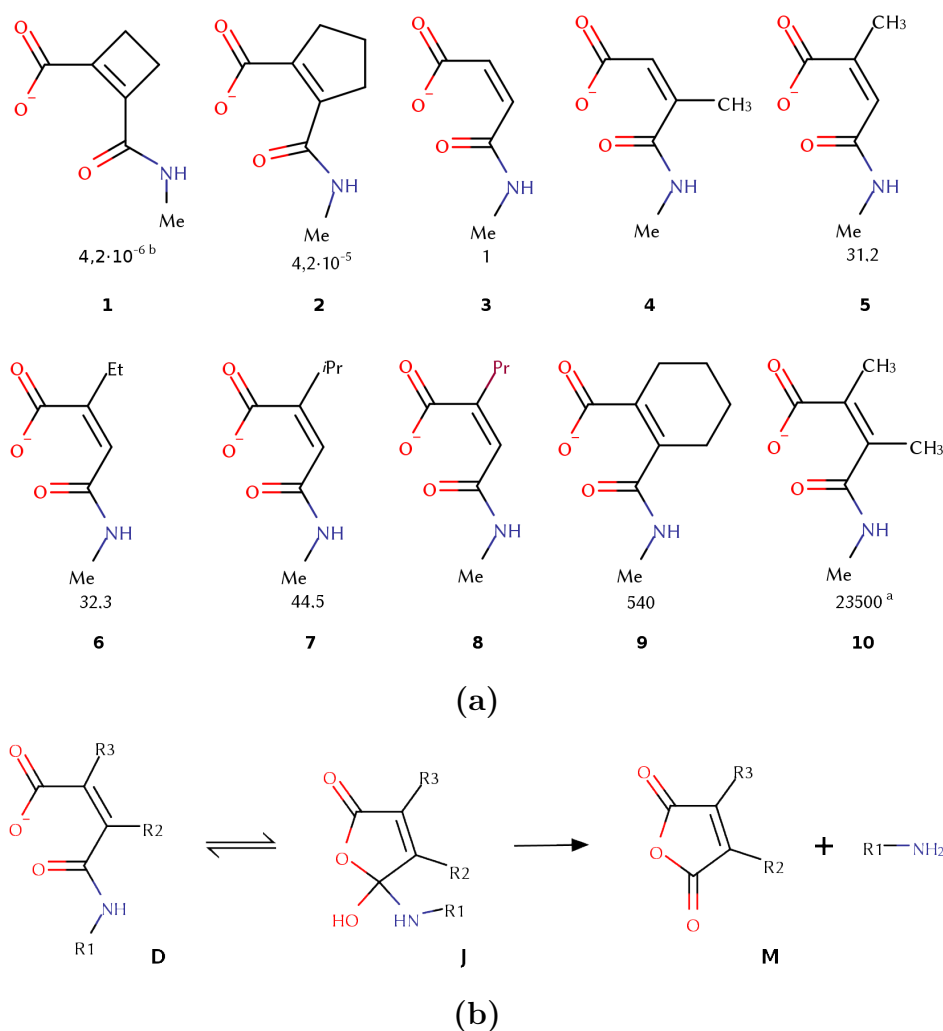


Figure 4 – (a) Substitutional kinetic effect in N-methyl maleamic acids for the cyclization reaction shown in (b). Such structure only admit vicinal disubstitutions. Available reaction rate constants k_{rel} available in the literature (relative to compound 3, measured at 39°C) are shown under each compound [68]. ^aOriginally estimated from a similar structure [68]. ^bEstimated from 100°C measurements due to slow reaction rate [68]. (b) Intramolecular hydrolysis of the amidic bond of *N*-alkyl substituted maleamic acids, giving rise to the formation of maleamic anhydride derivatives [68, 94, 95].